Developing and testing a sprayable overlay of Strain Hardening Cement-based Composite for retrofitting of unreinforced load bearing masonry walls.

by

Leon Roode de Beer

Thesis presented in partial fulfilment of the requirements for the degree of Master of Engineering in Structural Engineering in the Faculty of Engineering at Stellenbosch University

Supervised by:
Prof. G.P.A.G van Zijl

December 2016

Declaration

By submitting this thesis electronically, I declare that the entirety of the work contained therein is my own, original work, that I am the sole author thereof (save to the extent explicitly otherwise stated), that reproduction and publication thereof by Stellenbosch University will not infringe any third party rights and that I have not previously in its entirety or in part submitted it for obtaining any qualification.

Signature: .....

Date: .....

Abstract

In the Western Cape Province (South Africa) a large number of multi-storey buildings, built with unreinforced load bearing masonry (URM) were constructed before seismic resistance became a design standard requirement in 1989. The region lies in a light to moderate seismic zone in South Africa. It is foreseen that these buildings perform poorly during seismic activities due to their brittle in-plane shear failure mode. Retrofitting of existing URM structures are no easy task and few solutions have been suggested. A spray-able Strain Hardening Cement-based Composite (SHCC) overlay as retrofitting material is proposed for the materials superior tensile and shear properties while applying the overlay is simple.

SHCC is a fibre reinforced composite designed to form multiple fine cracks under tensile, shear and flexural load. The cracks are controlled to small widths, whereby significant toughness, or energy dissipation, is realised, while maintaining its resistance.

This thesis report results of determining the applicability and performance of retrofitting URM walls with a sprayable overlay of SHCC produced with local available material.

A spray-able SHCC was optimized for spray-ability as well as good adhesiveness to the masonry. Tensile strain capacity was tested throughout to determine the optimal mix having desirable fresh and hardened properties. SHCC free shrinkage, as well as the restrained shrinkage on the surface of the SHCC overlay were measured. The tests showed that restrained overlay shrinkage did not lead to visible debonding or cracking.

The interfacial bond and multiple cracking for energy dissipation in a seismic event were investigated using the triplet shear test. The preferred failure mechanism is described and designed for by restricting the overlay thickness to allow multiple crack formation in the overlay, instead of overlay debonding. Design guidelines to ensure that energy dissipative failure mechanisms indeed occur during in-plane shearing action are presented. The tests showed that the SHCC overlay is a viable solution as the shear strength and energy absorption capacity increased manifold.

Results from large scale shear wall validation tests are presented and the data was used to formulate a design model. The tests showed that multiple cracks form in the overlay, along with an increased in-plane shearing resistance compared with reference URM walls.

It can be concluded that spray-able SHCC is a viable retrofitting solution for the seismic resistance of URM and further development and testing is encouraged to optimize and implement the use of this retrofitting strategy.

Uittreksel

In die Wes-Kaap (Suid-Afrika) is daar 'n groot aantal meer-verdieping geboue, gebou met ongewapende lasdraende messelwerk (URM) voor seismiese weerstand 'n ontwerpstandaard vereiste geword het in 1989. Die streek lê in 'n ligte tot matige seismiese streek in Suid-Afrika. Daar word voorsien dat hierdie geboue swak sal vaar tydens seismiese aktiwiteite as gevolg van hulle bros in-vlak skuif falingsmode. Versterking van bestaande URM strukture is geen maklike taak nie en etlike oplossings is al voorgestel. 'n Spuitbare vervormingsverhardende sement-gebaseerde saamgestelde materiaal (SHCC) as oorlaag materiaal word voorgestel vir die materiaal se uitstekende trek en skuif eienskappe terwyl die toepassing van die oorlaag eenvoudig is.

SHCC is 'n veselversterkte saamgestelde material, ontwerp om menigvuldige fyn krake te vorm as trek, skuif of buig kragte aangewend word. Die krake se wydte word beperk, waardeur taaiheid en energie geabsorbeer word, terwyl die weerstand gehandhaaf word.

Hierdie tesis rapporteer resultate oor die bepaling of 'n SHCC oorlaag, gemaak van plaaslike materiale, as versterking op URM mure toepaslik is, asook die ekstra weerstand en duktiliteit wat dit verskaf. Vrye krimp, asook belemmerde krimp op die oppervlak van 'n SHCC oorlaag is gemeet. Die toetse het getoon dat belemmerde krimp van 'n oorlaag nie lei tot sigbare krake of lostrek vanaf die bakstene nie.

Die intervlak verband sterkte en veelvoudige krake vir energie absorbsie in 'n seismiese gebeurtenis is ondersoek met behulp van die 'triplet' skuiftoets. Die voorkeur falingsmeganisme word beskryf en voor ontwerp deur die beperking van die oorlaag dikte, sodat veelvoudige krake in die oorlaag kan vorm in plaas van faling van die verband tussen die SHCC en bakstene. Ontwerp riglyne om te verseker dat die energie-absorberende falingsmeganisme inderdaad voorkom tydens in-vlak skuif aksie word verskaf.

Resultate van grootskaalse skuif muur toetse word aangebied en die inligting is gebruik om 'n ontwerp model saam te stel. Die toetse het getoon dat meervoudige krake in die SHCC oorlaag vorm, saam met 'n verhoogde in-vlak skuif weerstand in vergelyking met die kontrole URM mure.

Uit die studie kan die gevolgtrekking gemaak word dat spuit-SHCC 'n toepaslike oplossing vir die seismiese versterking van URM is en dat verdere ontwikkeling en toetsing aangemoedig word om die materiaal te optimeer en te implementeer as 'n versterkingsmetode.

Acknowledgements

I would like to express my great appreciation to my supervisor, Professor Gideon Van Zijl, for his guidance, motivation, support and great knowledge that all contributed tremendously to this research project.

I would like to express my sincere appreciation to the following persons:

- Mr J. van der Merwe for his help and guidance during the planning and construction of the test setup. I thank him for the time, lessons and skills he taught me in the workshop.
- Stephan Zarenka, for his assistance in the laboratory and conducting of the tests.
- The laboratory staff from the University of Stellenbosch for their support and help with the inserting and removing of the large specimens.
- The Department of Civil Engineering at the University of Stellenbosch for allowing me to conduct the research over the time period of two years and supplying all the necessary tools and materials.
- My office colleagues and friends for all the support and creating an friendly environment and keeping me motivated during the long and tough hours.

I would also like to express my aprreciation for my family and friends for there support, love and motivation.

My greatest appreciation goes out to Anjali de Beer, for your loving support and becoming my wife in this period.

Above all, thanks to God for my personal abilities, strength and guidance during this project.

Contents

List of Figures

List of Tables

Nomenclature

A_{mb}	Mortar brick contact area
A_{SHCC}	Bonded area of the overlay
b	Breadth
C_{ε}	Constant accounting for combined influences of relative member dimensions
d	Depth
d_0	Slump cone diameter
d_1	Maximum diameter of slump spread (no external vibration)
d_2	Diameter perpendicular to d_1 (no external vibration)
D_1	Maximum diameter of slump spread (after external vibration)
D_2	Diameter perpendicular to d_1 (after external vibration)
e	Eccentricity
E	E-modulus
E_O	Modulus of elasticity of the overlay
E_S	Modulus of elasticity of the substrate
E_{SHCC}	Elastic Modulus of SHCC
f_b	Brick compressive strength
$f_{composite}$	Characteristic shear strength of clay masonry with a SHCC overlay
f_{cm}	Mortar compressive strength
$\bar{f}_c$	Average tensile strength at first crack
f_{mb}	Mortar brick shear bond stress
f_R	Frictional shear strength
f_{SHCC}	SHCC shear strength

$f_{SHCC}*$	Effective characteristic shear strength of SHCC
f_t	Tensile strength
$\bar{f_u}$	Average ultimate tensile strength
f_y	Yield stress
f_v	Characteristic shear strength
$f_{\tau SHCC}$	Bond shear strength between the brick and SHCC, (MPa)
F_v	Shear force
F_{vt}	Tension to effective shear stress ratio
g_A	Design vertical pressure
g	Ground acceleration
h	Height
l	Length
l_s	Height of triplet specimen
r_0	Stress at the start of the test $t = 0$
r_t	Stress after time t
R^2	Correlation coefficient
R_{char}	Reduction of F_{vt} from a average to characteristic value with a 95% exceedance probability.
RF_b	Reduction Factor for the bond
R_H	Relative humidity
S	Shear force
t	Time or thickness
t_0	Age at time of loading
t_{SHCC}	Thickness of the SHCC overlay
V	Vertical force
V_{SHCC}	Shear strength of cross sectional area of SHCC
w	Relaxation value
$\bar{\varepsilon_u}$	Average ultimate tensile strain

γ	Deformability (no external vibration)
Γ	Deformability (after external)
ε_0	Strain corresponding to stress σ_0
ε_{FSS}	Overlay free shrinkage strain
$\varepsilon_{restr.0,I}$	iRestrained overlay strain at the interface
ε_u	Ultimate strain
θ_R	Residual friction coefficient
σ_0	Pre-stress
σ_{tf}	First crack stress
$\sigma_{O,I}$	Direct stress in the overlay
Ψ_O	Relaxation function
ϕ	Initial shear bond strength

Abbreviations

ASTM	American Society for Testing and Materials
C	Cement
CAC	Calcium Aluminate Cement
CBM	Cement-Based Materials
CoV	Coefficient of Variance
DTT	Direct Tensile Tests
ECC	Engineered Cement-based Composite
E-Modulus	Modulus of Elasticity
FA	Fly Ash
FEM	Finite Element Method
FRP	Fibre Reinforced Polymer
FRC	Fibre Reinforced Concrete
GGCS	Ground Granulated Corex Slag
Hf	Horizontal facing side
HPC	High-Performance Concrete
HPFRCC	High-Performance Fibre Reinforced Cement Composite
LC	Load Cell
LVDT	Linear Variable Differential Transformer
MT	Modified Triplet
MTM	Materials Testing Machine
NSM	Near Surface Mounted
OPC	Ordinary Portland Cement
q	Behaviour factor

RC	Reinforced Concrete
SANS	South African National Standard
SCC	Self Compacting Concrete
SHCC	Strain Hardening Cement based Composite
SUN	Stellenbosch University
SP	Superplasticiser
SW	Shear Wall
SWS	Shear Wall Specimen
T	Triplet
UHPC	Ultra-High-Performance Concrete
URM	Unreinforced load bearing Masonry
UTT	Uni-axial Tensile Tests
VA	Viscous Agent
Vn	Vertical non-facing side
w/b	water binder ratio

Chapter 1

Introduction

Masonry is the most well known composite building material around the world. Masonry bricks are made of clay, calcium silicate, natural stone, concrete and fibre composites to name a few. This all round available building material has been used for millennia and is still one of the primary building materials for low-rise buildings in South-Africa. Most houses, office complexes and apartments up to four storeys are built with un-reinforced load bearing masonry (URM). Generally, masonry structures are good in resisting gravity loads but perform poorly when subjected to lateral loadings, such as seismic loads caused by earthquakes. The reasons for this are its high compressive strength, but low tensile strength and brittle shear failure mode.

One does not have to look far back in history (Christchurch-2011, Chile-2015 etc.) to see the poor performance of URM buildings during seismic activities. Brittle in-plane shear failures observed as diagonal cracking are the main cause of collapse for URM buildings during seismic activities. Seismic design requirements were only introduced in 1989 in South Africa, meaning that most of the URM buildings in the South Western region of the Western Cape province are not adequately designed for seismic activity, putting a large number of lives at risk.

Strain Hardening Cement-based Composite (SHCC) is a type of High-Performance Fibre Reinforced Cement Composite (HPFRCC) that has been engineered to have high ductility and can resist tensile load at a strain of more than 3 % and up to 6 %, compared to 0.01 % in normal concretes. Having a strain capacity 300 times more than normal concrete gives SHCC a high energy absorbing capacity. This makes an ideal construction material for seismic regions, providing highly ductile tensile resistance after concrete or mortar have failed.

Using SHCC as a retrofitting and strengthening overlay solution for URM buildings has been proposed and researched by individual researchers, but much still needs to be done to understand the composite failure mechanisms behaviour given the variability in materials. To utilise the ductility of SHCC, failure through the material should occur and not debonding as debonding leads to a brittle failure mode. Shotcreting the SHCC simplifies its application onto URM walls, but brings new challenges for the material fresh properties.

The study reported in this thesis addresses the characterization and performance of clay brick masonry and SHCC individually and as a composite to predict in-plane shear strength. Mathematical models to predict the performance are proposed to aid designers in understanding the material and behaviour.

1.1 Motivation

As engineers, it is our responsibility to ensure that structures are designed and constructed to be safe, now and in the future. With new knowledge of building materials and seismic activity, one also has to evaluate work completed in the past to ensure that the structure are structurally sound. This study aims to help engineers with a solution to retrofit URM buildings vulnerable to seismic activities using a spray-able overlay of SHCC.

1.2 Outline

The motivation and proposal for this study documented in this thesis come from the shortcoming, in research and need for retrofitting. The development of a suitable spray-able SHCC through to the large-scale testing of URM retrofitted shear walls was performed.

In Chapter two a theoretical background of the independent materials, seismic performance and test methods is given based on findings of other researchers.

In Chapter three the material development of shotcrete SHCC is discussed taking deformability, shrinkage and tensile strain capacity into account.

In Chapter four the experimental design of testing the in-plane shear performance of the composite is discussed. Small scale characterising tests are followed by large-scale validation tests.

The results from the experimental testing are elaborated in Chapter five, with interpretations and mathematical predictions for design.

Conclusions are drawn in the final chapter together with recommendations for further work. Finally, this is succeeded by the bibliography and appendices where additional photographs and experimental data can be found as referenced in the document.

Chapter 2

Literature Review

Retrofitting is no new topic of research and various researchers have investigated solutions for retrofitting of masonry structural elements. The behaviour of SHCC retrofitted URM walls subjected to in-plane shear stresses is presented in this chapter together with other retrofitting solutions from various researchers at other institutions. Typically, the in-plane characteristics of an URM wall dictate the structural integrity of the complete building, as these walls transfer the lateral inertia forces, caused by an earthquake, due to their relative high stiffness compared to walls orientated in the out-of-plane movement direction. The in-plane shear strength and ductility of masonry are thus studied in this research. There has been limited research on SHCC retrofitting of URM walls and no research at all using local products and materials.

The literature study addresses four categories that are all relevant to the poor performance of URM during seismic activity and how to retrofit these structures. Firstly, seismic action and masonry behaviour during these events are elaborated. Secondly, clay brick masonry and its mechanical properties are studied. Thirdly, SHCC as a spray-able construction material is discussed, considering its fresh and hardened state, and lastly the composite behaviour, mechanical performance and testing techniques on a small and large scale of the composite behaviour of masonry with an SHCC overlay.

2.1 Seismicity in South-Africa

The South Western part of the Western Cape province in South Africa is a low to medium seismically active region with peak ground accelerations of 0.15 g. This can be seen from the seismic hazard map shown in Figure 2.1 from SANS 10160-4:2011. The first seismic loading and design standard for South Africa was however only introduced in 1989 and since then updated to the current SANS 10160-4:2011. There is a need to retrofit buildings dating from before 1989, in order to bring them to the required level of seismic resistance.

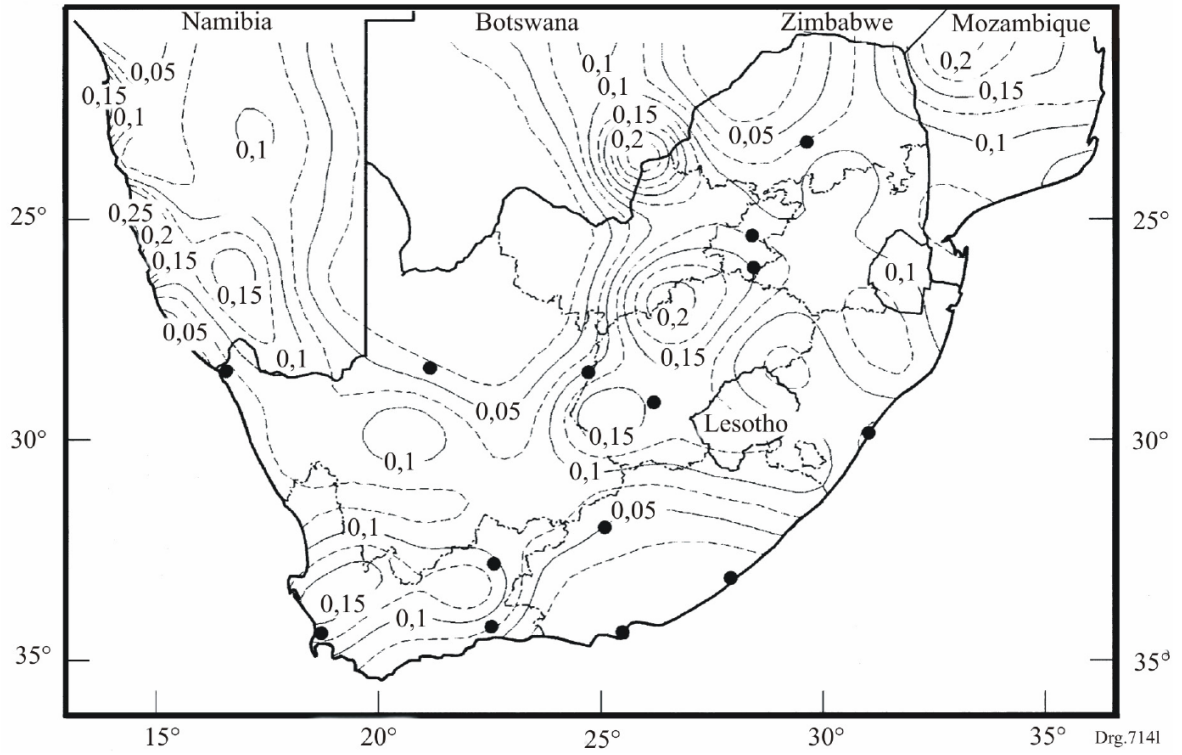

Figure 2.1: Seismic hazard map of South Africa 10 % in 50 years nominal peak ground acceleration, expressed in earth gravity acceleration ($\boldsymbol{g}$) (9.81 m/s^2), extract from SANS 10160-4:2011.

2.1.1 Design considerations using SANS 10160-4:2011

In this section a short summary of the basis of SANS 10160-4:2011 is given. Key design considerations impacting the study documented here are discussed.

"The earthquake motion at a given point on the surface is represented by an elastic ground acceleration response spectrum called elastic response spectrum.

The horizontal seismic action is described by two orthogonal components considered as independent and represented by the same response spectrum.

In order to avoid explicit inelastic analysis in design, the capacity of the structure to dissipate energy through ***ductile*** *behaviour is taken into account by reducing the elastic response spectrum by a behaviour factor,* $\boldsymbol{q}$*. The normalised design response spectra,* $S(T)/a_g$*, corresponding to the ground condition types defined in table 1, are given in figure 2 for 5 % damping and for a behaviour factor of,* $q = 1{,}0$*."* Extract from SANS 10160-4:2011

For further detail on the design procedure the reader is referred to SANS 10160-4:2011, but the basis of a dynamic inertia force being converted to a static horizontal force with the structure having a certain behaviour (ductility and energy dissipation capacity) is what is of importance in this document.

Masonry structures are usually relatively regular and load paths are not hard to find or predict. This helps designers also when retrofitting is necessary as only critical elements might be treated to ensure a safe structure. Structural regularity and simplicity are also strongly advised in SANS 10160-4:2011.

It is important to also keep in mind that horizontal seismic motion is a multi-directional phenomenon and URM buildings should be able to resist horizontal action in any direction. This also helps for retrofitting as most buildings have a problem only in one direction in isolated places where shear forces are concentrated around window openings or shorter walls. This thesis does not cover the whole seismic design process and how forces should be determined and distributed. However, a few important aspects to take note of for URM during seismic design are stated. These structures have a high self-weight that contributes to horizontal inertia forces during seismic action. URM are also relatively stiff structures with low natural vibration periods leading to higher lateral forces.

Lastly, the low ductility in URM cause designers to design these structures to resist almost elastic response forces. This is taken into account, as previously stated, through the behaviour factor q. The effect ductility has on the lateral force can clearly be seen in Table 2.1. This extract from Table 4 of SANS 10160-4:2011 shows the design q factors to be used for bearing wall systems. The equivalent static force on a RC wall, correctly detailed, is reduced by a factor of 5, compared with 1.5 for URM.

More ductile failure can thus ensure a lower strength demand of the structure. Using SHCC to ensure ductility (elaborated in Section 2.3) and a higher q factor could ensure safer URM structures.

Table 2.1: Behaviour factor, q, for structural systems. (Extract from SANS 10160-4:2011 Tabel 4).

Structural system	**Detail**	**Behaviour factor (q)**
Bearing wall system	Unreinforced masonry walls (see annex A)	1.5
	Reinforced concrete walls (detailed in accordance with SANS 10100 and annex B)	5.0
	Reinforced concrete walls not detailed in accordance with annex A)	2.5
	Reinforced masonry walls (with reinforcement provided in both the horizontal and vertical directions, all designed according to the requirements for reinforced masonry)	2.5

2.2 Masonry

The failure of masonry is complex and difficult to model. The interaction between the two constituent materials has to be quantified together with their individual material properties. Designers are however aided by design guides such as the SANS 10164:1 Structural use of unreinforced masonry, to design masonry elements to resist the required forces. Elements in axial compression, elements in bending, as well as in-plane shear are handled in this code. This thesis focusses on the in-plane shear strength that is described by the Coulomb-friction type model as follows in SANS 10164-1:1989:

$$f_v = 0.15 + 0.6 \cdot g_A \tag{2.1}$$

Where

f_v	is the characteristic shear strength of masonry, (MPa)
g_A	is the design vertical load per unit area, (MPa)
0.15 *and* 0.6	is the initial shear strength and friction angle constants of the joint respectively

The triplet shear test (BS EN 1052-3, 2002), where the centre brick of three mortar bonded bricks is pushed through, is normally used to determine the shear parameters in Equation 2.1. This will be further elaborated later in this document in 4.3.2.

2.2.1 Masonry structures

The Western Cape has a large number of multi-storey URM buildings, from office buildings through to apartment blocks. Government funded housing as shown in Figure 2.2 is also constructed from URM. Typically, solid and hollow clay bricks, concrete blocks and calcium silica units have been used in the Western Cape. This thesis concentrates on solid clay brick masonry to limit the scope of investigation, but future work of the research group will consider concrete blocks.

Studies conducted by Schaaf (2009), Hancilar et al. (2008) and Van der Mersch (2015) have showed that URM structures are at risk of collapse during an earthquake and a need for evaluation of historic and older masonry buildings' earthquake resistance exists. A large number of fatalities worldwide due to earthquakes and buildings collapsing on people is concerning. In 2011, 185 people lost their lives in the Christchurch earthquake while over 8800 people lost their lives, and more that 21000 people were injured in the 2015 Nepal earthquakes.

Although this study focussed on the in-plane shear strength, it should be noted that out-of-plane and localized failures during an earthquake can lead to toppling wall parts and flying

bricks injuring or killing people. An SHCC overlay can possibly tie the bricks together, and prevent these flying bricks.

Figure 2.2: Typical URM building in the Cape Flats.

Figure 2.3 shows the characteristic diagonal shear cracks that occur in masonry during an earthquake. Similarities in building layouts can also be seen between the buildings where walls are build at right angles and windows openings exist at regular intervals. Windows create discontinuity and weakness by reducing the shear area. It is in these areas where failure occurs. In-plane shear cracks that occur during seismic activities are brittle failures and lead to collapse. A ductile failure with higher energy dissipation is desirable.

(a) Typical diagonal cracks in bottom storey. (b) Multi-storey building after earthquake.

Figure 2.3: Diagonal shear cracking of URM walls after earthquakes.

2.2.2 Failure modes of URM walls

Seismic action causes displacements in three dimensional space. These displacements induce inertia forces which was explained in (2.1.1). These forces cause both out-of-plane and in-plane forces. As the in-plane stiffness of walls is significantly higher than the out-of-plane stiffness, the lateral forces are resisted by the in-plane walls, in shear. Any collapse or failure, in-plane and out-of-plane must be prevented at all cost. This is why structural elements must be tied together. If well-tied, the increased in-plane resistance will also keep out-of-plane walls upright

or from collapsing altogether.

The principal in-plane failure mechanisms of URM walls subjected to earthquake actions can be summarised as shown in Figure 2.4 (Tomazevic, 1999). Combinations of theses failure modes can also occur during seismic action.

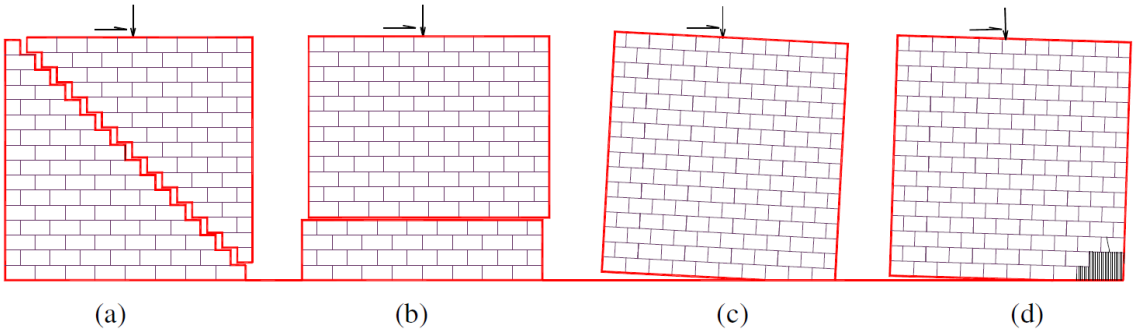

Figure 2.4: In-plane failure modes of a laterally loaded URM wall: a) Shear failure, b) Sliding failure, c) Rocking failure, and d) Toe crushing.

2.3 Strain Hardening Cement-based Composite (SHCC)

2.3.1 Material properties

All of the properties discussed in this section are for SHCC that has been cast into moulds, as this is the standard way of manufacturing samples and structural elements. Spray-able SHCC and its small differences will be discussed in the next Section (2.4) of this chapter.

SHCC is a type of High-Performance Fibre Reinforced Cement Composite (HPFRCC) that has been engineered to have high tensile ductility and can resist tensile load at a strain of more than 3% and up to 6% compared to normal concretes 0.01%. The behaviour of SHCC after the initiation of the first crack is its fundamental mechanical property. An increase in post-cracking strength can be observed, together with multiple cracks leading to high ductility and energy absorption. This makes it ideal for earthquake loading application, providing highly ductile under tensile resistance after normal concrete or mortar would have failed.

2.3.1.1 Tensile behaviour of SHCC

The fundamental difference between SHCC and ordinary fibre reinforced concrete (FRC) is the strain-hardening response that accompanies the ductile behaviour of SHCC. FRC displays a decline in strength with an increase in strain beyond the first crack, which is referred to as strain-softening. Strain-hardening behaviour, on the other hand, is a behaviour that displays an increase in post-cracking strength, accompanied by the formation of multiple cracks, not always visible to the naked eye. A typical tensile response of SHCC is shown schematically in Figure 2.5 and compared to a typical response of ordinary concrete and FRC.

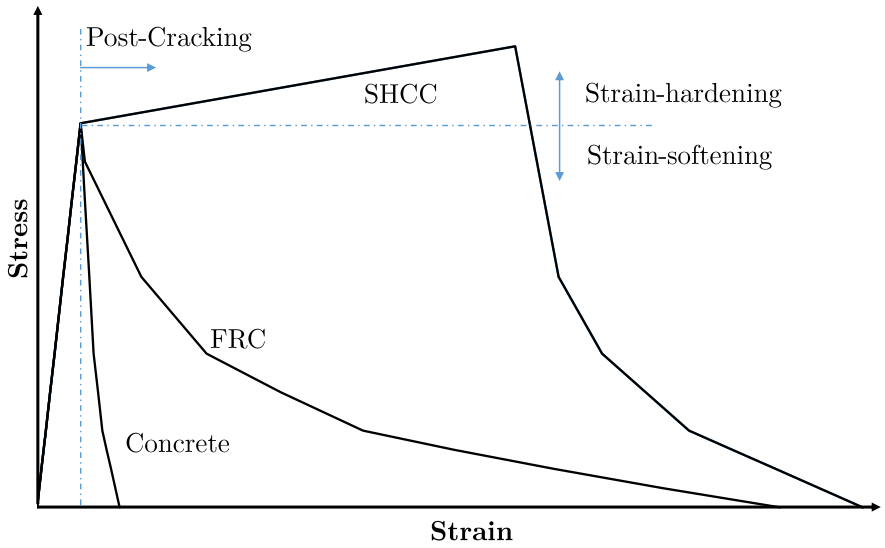

Note: The strain up to first crack is magnified 10 times as well as the strain of the normal concrete post-cracking. This was done to make the graph easier to interpret

Figure 2.5: The tensile stress-strain response of SHCC compared to FRC and ordinary concrete schematically.

Strain hardening is achieved by multiple cracking of the matrix. The material matrix cracks at its weakest point under direct tensile load. Without any fibres, the material would fail completely. If fibres are used to reinforce the matrix, the fibres will carry the load by bridging the crack.

In the case of FRC, the fibre crack bridging capacity is less than the cracking strength of the concrete, thus, the crack widens and the load is reduced if the strain is increased. In the case of SHCC, the fibre crack bridging capacity is more than matrix capacity and thus, the load is sustained after cracking of the matrix. If the strain is then increased, the load will increase and the matrix will crack at the next weakest point which is stronger that the first cracking point, thus an increase of the stress is found. This ongoing cracking and bridging process will continue until the load becomes greater than the crack bridging capacity of the fibres at any of the multiple cracks. At this point a localising crack will form at one of the multiple cracks and strain softening will start. Multiple cracking can be seen in Figure 2.6, where SHCC was tested under direct tension.

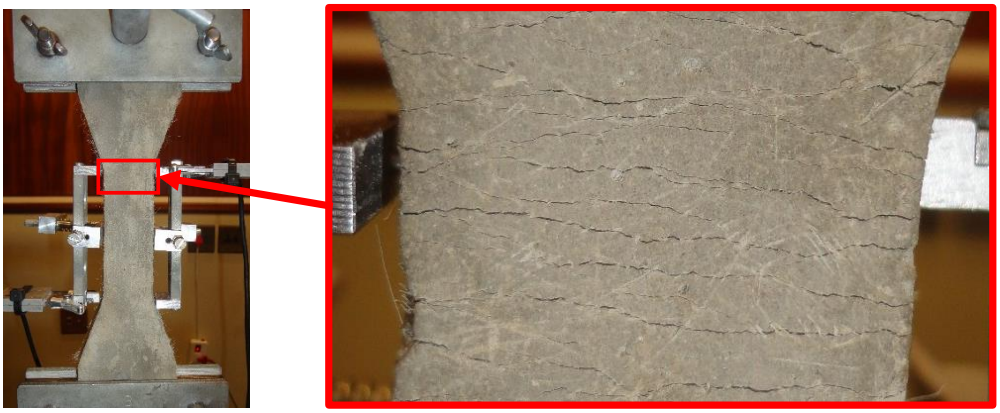

Figure 2.6: Uni-Axial Tensile test of SHCC depicting the multi-cracking ductile failure.

Boshoff (2007) pointed out that the unloading and reloading behaviour of SHCC is of importance, especially with regard to earthquake loads. A typical result of tensile unloading and reloading tests that were done at the University of Stellenbosch (SUN) is shown in Figure 2.7. It is observed that the stiffness decreases with higher tensile strain during loading and unloading, but the ultimate strain and strength can still be reached. This property is advantageous in earthquakes and especially URM as for a lower stiffness the fundamental period of the structure would increase, leading to lower base shear forces, while dissipating energy with each cycle of movement without losing its ultimate strain or stress capacity. For more details on the reverse cyclic response of SHCC, the reader is referred to Kesner et al. (2003).

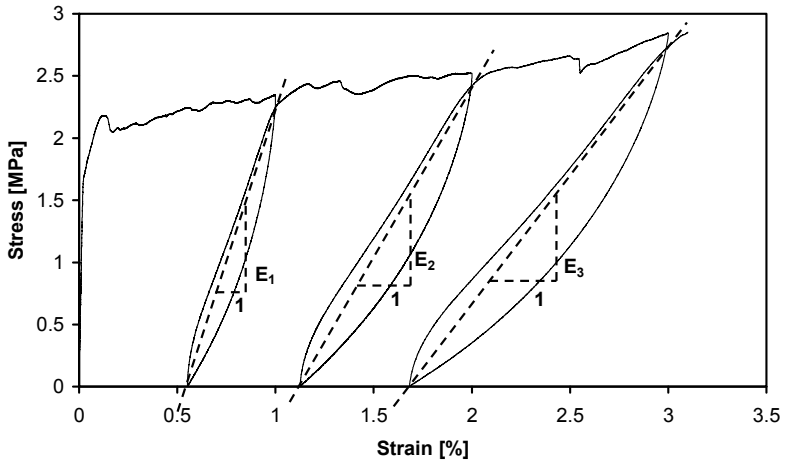

Figure 2.7: The unloading and reloading tensile behaviour of SHCC adopted from Boshoff (2007)

2.3.1.2 Compression behaviour of SHCC

The compressive response of SHCC up to ultimate compressive stress is approximated to be linear elastic after which strain softening post peak response occurs, as in normal concrete. While high strength (50 MPa +) SHCC has been developed by Wang and Li (2006) and Sahmaran et al. (2015), normal SHCC compressive strengths are in the range of 20-40 MPa cube strength. SHCC also has a similar failure mode as normal concrete in compression with a strain softening behaviour after peak load. As for normal concrete, SHCC's compressive strength is approximately 10 times the tensile strength (Visser, 2007).

2.3.1.3 Elastic Modulus of SHCC

SHCC has a relatively low Modulus of Elasticity (E-Modulus), and that can mainly be ascribed to the fact that there is lower aggregate content and no coarse aggregate in the matrix. The E-Modulus is usually determined by applying the secant method to direct tensile test results. Shang (2006), determined the E-Modulus of SHCC at 14 day strength to be between 7.5 and 10.0 GPa during his studies at SUN. These low E-Modulus are due to entrained air, similar tests done on

normal SHCC at 28 days showed that the E-Moduli increases and may roughly be double at this higher age (Van Zijl, 2005).

The secant method takes the stress at one-third of the first cracking stress and a low pre-stress ($\sigma_0 = 0.1\,\mathrm{N/mm^2}$) and the corresponding strains, to compute the E modulus as follow:

$$E_{SHCC} = \frac{\frac{1}{3}\sigma_{tf} - \sigma_0}{\varepsilon_{\left(\frac{1}{3}\sigma_{tf}\right)} - \varepsilon_0} \times 10^{-3} \tag{2.2}$$

Where

E_{SHCC}	= elastic modulus of SHCC, (GPa)
σ_{tf}	= first crack stress, (MPa)
σ_0	= pre-stress, usually equal to 0.1, (MPa)
$\varepsilon_{\left(\frac{1}{3}\sigma_{tf}\right)}$	= strain corresponding to stress $\frac{1}{3}\sigma_{tf}$
ε_0	= strain corresponding to stress σ_0

2.3.1.4 Shear behaviour of SHCC

Research by Shang (2006) on the shear performance of SHCC led to the development of a shear test based on the Iosipescu shear test (Iosipescu, 1967). The SHCC tested showed an ultimate shear strength to first cracking strength ratio of 2.25, and a ratio of 1.5 for the ultimate shear strength to the ultimate tensile strength. SHCC forms multiple cracks in shear at an angle greater than 45°, dominated by the principal stress direction. This is possible due to the ductility in tension, with resistance maintained or increased beyond initial cracking to enable the reserve compressive resistance to be mobilised. Numerical models were also developed and presented by Van Zijl (2007) for the same tests.

2.3.2 Matrix constituents' properties

The same ingredients used in FRC such as binder, water, sand, fibres and chemical additives are used in SHCC. It is, however, the optimal combination of these constituents through micro-mechanical considerations that leads to SHCC ductile behaviour under tensile strain. There is no coarse aggregate in SHCC, as coarse aggregates cause higher fracture toughness of the matrix, which adversely affects the ductile behaviour. Coarse aggregate also has a negative effect on fibre distribution and crack bridging capacity of the small fibres. Generally, 2% by volume of fibres are adequate, leading to similar mixing procedures to that of conventional concrete. (Boshoff, 2007).

Consolidated SHCC contains three components namely cement-based matrix, fibres and fibre-matrix interface. To attain the unique ductile behaviour, each component needs to be proportioned correctly according to its mechanical and geometric properties. Admixtures are incorporated into the mix to enhance the fresh state ensuring a uniform spread of constituents that is vital for the optimal functioning of micro-mechanical mechanisms. This all benefits the consolidated state.

2.3.2.1 Fibres

Several different types of fibres such as Poly-Ethylene and Polyvinyl Alcohol (PVA) fibres have been used in SHCC. All research done on SHCC at SUN was with PVA fibres. Forming the basis of this study, PVA fibres was also used in this research. These fibres have a high tensile strength (f_t) and E-modulus (E). Fibre breakage at the crack regions will lead to brittle behaviour of the composite. PVA fibres avoid or restrict this occurrence by slipping from the matrix as opposed to rupturing. A fibre length of 12 millimetres (mm) is most commonly used, for its good fibre dispersion and workability in the fresh state. A fibre length of 8 mm was used in this study for pumpability and spray-ability as explained in Section 3.1, but it should be noted that the shorter fibres do not adversely influence the ductility of the material or other properties discussed above. The PVA-fibres properties are shown in Table 2.2.

Table 2.2: Properties of PVA-fibres (Stander, 2007).

Type	Diameter$_{[mm]}$	Length$_{[mm]}$	$f_{t,f[GPa]}$	E $_{[GPa]}$	$\varepsilon_{u,f[\%]}$
PVA-REC15	0.04	8	1.6	37	6

2.3.2.2 Binder

The binder consisted of Ordinary Portland Cement (OPC CEM I 52.5 N) and Fly Ash (FA) in this research, but Ground Granulated Corex Slag (GGCS) has also been used by other researchers (Song, 2005). OPC CEM I 42.5N was previously used at this institution but is no longer available in South Africa. The added strength, however has a very small effect if any.

2.3.2.3 Admixtures

Admixtures are chemicals that are added to the concrete immediately before or during mixing and significantly modify its fresh, early age or hardened state to ensure economic or physical advantages. Normally only small quantities are required, typically $0.1 - 2\%$ by weight of the binder (Stander, 2007). The two admixtures that were used in this research and in previous research at this faculty are Superplasticiser and Methyl Cellulose (Viscous Agent).

Superplasticiser (SP)
Known as workability aids, it increases the fluidity or workability of cement paste or concrete. Superplasticiser is also referred to as high-range-water-reducing-agents. The low water binder (w/b) ratio together with the addition of methyl cellulose and fibres leads to a stiff mixture with low viscosity. The addition of SP aids this workability problem. The mode of action induced by SP, is purely physical, a combination of joint repulsion and steric hindrance between cement particles, creating less friction when the particles move. The behaviour of any particular combination of SP and cement will depend on several factors other than the admixture type, including the cement composition, the cement fineness and the w/b ratio.

Methyl Cellulose
Also known as Viscous Agent (VA), causes an increase of intermolecular shear force of the fresh concrete. Thus it acts as a dispersion agent and assists in the uniform dispersion of the fibres in the mix. VA is used to prevent segregation and wash out of fresh concrete. This is of particular importance when extruding, pumping or spraying SHCC to ensure that segregation in the form of water being squeezed out under pressure, does not occur. The VA product used in this research was Chryso Aquabeton ZA, which comes in the form of a powder. The addition of Chryso Aquabeton ZA reduces the workability, but this should be taken into account during mix design and trials. An optimal SP dosage for the particular w/b ratio should be found to compensate this workability loss.

2.3.2.4 Fine Aggregate

It is important to have a good sand grading to ensure good compaction of the cement-based matrix. Finer gradings ensure a lower matrix fracture toughness, which conforms to micro-mechanical models of strain-hardening. This suggests that a matrix with lower toughness (in comparison to concrete) should require a smaller number of fibres to make the transition from strain softening to strain hardening mode of failure. Fine silica sand supplied by Console with a maximum particle size of 0.2 mm was used in this research, as this sand was previously used at SUN for SHCC by Paul (2015). This saves time to sieve and blend the correct fractions of crusher dust and Philippi (dune) sand as performed by Stander (2007) and Boshoff (2007).

2.4 Shotcrete process

Shotcrete is the process where concrete is pumped and conveyed through a hose to a nozzle where it is pneumatically projected at high velocity onto a surface. Shotcrete can be reinforced by conventional steel reinforcing bars, mesh or fibres. The fibres can be steel or synthetic. Shotcrete can refer to dry- or wet-mix shotcrete, however, dry-mix shotcrete is most commonly referred to as gunite and wet-mix as shotcrete. Dry-mix shotcrete or gunite is where dry material is conveyed through the hose and water and air is added at the nozzle. The operator determines the amount of water. This is most commonly used in slope stabilisation and mining application. Wet-mix shotcrete is where ready mixed concrete or mortar is pumped through a hose and

compressed air at the nozzle pneumatically spray the concrete. The impact on the surface compacts the concrete.

2.4.1 Wet-mixture SHCC Shotcrete

Kim et al. (2003) were the first researchers that developed SHCC for wet-mixture shotcreting, while maintaining tensile strain-hardening behaviour in the hardened state by employing a parallel control of micro-mechanics and rheology-based design. The rheological properties are of most importance for a successful spray-able SHCC. The fresh material should have the consistency and fluidity for it to be effectively conveyed through a hose and nozzle without segregating. Once the SHCC is sprayed onto the surface, it should be viscous enough to stay adhered to the surface and be cohesive enough not to segregate (Kim et al., 2003; Bruedern et al., 2009). To achieve such different fluid properties of the fresh mixture while keeping the ductile performance of SHCC, the method to control the processing parameters and micro-mechanical parameters in a parallel manner was adopted by Kim et al. (2003).

Calcium Aluminate Cement (CAC) was introduced to the SHCC mix by Kim et al. to enhance the viscosity and adhesiveness development over time through flocculation onset by CAC. Rheological tests on fresh cement paste and deformability tests on the mortar matrix as well as SHCC were conducted.

Figures 2.8a and 2.8b graphically show the effect of SP and CAC, respectively. It is found that SP controls the initial deformability, while CAC controls the rate of deformability loss. CAC increases the initial deformability, but after a short period of time, flocculation of particles causes a decrease in deformability. A similar approach was adopted in the study documented in this thesis, and more information on the calculation of deformability can be found in Section 3.1.2.1.

Using this information, the correct deformability for shotcreting can be determined for a certain rest time. The rest time is defined as the time after mixing has stopped and shotcreteing starts. The shotcrete pump, spray nozzle and air supply determine the deformability needed/required and will be elaborated in Chapter 3.

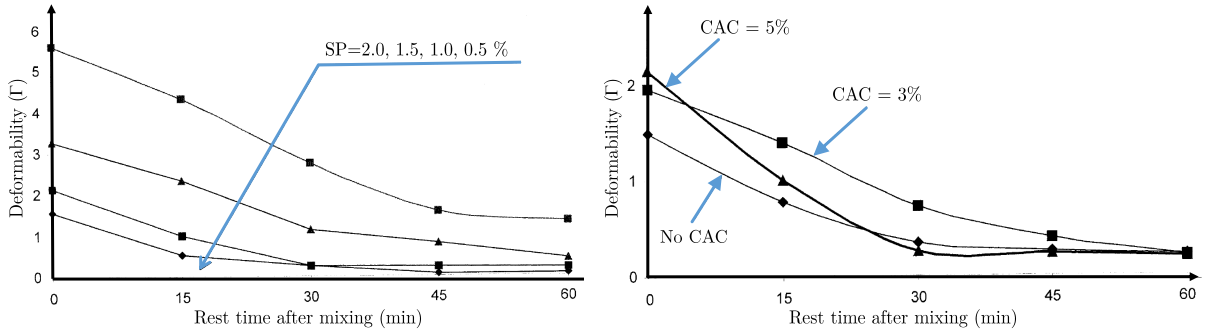

(a) (b)

Figure 2.8: Changes in deformability (Γ) of mortar matrix mixture, as function of rest time for: (a) effect of SP concentration (VA = 0.05%, CAC = 5.0%); and (b) effects of CAC dosage (SP = 1.0%, VA = 0.05%) as presented in (Kim et al., 2003).

2.5 Shrinkage mechanism and effects

Cement based materials' dimensional instability are caused by shrinkage and creep. This instability leads to complex stresses arising when restrained in composite systems, where two unique materials have different deformation needs at different times. If this characteristic of cement-based materials is not properly considered and addressed it can be detrimental and lead to cracking and debonding, both of which processes could cause premature failure. Shrinkage from all of its sources will be shortly discussed next, followed by the effect of restraining this shrinkage by bonding a material to another. Performance predictions from the literature will then be evaluated, together with shrinkage of SHCC as a bonded overlay.

2.5.1 Shrinkage mechanism

Shrinkage is the decrease in volume of both fresh and hardened concrete over time. Shrinkage is the result of moisture movement out of, or within concrete because of the surrounding environment and hydration process. (Alexander and Beushausen, 2009). Autogenous shrinkage due to the hydration process involving the water and cement, and drying shrinkage due to moisture diffusion are usually the main contributors to the total shrinkage. It is not necessarily known in advance what mechanism may dominate (amongst plastic, chemical and drying shrinkage) and it is important for the materials specialist to know and consider the various mechanisms when considering retrofitting intervention design.

Shrinkage is affected by both intrinsic and extrinsic factors. Intrinsic factors include cement paste content, water binder ratio, aggregate type, size and quantity, whereas extrinsic factors include member geometry, relative humidity and temperature. For more in-depth discussion of these factors please refer to Chilwesa (2012).

The four main types of shrinkage are plastic shrinkage, autogenous shrinkage, drying shrinkage and carbonation shrinkage and are briefly discussed hereafter.

2.5.1.1 Plastic shrinkage

Plastic shrinkage occurs when there is a rapid surface water reduction/removal from the concrete during early ages (the few hours between placing and final setting of concrete). Plastic shrinkage takes place when the evaporation rate exceeds the bleeding rate of the concrete. Combrinck (2016) showed that if excessive surface moisture loss occurs, a drop in capillary pressure may produce tensile strains. If the fresh concrete is restrained, these stresses exceed those needed to cause cracking in fresh concrete with low strength. Concrete elements with a high surface area to volume ratio, such as bonded overlays, are susceptible to early age cracks especially when subjected to dry, hot and windy weather conditions. These conditions should thus be avoided. Proper curing is vital in controlling plastic shrinkage cracking (ACI Committee 224, 2007).

2.5.1.2 Autogenous shrinkage

Autogenous shrinkage is the volume reduction of concrete due to internal water consumption by the hydration reaction. This starts taking place at an early age (immediately after setting) due to the hydration reaction consuming the internal water, whereafter the rate drops rapidly (Alexander and Beushausen, 2009). The reactant volumes are more than the hydration products, leading to a volume reduction during the hydration process. Autogenous shrinkage is relatively low in normal concretes with w/b ratios above 0.4. However in High-Performance Concrete (HPC) and Ultra-High-Performance Concrete (UHPC), autogenous shrinkage can be considerable and in the same order as drying shrinkage due the large amount of cement and hydration product.

2.5.1.3 Carbonation shrinkage

Carbonation shrinkage is the reduction in volume resulting from the reaction of hardened cement paste and the carbon dioxide (CO_2) from the ambient environment (Alexander and Beushausen, 2009). The initial step of the reaction is the dissolving of (CO_2) in the pore water, consequently, if there is very little or no pore water, carbonation shrinkage cannot occur. (Boshoff, 2007)

2.5.2 Relaxation and creep behaviour

Relaxation and creep are both results of the visco-elasticity of Cement-Based Materials (CBM). Tensile relaxation is defined as the decrease of force or stress over time under a sustained strain, while creep is the increase of strain of a material under constant force or stress (Boshoff, 2007; Chilwesa, 2012).

Relaxation and creep behaviour of CBM is difficult to accurately predict without testing a range of parameters. The main parameters affecting the relaxation/creep capacity is the w/b ratio, aggregate type and volume, stress level, time of loading, curing age and post-cracking behaviour in fibre reinforced CBM.

For in-depth explanations on the mechanisms of relaxation and creep the reader is referred to Neville (1970) and Boshoff (2007). In this thesis, only a short description is given to ease reading of the next section 2.5.3 of this chapter.

2.5.3 Bonded overlays behaviour under restrained shrinkage

Restraint to shrinkage is a broad term used to describe the prevention of concrete elements to freely expand or shrink. This restraint can be in the form of already in place concrete or steel elements that the new element connects to, or in a composite configuration such as bonded CBM overlays and repair patches. During the lifetime of the bonded overlay, it would want to shrink, and when restrained, tensile stresses would arise.

Tensile stresses due to restrained shrinkage depend on a number of time-dependent properties of the overlay, substrate and bond. The CBM overlay's shrinkage, relaxation, elastic modulus, tensile strength as well as the degree of restraint, surface area and environment all play a role. If these tensile stresses exceed the strength of the overlay at any given time, the overlay will crack.

According to Carlsward (2006), restrained shrinkage is the main cause of cracking in bonded overlays. Figure 2.9 shows examples of shrinkage cracking and debonding.

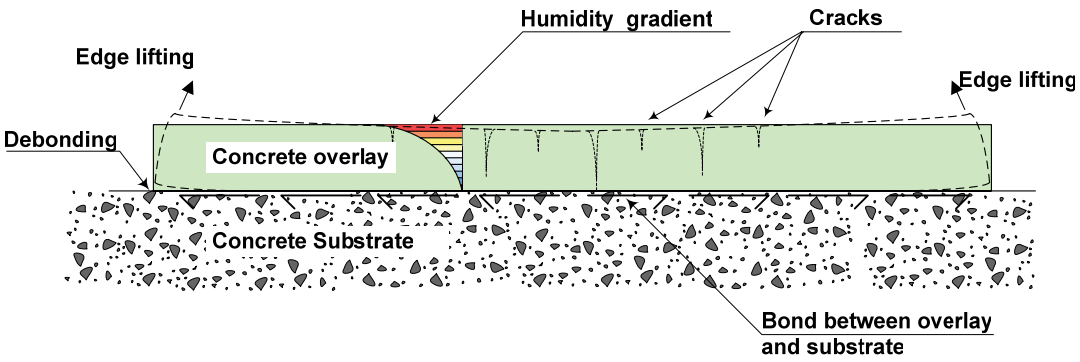

Figure 2.9: Cracking, debonding and edge lifting in concrete overlays as presented in Carlsward (2006).

Various studies regarding the prediction of stress development from restrained deformations in overlays have been conducted. Characteristics of the tensile relaxation are often obtained from creep results as in the work by Loser R (2009). In experiments discussed by Beushausen and Alexander (2006) the ultimate relaxation of a specimen subjected to sustained, constant strain was achieved only after 72 hours. The relaxation value $w(t)$ is defined as the percentage stress released during a certain period and calculated according to Equation 2.3.

$$w(t) = 100(1 - \frac{r_t}{r_o}) \tag{2.3}$$

Where

$w(t)$	is the relaxation value, (%)
r_t	is the stress after time t, ($t = 72h$ for ultimate relaxation)
r_0	is the stress at the start of the test $t = 0$

2.5.4 Restrained shrinkage of bonded overlays performance prediction models

Chilwesa (2012) followed the work done by Beushausen and Alexander (2006) and conducted a range of tests to develop a prediction model that is discussed in this section. The stress distribution through the overlay for different overlay thicknesses can be found in Beushausen and Alexander (2007).

The prediction of stresses and cracking onset in restrained bonded overlays due to shrinkage, requires information on the different material properties and how they interact with each other. It is not possible to calculate tensile stresses from the product of the instantaneous elastic modulus and free shrinkage strain, because of the effect that relaxation has over time and stress level. Factors such as rate of overlay shrinkage, increase in elastic modulus and tensile strength together with relaxation capacity over time complicate stress predictions.

Beushausen (2005) found it easier to look at the result of direct stresses alone before considering other influences. For a fully bonded overlay the instantaneous elastic strain of the overlay Equation (2.4) at the interface is as follows:

$$\varepsilon_{restr.0,I} = (\varepsilon_{FSS} - \frac{\varepsilon_{FSS}}{1 + \frac{E_s}{E_o} \times (C_\varepsilon)}) \tag{2.4}$$

Where

$\varepsilon_{restr.0,I}$	is the restrained overlay strain at the interface
ε_{FSS}	is the overlay free shrinkage strain
E_S	is the modulus of elasticity of the substrate
E_O	is the modulus of elasticity of the overlay
C_ε	is the constant accounting for combined influences of relative member dimensions and strain profile characteristics

From this strain ($\varepsilon_{restr.0,I}$), the stress at the interface can be determined. However in bonded concrete overlays direct elastic stresses do not remain constant as the overlay is subjected to relaxation and the substrate creep. Therefore, the contributions were included by Beushausen (2005) in Equation 2.5 and by substituting Equation 2.4 into Equation 2.5, Equation 2.6 was developed to calculate the time-dependent stress in the overlay. It is worth noting that all variables in Equation 2.6 are time-dependent.

$$\sigma_{O,I}(t) = (\Psi_O(t,t_0)(\varepsilon_{FSS}(t) - \varepsilon_I(t))) \cdot E_O(t) \tag{2.5}$$

Substituting Equation: 2.4 into 2.5 yields:

$$\sigma_{O,I}(t) = \Psi_O(t,t_0) \cdot \left(\varepsilon_{FSS}(t) - \frac{\varepsilon_{FSS}(t)}{1 + \frac{E_s}{E_o(t)} \times (C_\varepsilon)}\right) \cdot E_O(t) \tag{2.6}$$

Where

$\sigma_{O,I}(t)$	= direct stress in the overlay at the age t
t	= age at time of testing
t_0	= age at time of loading
$\Psi_O(t,t_0)$	= relaxation function within the period $(t - t_0)$
	The rest of the parameters have been described earlier

2.5.5 Bonded overlay cracking prediction

Cracking age can be determined by determining the intercept of the tensile strength and instantaneous tensile stress (actual tensile stress after stress relaxation) over time, on a graph. The point on the graph at which the elastic stress exceeds the tensile strength depicts the age at which cracking would occur if the effect of stress relaxation were ignored. This is demonstrated in Figure 2.10.

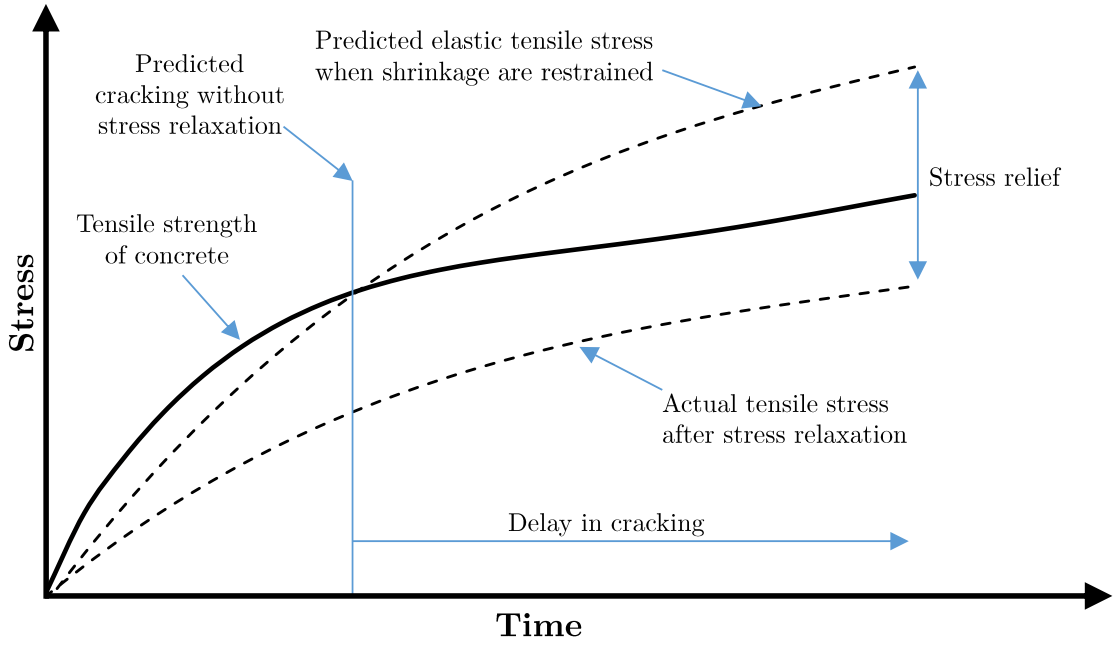

Figure 2.10: Influence of shrinkage and creep on concrete cracking adopted from Chilwesa (2012).

From Section 2.5.4 and Figure 2.10, it is clear that the prediction of restrained shrinkage performance is no easy task as one needs a lot of material properties over time. All three lines in Figure 2.10 can move up, down, left or right with endless combinations. All previous studies were conducted on repair mortars and normal cement based mortars, with no in-depth research done on SHCC. Although much research has gone into SHCC on the strength, elastic modulus and tensile strain capacity over time, and even research on SHCC creep performance (Boshoff, 2007), no research on the relaxation capacity of SHCC at different ages has been conducted. The substrate material also plays an important role in providing restraint, and would differ for concrete and masonry.

Li (2006) has conducted quantitative tests on the cracking of SHCC overlays and found SHCC to show multiple cracks visible to the eye. Crack widths are typically in the range 10 to 100 micrometer (Van Zijl and Wittmann, 2011). This was however not the case in this research as discussed in Section 3.3.3.

Shrinkage of SHCC tend to be more than that of normal concrete, because of the relatively low overall volume portion aggregate (sand) in SHCC (typically 20%) compared to concrete's (sand + stone) (typically 70%). The low (0.35) w/b ratio of SHCC means that autogenous shrinkage can also play a role, were this was ignored in previous research on concrete and mortar. The post cracking and ductile behaviour of SHCC implies that even after initial cracking the overlay may still be fully functional, this is further elaborated in Section 3.3.3. Self-healing properties of SHCC can also further repair initial cracks caused by shrinkage.

2.6 Retrofitting techniques

Retrofitting is no new topic of research and has a wide range of applications and purposes, for example corrosion protection, structural integrity and aesthetic appearance. This research project focused on structural retrofitting of URM buildings vulnerable to in-plane shear failure. Other retrofitting techniques to address this problem will be summarised here with some pros and cons.

2.6.1 Fibre Reinforced Polymer (FRP) strips

FRP strips as a retrofitting method for URM walls have been experimentally studied eg. (Zhou et al., 2013; ElGawady et al., 2004; Van Zijl et al., 2004; Van Zijl, 2004). The method entails using FRP strips made of a range of fibres (carbon, glass, basalt) to externally reinforce a wall in different patterns as shown in Figure 2.11a. The strips are externally bonded using epoxy type glue. Problems with the practical application arise when having to wrap a wall with continuous edges, and making walls aesthetically pleasing after applying the strips. Most of the tests also showed debonding to be a big problem.

2.6.2 Near Surface Mounted (NSM) reinforcement with steel bars

NSM overlays reinforced by steel bars have been researched by eg. ElGawady et al. (2006). The strengthening system consists of steel reinforcement mesh (sometimes mechanically anchored to masonry) covered by conventional shotcrete as shown in Figure 2.11b below. Conventional shotcrete causes significant waste that has to be removed leading to additional cost.

(a) FRP Strips.

(b) NSM with steel mesh reinforcement.

Figure 2.11: Retrofitting techniques for URM, adopted from Zhou et al. (2013) and ElGawady et al. (2006).

2.6.3 Bonded Overlays using Engineered Cement-based Composites (ECC) and SHCC

Bonded overlays using ECC and SHCC have been tested by several other researchers eg. Lin et al. (2014), Esmaeeli et al. (2013) and Dehghani et al. (2015) and have demonstrated enhanced ductility and shear strength when compared to unstrengthened masonry elements. The easy application, excellent performance and aesthetically neutral look make it ideal. The system is elaborated comprehensively in Chapter 3 and not explained further here.

Lin et al. (2014) did a comprehensive study on clay and concrete brick masonry, investigating the in- and out-of-plane strengthening using ECC. He found that the ductility of the strengthened elements to be 220% that of the as-build and a strength increase between 130% and 514% for different masonry and overlay thicknesses. The ECC material used however only had a strain capacity of 0.15% compared to the 2% plus strain capacity of the SHCC used in this thesis. Characterising tests together with large-scale tests have also not been conducted, with Dehghani et al. (2015) and Bruedern et al. (2009) only looking at characterising shear behaviour with triplet tests.

2.7 Test methods for testing in-plane shear strength of masonry

Various test methods were researched to obtain the best methods that can be performed at SUN with the available testing equipment. Test methods for material characterization as well as structural system testing used by other researchers are summarised in this section. It must be kept in mind that only material properties relevant to in-plane shear failure mechanism of URM and URM with a SHCC overlay were investigated in this research.

2.7.1 Material characterising tests

Characterising tests for masonry, SHCC and SHCC bonded on masonry were investigated. All of the tests conducted during the characterising of the different materials are standard test procedures from either the American Society for Testing and Materials (ASTM), British Standard (BS EN) or South African National Standard (SANS) except for the uni-axial tension test of SHCC which was performed according to the guidelines described by Van Zijl et al. (2016). A modified triplet test was also performed to characterise the shear behaviour of the composite, but further detail can be found in Chapter 4.

2.7.2 Large scale in-plane shear test methods

A large number of variations of shear test methods exist, with the diagonal compression test (ASTM E519, 2002) being the only standardised test in international codes as of yet. Results produced by different test methods vary accordingly. Non standard test methods are implemented in comparable studies. Different parameters such as specimen size, aspect ratio, vertical compression level, loading rate, boundary conditions, etc. all augment this variation. Careful consideration needs to be undertaken to find the best-suited test method simulating reality and inducing the correct failure mechanism.

A test method that has the following outcomes was looked for:

- Induce diagonal shear cracks as depicted in Figure 2.12. This is important as this failure mechanism is what was observed in URM buildings during past earthquakes. Inducing other failure mechanisms does not help to test the material for the specific need of strengthening the in-plane shear resistance. It should be noted that other failures like tension failure might occur prior to diagonal shear failure, but the ultimate failure should come from diagonal tension failure.
- Tested under normal working imposed self-weight (of upper storeys) that will be experienced in walls of a URM building walls. As the shear strength of a masonry bed joint is a function of vertical compression, as shown in Equation 2.1.
- Sample size must be comparable to wall elements between windows in a URM building.
- Similar boundary conditions during testing to that experienced by a wall in a URM building.

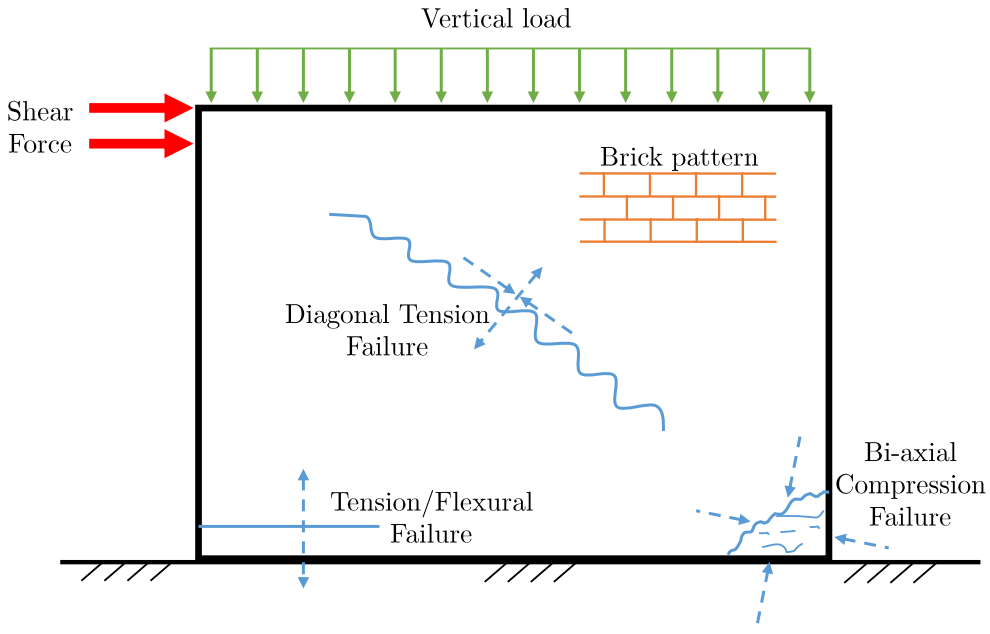

Figure 2.12: Modes of failure for a wall panel loaded in shear as described by Page (1989).

Keeping in mind the outcomes listed on the previous page, different test methods are described.

1. The diagonal compression test method is the easiest and most straight forward test method that is possibly the reason why it is the only standardised test (ASTM E519, 2002). As shown in Figure 2.13a, indirect tensile forces along the diagonal are induced by compression along the perpendicular diagonal. Shortcomings of this test are that no vertical pressure simulating self-weight can be applied. The top and bottom edges are also free where a URM wall would be continuous and have confinement at both edges. Multi-directional cyclic testing is also not possible with this test method.

2. Diagonal shear with fixed vertical load test method (Figure 2.13b) is considered by the author to be close to reality, except that the vertical load does not stay constant. Van Zijl (2004) showed that this can considerably enhance shear performance as the vertical load increases during the shearing action due to dilatancy behaviour of masonry bed joints. For all the test methods to follow, including this test method, the load is applied over the top face through a load spreader beam made of concrete. The bottom of the wall is also confined and supported by a concrete beam fixed to a strong floor. This test method allows for cyclic testing, which Basoenondo (2008) showed to have a significant influence on the shear performance of masonry. Basoenondo found that a decrease of up to 50% can be found when testing masonry walls under cyclic loads instead of mono-directionally.

3. ElGawady et al. (2006) tested masonry walls and retrofitted masonry walls using FRP strips with a test method as shown in Figure 2.13c. The vertical load was kept constant by using a spring that was tensioned. Diagonal shear cracks were however not achieved as the vertical load was too low to counter the overturning moment created by the shear force. Rocking and toe-crushing failures were observed, which are a result of tension failure and concentrated compression forces at the toe due to overturning. Keeping the vertical force constant at a reasonable pressure and inducing a shear failure was found to be hard if not impossible and will be discussed later in Chapter 4.

4. Advanced control shear tests have been conducted by eg. Matsumura (1990) with similar test setups as shown in Figure 2.13d . The vertical, as well as horizontal loads, were computer controlled by hydraulic actuators. Being the most accurate and controlled test, it is also the most time and resource consuming.

5. Shear test using steel rods to apply vertical forces. This test is similar to test method 2, however, the vertical force is distributed more evenly and load controlled by a central hydraulic pressure gauge. With the steel rods' stiffness's being orders of magnitude less than stiff beams as in test method 2, this allows for some vertical movement without too large vertical force increase during shearing and dilatancy behaviour.

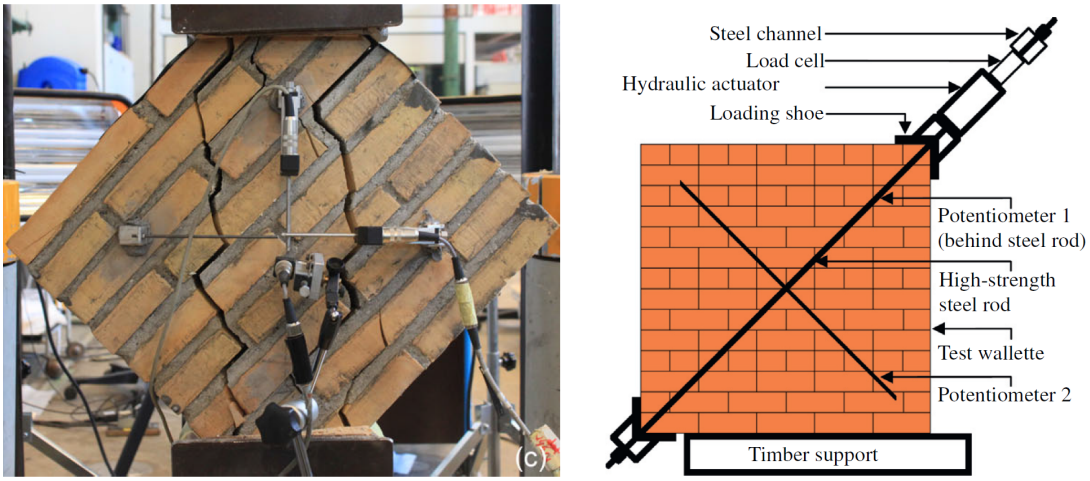

(a) Test method 1 Diagonal Compression.

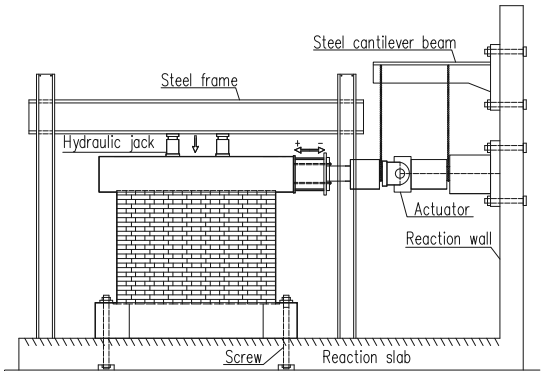

(b) Fixed vertical compression.

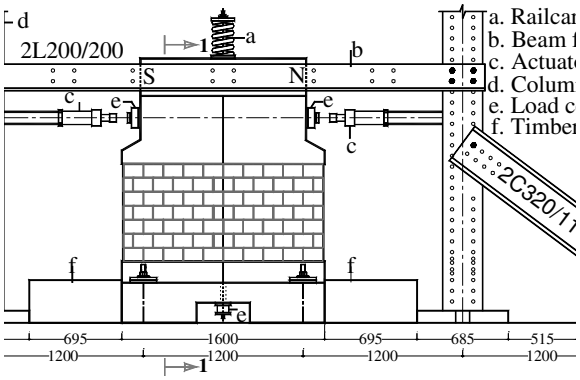

(c) Constant vertical compression by spring.

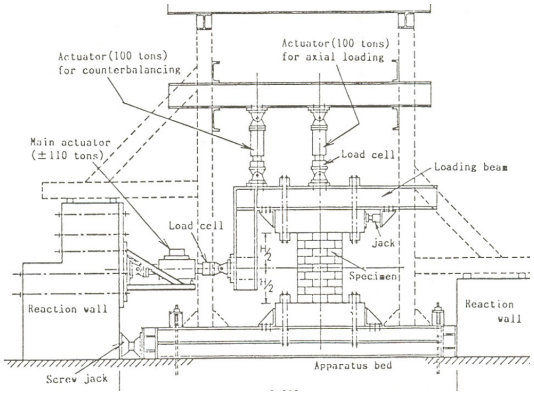

(d) Vertical and shear displacement controlled.

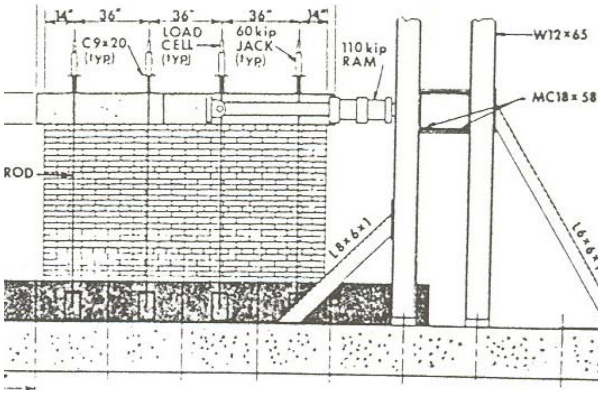

(e) Vertical compression through tensioned rods.

Figure 2.13: Test Methods.

2.8 Concluding summary

The understanding and characterisation of the shear performance of SHCC bonded to masonry as an overlay are important for fundamental research as well as guidelines for structural use of the material in retrofitting. Knowledge of the fundamental mechanisms of failure in masonry, as well as SHCC, is required before any characterization of the composite behaviour can be performed. A few works have been published on locally produced SHCC and ECC retrofitting as discussed in Section 2.3 and 2.6.3 respectively, but a study for South-African design purpose, using SHCC on locally produced clay masonry is required. This forms the basis of the experimental work presented in the remainder of this thesis. This was done through material development of sprayable SHCC, followed by testing of the material at a small characterisation level and concluded by large-scale shear wall testing to validate proposed design guidelines.

Chapter 3

Spray-able SHCC Material development and characterization

The material development phase documented in this chapter entails adjusting a standard SHCC-mix design, used previously at Stellenbosch University, to produce a spray-able SHCC with favourable fresh and hardened properties. The material development process was divided into three parts, which form the three sections of this chapter:

1. The SHCC material was adapted for the correct fresh properties, adhesion and viscosity development rate so that it can be applied successfully by spraying onto masonry.
2. Material characterisation tests for tensile and compressive behaviour were performed to hardened SHCC that was cast as well as sprayed to establish whether the material kept it's mechanical properties.
3. Free and restrained shrinkage was measured on separate sprayed SHCC specimens.

3.1 Shotcrete machine and spray-ability testing

For SHCC to be efficiently applied by spraying, the fresh material should have the consistency and fluidity for it to be conveyed through a hose and nozzle without segregating. Once the SHCC is sprayed onto the masonry, it should be viscous enough to remain adhered to the masonry and be cohesive enough not to segregate (Bruedern et al., 2009; Kim et al., 2003).

3.1.1 Shotcrete Machine

The shotcrete machine used in this research is a Rockcrete-TSL, as shown in Figure 3.1a, shotcrete machine manufactured in South-Africa by Rockcrete Equipment (PTY) LTD. The machine has a pumping rate of 10 l/min and can accommodate a maximum aggregate size of 4 mm. The pump makes use of a rotar-stator for pumping up to pressures of 35 Bar. The standard nozzle, supplied with the machine, is a mortar-spray nozzle with air supplied to the middle of the material flow as shown in Figure 3.1b.

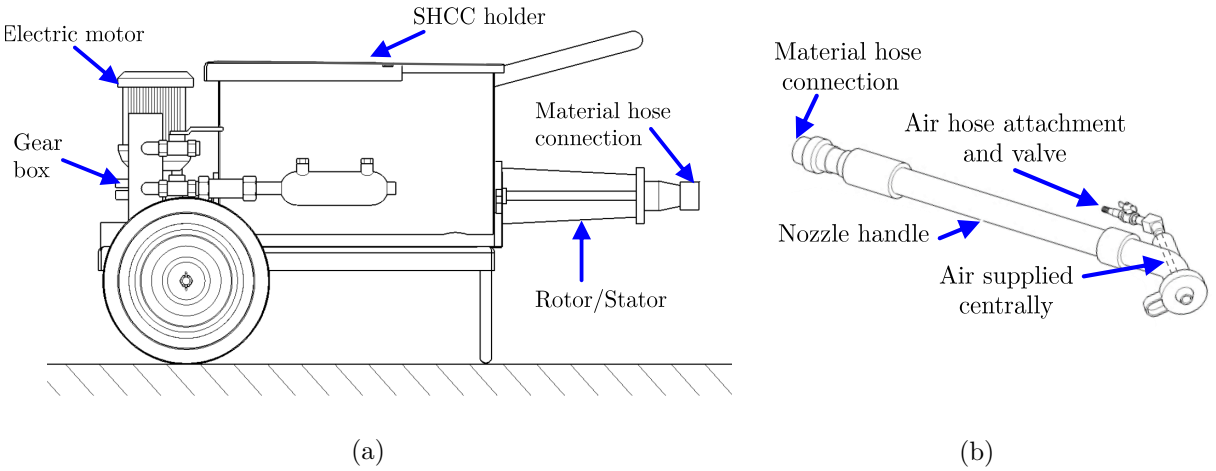

Figure 3.1: (a) Rockcrete TSL shotcrete machine; (b) Mortar spray nozzle.

Problems with the spray angle and air pressure were identified during initial testing, while using a standard SHCC mix design from Paul (2015). Using the standard mortar nozzle, the SHCC was sprayed at a wide angle, leading to wastage as depicted in Figure 3.2. The single central air supply was also not sufficient and lead to the SHCC being sprayed with low velocity and energy and resulted in poor compaction. The nozzle had to be kept close to the spray surface resulting in the airflow, blasting off already sprayed material. An alternative nozzle with air supplied along the full circumference of the material is advised in literature. Different shapes and sizes of these nozzles are available, however it was opted to manufacture a nozzle specifically for the material hose, air supply hoses and fittings on the machine. The design drawing is presented in Figure A.1, in Appendix A. The new nozzle supplies air around the circumference, behind the material. The nozzle also has a longer barrel directing the flow, leading to a smaller spray angle as shown in Figure 3.2. The addition of an extra air hose doubled the air being supplied and significantly improved the spray velocity and compaction. It was possible to hold the nozzle further away and no material was blasted off. Shotcrete is not an exact science and requires experience from the operator that controls the air flow and spray direction. Different size machines will also be able to spray at different rates and consistencies. The circumferential air supply nozzle was used for all testing documented further in this thesis.

Figure 3.2: Left: Standard mortar nozzle with wide spray angle; Right: Circumferential air supply nozzle with small spray angle.

3.1.2 Experimental setup and tests

The starting mix design was taken from Paul (2015). As test parameters, two types of locally available CAC at various cement-replacement percentages were considered. The criteria for acceptance were the slump flow of the fresh SHCC over time and the spray-ability and adhesion to the masonry substrate.

3.1.2.1 Deformability test for fresh SHCC using small slump cone

CAC was used to enhance the viscosity development and cohesiveness of the fresh SHCC. The type of CAC and the percentage cement replaced by CAC were varied. Two types of locally available CAC were tested, namely Ciment Fondu containing 34% alumina and Secar 51 with 51% alumina. The dosage of superplasticizer was initially adjusted to control the initial viscosity, to achieve good mixing and sufficiently high slump flow for all mixes. The small slump cone of diameter $d_0 = 100$ mm was used to measure the SHCC flow-ability over time in the same manner as described in Kim et al. (2003). No external vibration was applied at first, to consolidate the fresh SHCC. Immediately after the slump cone was lifted the SHCC tended to collapse and spread. The maximum diameter of the spread, d_1, and the diameter perpendicular to it, d_2, were measured. External vibration was then added to perform a standard mortar slump test according to ASTM C1437 (2007). The maximum diameter of the spread, D_1, and the diameter perpendicular to it, D_2, were measured. The deformability (γ) for d_1 and d_2, and (Γ) for values D_1 and D_2 was then calculated as follows:

$$\gamma = \frac{(d_1 \times d_2) - {d_0}^2}{{d_0}^2} \tag{3.1}$$

The first slump flow value ($t = 0$ min) was taken directly after the seven minute stage mixing of the SHCC, and thereafter at fifteen minute intervals. Standard SHCC mixing procedures as described by Boshoff (2007) were followed.

3.1.2.2 Spray-ability and adhesion to the masonry substrate testing

The experimental set-up consisted of a small 450 mm x 450 mm masonry wall shown in Figure 3.3a, inside a wooden box with a 30 mm deep edge. The wall was used to test the overlay thickness that could be applied for various rest times after mixing, for various mix designs and concentrations of CAC. The overlay thickness of material build-up that did not run down was measured as shown in Figure 3.4a before trowelling it flat as shown in Figure 3.3b, and measured again as shown in Figure 3.4b.

The spray process can be seen in Figure 3.3. After the SHCC was trowelled flash with the wooden frame, the overlay adhesion was assessed to ensure that no run-down occurs or that the

SHCC slowly starts to creep due to gravity. The wall was then cleaned and washed off with water before sprayed again at the next rest time (every 15 minutes).

(a) (b) (c) (d)

Figure 3.3: Overlay thickness and adhesion test.

(a) (b)

Figure 3.4: (a) 80 mm thick SHCC spray on thickness before trowelled flat; (b) 32 mm SHCC overlay, with good adhesion and no run down.

3.1.3 SHCC shotcrete-ability results and disscusion

The effect of the CAC can be seen clearly in Figure 3.5, where a standard slump test according to ASTM C1437 (2007) was performed at $t = 0$ and $t = 25$ min after mixing. These slump flow values were used to calculate γ and Γ respectively, using Equation: 3.1.

The results are shown schematically in Figures 3.6 and 3.7. The control mix (without any CAC) shows a significantly slower decrease in slump flow, compared to the mixtures containing CAC. The amount of cement replaced by CAC varied between 0 and 10% by mass of cement. Higher dosages of CAC led to a higher rate of deformability loss. The higher percentage aluminate content in Secar also led to a higher rate of deformability loss, compared to the Ciment Fondu for the same dosage. From Figure 3.7 it can also be observed that the Secar has a larger effect on the deformability at $t = 0$ than the Fondu mixes, and the amount of SP would have to be adjusted if the same initial workability is needed. The rate of decrease is directly proportional to the amount of aluminate content added. The rate of deformability loss for 5% replacement with Ciment fondu with alumina content of 34% is similar to that of 3% replacement with Secar with alumina content of 51%. Figures 3.6 and 3.7 can be used to estimate the amount of CAC needed for a certain rest time.

Following Lin et al. (2014), that found that a 30 mm overlay has the optimal strengthening effect, with larger thickness's a decreased effectiveness was observed. A mixture that can be sprayed to an overlay thickness of at least 30 mm after 15 minutes of waiting time after mixing, was chosen. The overlay consistency was also assessed visually. After several trials it was determined that for a deformability of $\gamma < 0.3$ and $\Gamma < 1.3$, corresponding to a slump flow of 115 mm and 152 mm respectively, the mixtures adhesion and viscosity were adequate for easy pumping and spraying to thickness of up to 50 mm. A maximum thickness of 80 mm was achieved with $\Gamma = 1.1$. For $\Gamma < 1.1$ the workability was too low and the SHCC could not be pumped.

Based on the results discussed above and shown in Figure 3.7, it was decided to use a CAC dosage of 5% of Secar for the rest of the research documented in this thesis.

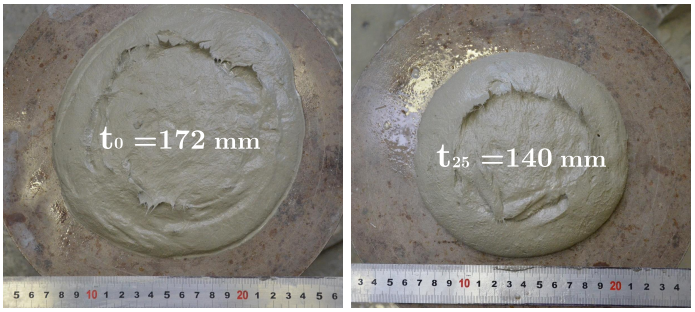

(a) (b)

Figure 3.5: (a) Slump directly after mixer stopped ($t = 0$); (b)Slump after 25 minutes rest.

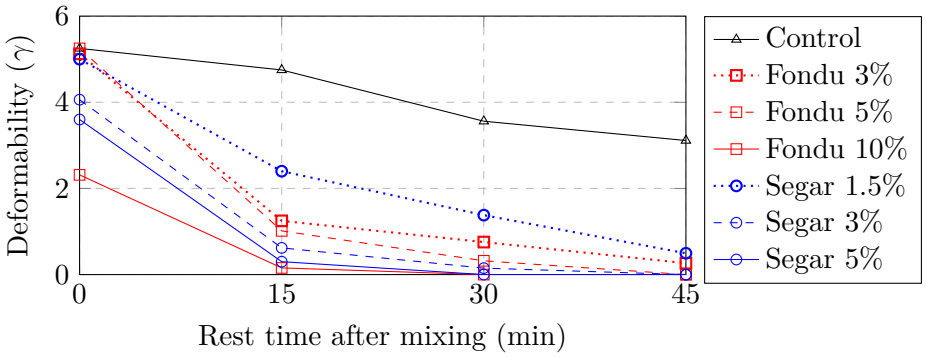

Figure 3.6: Deformability (γ) over time for different CAC's and dosages.

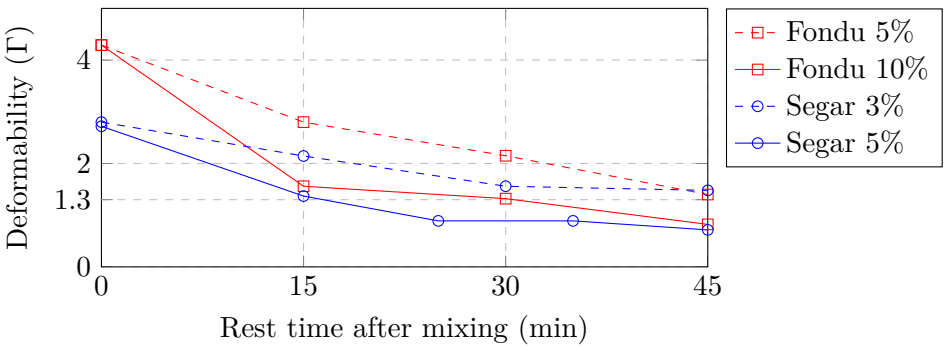

Figure 3.7: Deformability (Γ) over time for different CAC's and dosages.

3.2 Uni-Axial Tension Tests

Uni-axial Tensile Tests (UTT), or Direct Tensile Tests (DTT) are the only tests that can be used to determine the tensile material properties of SHCC directly (Boshoff, 2007). As discussed in Chapter 2, the tensile behaviour of SHCC is what distinguishes it from normal mortar or concrete. Ensuring that sprayed SHCC still have strain hardening properties is of critical importance. Two variations of uni-axial tensile tests were performed in this research. Firstly as developed and described by Boshoff (2007), and secondly tests with larger specimens as described by Zang (2015). The two test setups are presented, followed by the experimental program and succeeded by test results.

3.2.1 Uni-axial Tension Test setup

Test method 1: A simple and practical specimen shape and test setup for larger number of tests during a day were used. Thinner specimens simulate thin layer application, while the larger specimens are more appropriate for thicker overlays. The relatively small, flat dumbell shape specimen, with a gauge length of 80 mm, width of 30 mm and thickness of 16 mm, as shown schematically in Figure 3.8 was used. SHCC was cast horizontally into the steel mould, and a lid was applied during vibration of the freshly cast SHCC to ensure a flat top surface each time. All samples were cast into steel moulds, protected and demoulded after 24 hours. They were subsequently water cured at $23 \pm 2\ ^{\circ}C$ for 13 days. The tests were performed in a Zwick Z250 Universal Materials Testing Machine (MTM) which has a capacity of 250 kN. The top clamp had a pinned connection and the bottom clamp a fixed connection as shown in Figure 3.10a. The strain was measured using an extensometer with a gauge length of 80 mm. The test was performed with the speed of the crosshead of the machine set at 0.5 mm/min. For more detail on the test, the reader is referred to (Boshoff, 2007).

Test method 2: Larger SHCC specimens and fixed end boundary conditions are recommended by RILEM (Van Zijl et al., 2016). Following this recommendation as well as the samples being larger and grind-able, this test was also used. Dumbbell specimens with a cross-section of d=40 mm $\times$ w=80 mm, and a gauge length (l_g) of 90 mm, as schematically shown in Figures 3.9 and 3.10b, were used. A single layer of fine steel wire mesh reinforcement (Figure 3.9), with a wire diameter of 0.6 mm was placed in the middle of the thickness of the sample at both ends, to ensure that failure occurs in the measured area and not at the clamps or transition zones. The samples were cast and sprayed into the moulds, protected by a plastic sheet and demoulded after 24 hours. The samples were water cured under the same conditions, as in test method 1. In this case, no lid was applied to the freshly filled moulds and the surface was only trowelled flat, leaving an uneven finish with a depth (d) of 41 ± 1 mm. The specimen was subsequently ground flat using a Kingtest sample grinding machine (shown in Appendix A, Figures A.2 and A.3) at the age of 13 days. This very precise grinding of the hardend sample ensured a depth tolerance of 0.05 mm, ensuring that the aligned pneumatic clamps do not induce a bending moment when clamping. Pneumatic clamps that extrude from both sides were used to clamp the 410 mm long

sample at the edges and provide a 'fully fixed' end condition as shown in Figure 3.10b. The test was performed with the speed of the crosshead of the machine at 0.6 mm/min leading to the same strain rate as for test method 1 described above.

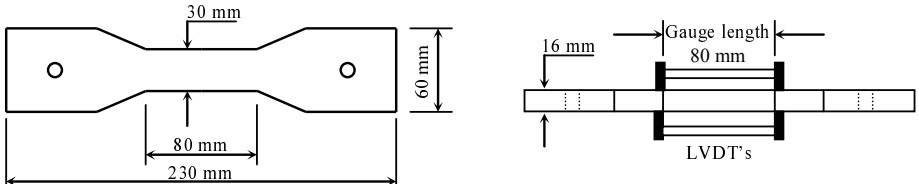

(a) (b)

Figure 3.8: Dimensions of the flat dumbbell specimen, (a) Top view; (b) Side view.

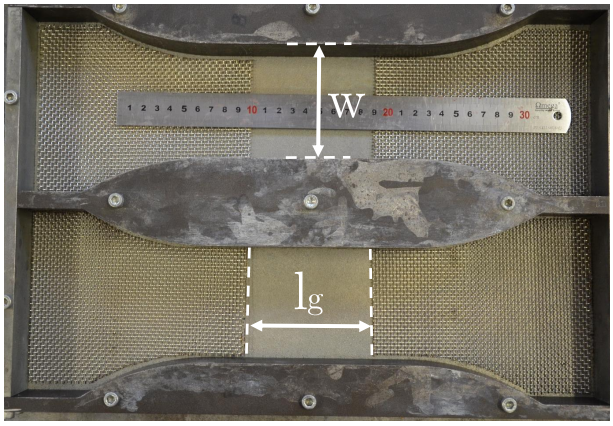

Figure 3.9: Large dumbbell moulds

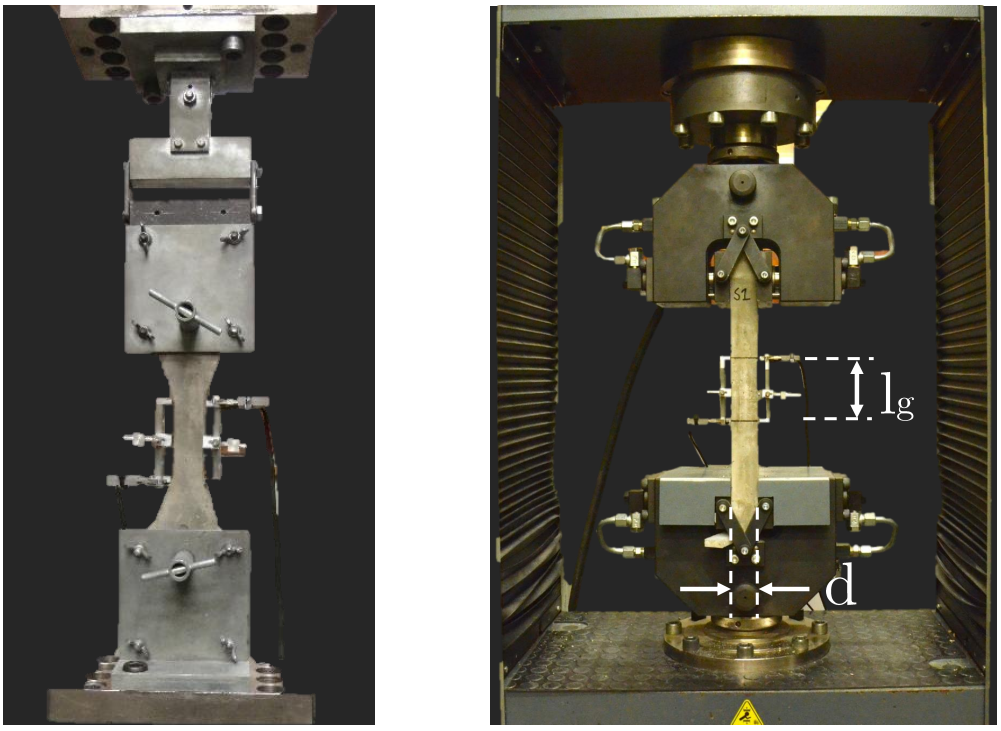

(a) (b)

Figure 3.10: UTT setup with BC (a) Pinned-Fixed ; (b) Fixed-fixed

3.2.2 Experimental test program

The water cement ratio and fly-ash replacement percentage were varied after the optimal CAC and superplasticizer dosages were determined, to achieve the appropriate mechanical properties in the hardened state. A reference SHCC mix from Paul (2015), was used as basis. The mix proportions are shown in Table 3.1. These proportions are calculated using the following ratios: water/binder (w/b) ratio of 0.33, aggregate/binder ratio of 0.49 and FA/C ratio of 1.2. The CAC replacement percentage of cement was varied at 0%, 3% and 5% replacement. The FA/C ratio was also tested at FA/C = 100%, 120% and 140% with 5% Segar CAC replacement.

Table 3.1: Mix proportions for the reference SHCC mix design.

Cement	Fly ash	CAC	Sand	Water	Fibre	SP	VMA	Total	
500	600	0	540	365	26	2.2	0.8	2034	kg/m^3

The effect that pumping and spraying has on SHCC's mechanical properties, was tested by casting big dumbbell specimens directly after mixing and spraying specimens after a rest time of 25 min. The SHCC was sprayed into the horizontally placed moulds. The SHCC mix used in these tests had a FA/C ratio of 1.4 and a CAC/C ratio of 0.05.

3.2.3 Results and discussion

The results of the FA percentage replacement tests is shown in Figure 3.11, with the labels indicating FA content as percentage of the cement mass. The strain is expressed as a percentage. The stress is calculated as the force reading divided by the actual dimensions of the section in the gauge area. It is apparent that a lower fly ash content leads to a higher tensile strength, but at a lower average ultimate tensile strain. The 140% fly-ash mix was selected for its high strain capacity.

The results of the CAC percentage replacement tests are shown in Table 3.2. The average tensile strength at first crack ($\bar{f}_c$), average ultimate tensile strength ($\bar{f}_u$) and average ultimate tensile strain capacity ($\bar{\varepsilon_u}$) were compared. It was found that the percentage of CAC has no clear influence on these parameters.

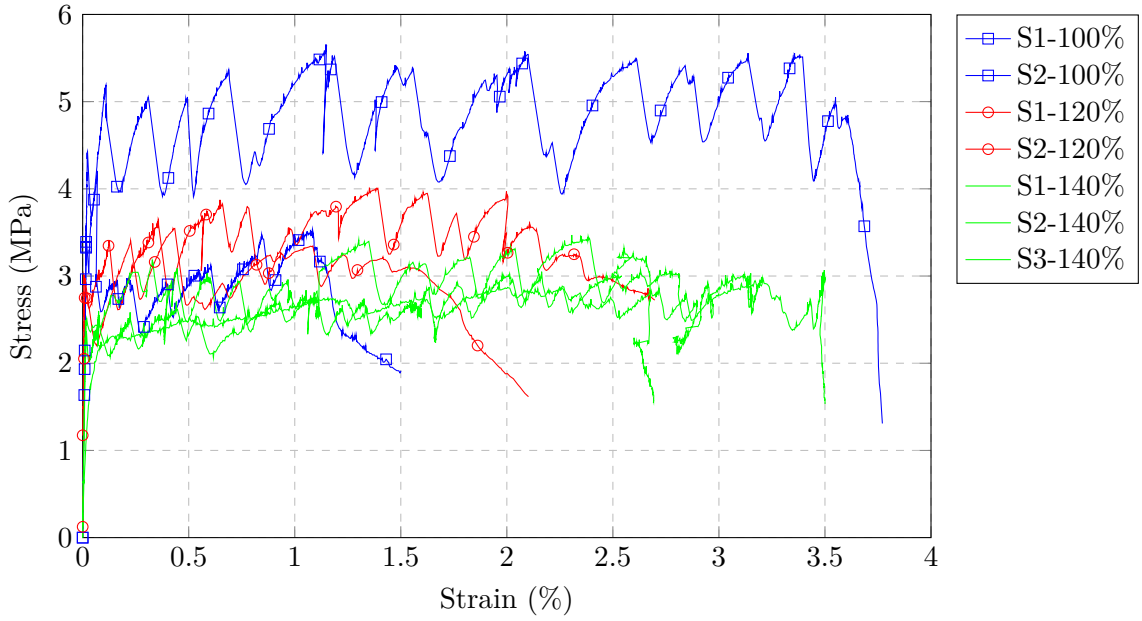

Figure 3.11: Direct tensile response at different FA/C ratios, deterimned from small dumbbell tests.

Table 3.2: DTT results at different CAC replacement percentages.

CAC	nr. of samples	$\bar{f}_c(MPa)$ (CoV)	$\bar{f}_u(MPa)$ (CoV)	$\bar{\varepsilon_u}$ (CoV)
0%	3	3.25 (5.29)	3.71 (4.09)	2.27 (27.53)
3%	2	2.79 (9.39)	3.77 (11.75)	3.06 (20.54)
5%	2	3.00 (0.47)	3.80 (8.96)	2.25 (28.20)

The tensile responses of SHCC specimens that were cast, compared with specimens that were sprayed into the moulds are shown in Figure 3.12 and summarised in Table 3.3. In Figure 3.12, the blue (cast) and red (spray) samples were of the same batch. An additional six sprayed specimens (green) were tested as quality control during the spraying of shear walls as described in Chapter 4. These results are also documented here as the same SHCC mixture was used.

The ultimate tensile strength of the sprayed specimens was on average 26.1% lower than that of the cast specimens, while the tensile strain capacity decreased by 32.1%. The average E-modulus (E-mod) was calculated from Equation 2.2 to be 15.26 GPa and was the same for both cast en sprayed samples. A phenomenon that was observed for the sprayed specimens, is the drop in stress after first cracking point, followed by strain hardening behaviour. This phenomenon was also observed by Boshoff (2007), when DTT was performed at high strain rates. The strain rate during all DTT tested however remained the same, and no explanation for this behaviour was found. Further mix modifications are envisaged to improve the mechanical properties of the sprayed specimens. However, the sprayed SHCC still had an average tensile strain capacity of 2.26%, which is considered to be sufficient for retrofitting application. Characteristic multiple cracking was also observed with the same crack spacing as typical cast SHCC (Figure 3.13). Further research to study the effect of the rest time before spraying on the tensile response is needed. Longer rest times (lower deformability) can cause air entrainment and poor homogeneity and fibre distribution during spraying.

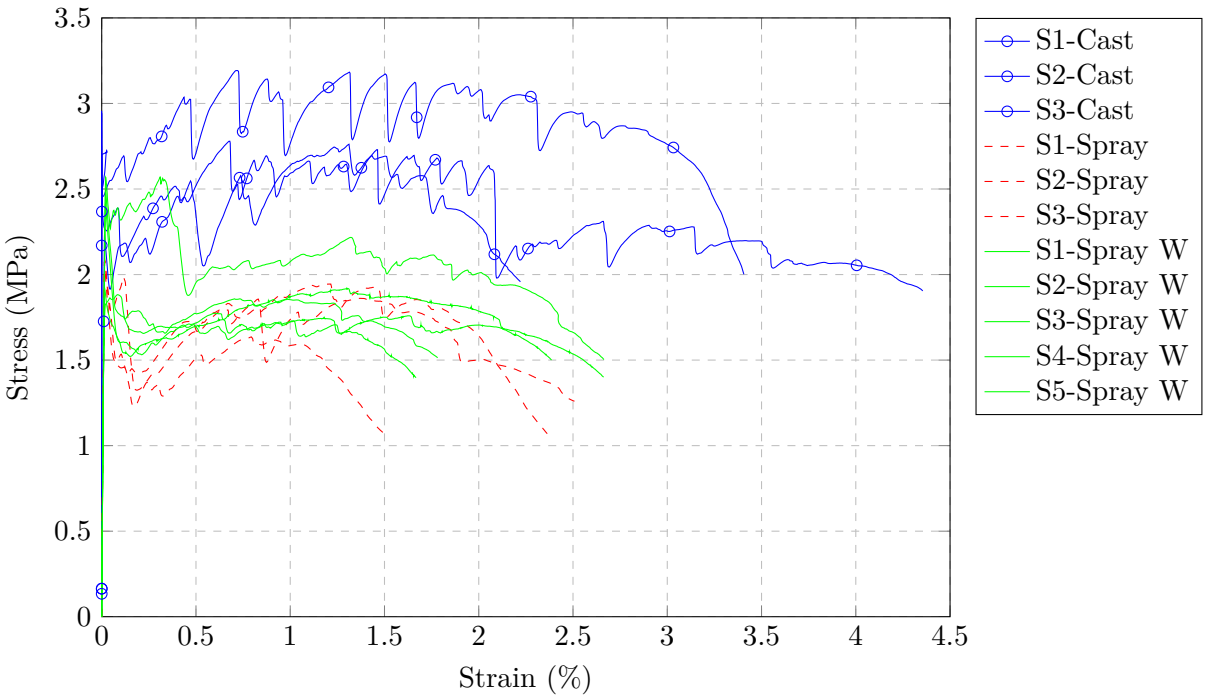

Figure 3.12: Direct tensile response of cast and sprayed SHCC.

Table 3.3: Direct tensile test results of cast and sprayed SHCC.

	nr of samples	$\bar{f}_c$ (MPa) (CoV)	$\bar{f}_u$ (MPa) (CoV)	$\bar{\varepsilon_u}$ (%) (CoV)	$E - mod$ (GPa) (CoV)
Cast	3	2.62 (11.54)	2.97 (7.27)	3.33 (32.10)	15.25 (1.94)
Sprayed	8	2.19 (11.93)	2.2 (11.87)	2.26 (23.35)	15.27 (3.72)
% Decrease		16.3%	26.1%	32.1%	-0.1%

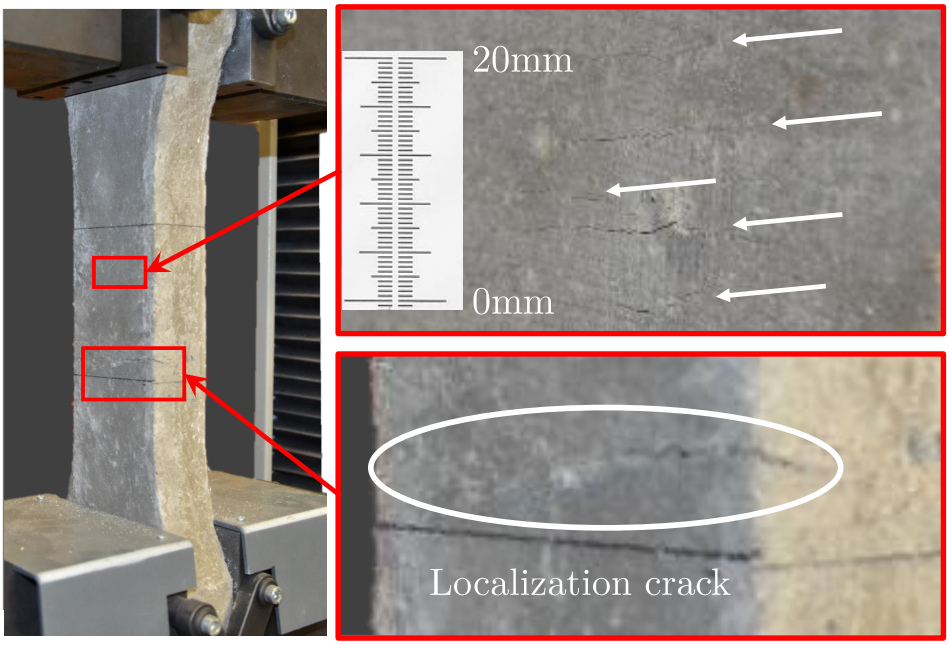

Figure 3.13: Uni-axial tension test.

3.2.4 Mix proportions of Spray-able SHCC used for all test documented further in this thesis

From the results discussed in Sections 3.1 and 3.2, a mixture was chosen. This mixture was used for all other tests documented further in this thesis. The mixture has a FA/C ratio of 1.4 and CAC/C ratio of 0.05. The CAC type was Segar 51. The mix proportions are shown in Table 3.4.

Table 3.4: Mixture proportions used in rest of thesis.

Cement	Fly ash	CAC	Sand	Water	Fibre *	SP	VMA	Total	
420	620	21	540	365	2 %	2.2	0.8	1995	kg/m^3

$*$ Fibre volume fraction

3.3 Shrinkage tests on free and restrained SHCC

The behaviour of SHCC under restrained shrinkage was investigated to determine what effect it has on the overlay and possibly predict whether the overlay will debond or crack due to shrinkage. The importance of characterising shrinkage behaviour of bonded overlays was discussed in Section 2.5.

3.3.1 Free shrinkage specimens

The shrinkage of prismatic specimens was determined by following the guidelines provided in BS ISO 1920-8: Determination of drying shrinkage of concrete for samples prepared in the field or in the laboratory.

SHCC was sprayed into steel moulds with a cross-section 100 mm × 100 mm and length 500 mm to create prisms to measure the free shrinkage of the overlay material. Demac targets were attached similar to Beushausen and Chilwesa (2013), using high strength Quickset® epoxy glue from Pratley adhesives, 24 hours after spraying the free shrinkage specimens. The targets were glued at a 100 mm gauge length as shown in Figure 3.14. The reference bar was used to position the targets before the glue hardened. The specimens were left unsealed on all surfaces and stored at $24 \pm 2\ ^{\circ}C$ and relative humidity of $65 \pm 5\%$. A hand-held demac extensometer with resolution of 0.001 mm was used to measure the length change as shown in Figure 3.14, by placing the pins within the centres of both targets. Readings were taken until three consecutive readings had the same value. This value was then noted as the reading. Four samples were used with 3 measurements on each sample. The zero reading was taken 6 hours after the targets were glued onto the specimen, thus at a specimen age of 30 hours. It should be noted that it is clearly not purely drying shrinkage that was measured, but overall dimensional change under the stated climatic conditions and continued hydration from the young age.

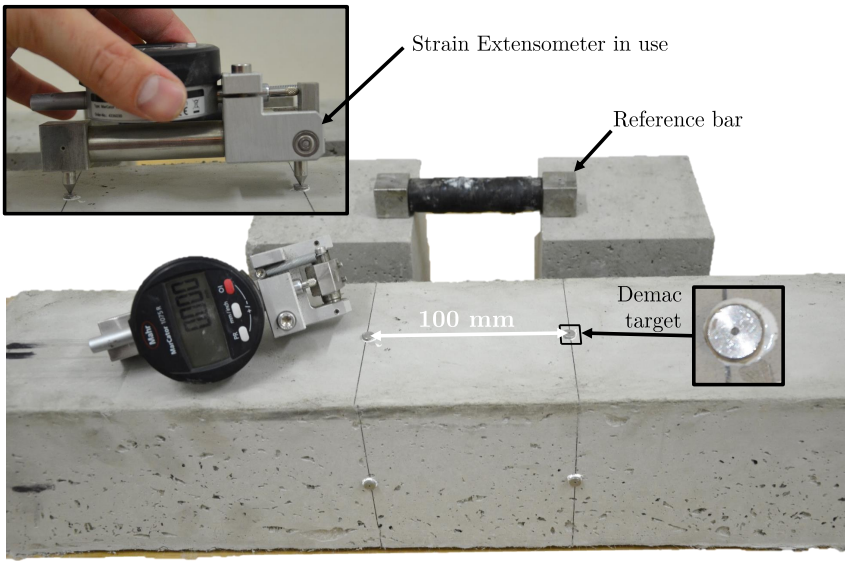

Figure 3.14: Free shrinkage test setup.

3.3.2 Restrained shrinkage test setup

Restrained shrinkage tests were conducted by spraying SHCC onto four masonry specimens that were constructed to represent typical running bond of masonry walls for both the smooth and grooved sides of the bricks. Typical horizontal restraint on the facing/smooth side (Hf) and vertical restraint of the non-face/grooved side (Vn) can be seen in Figure 3.15 (a) and (d) respectively. The specimen dimensions were 1030 mm× 220 mm. The specimens were left in laboratory conditions to cure for seven days and provide stiff restraint to the SHCC overlay. A 30 mm overlay of SHCC was sprayed onto a single side of each specimen and left to harden for 24 hours before a Linear Variable Differential Transformer (LVDT) was attached similarly to the demac targets, as shown in Figure 3.15 (c) to measure deformation on the outer face of the SHCC over a gauge length of 500 mm (Figure 3.15 (d)). A computer was used to digitally log readings from the LVDT's every hour for 56 days.

The shrinkage behaviour of restrained SHCC overlays, on samples with dimensions of 1150 mm×935 mm, was also assessed. The overlay was sprayed onto the smooth side of the bricks and water cured for 7 days after hardening, by wetting the overlay daily, with a sprinkler. After 14 days the cracking of the overlay was assessed.

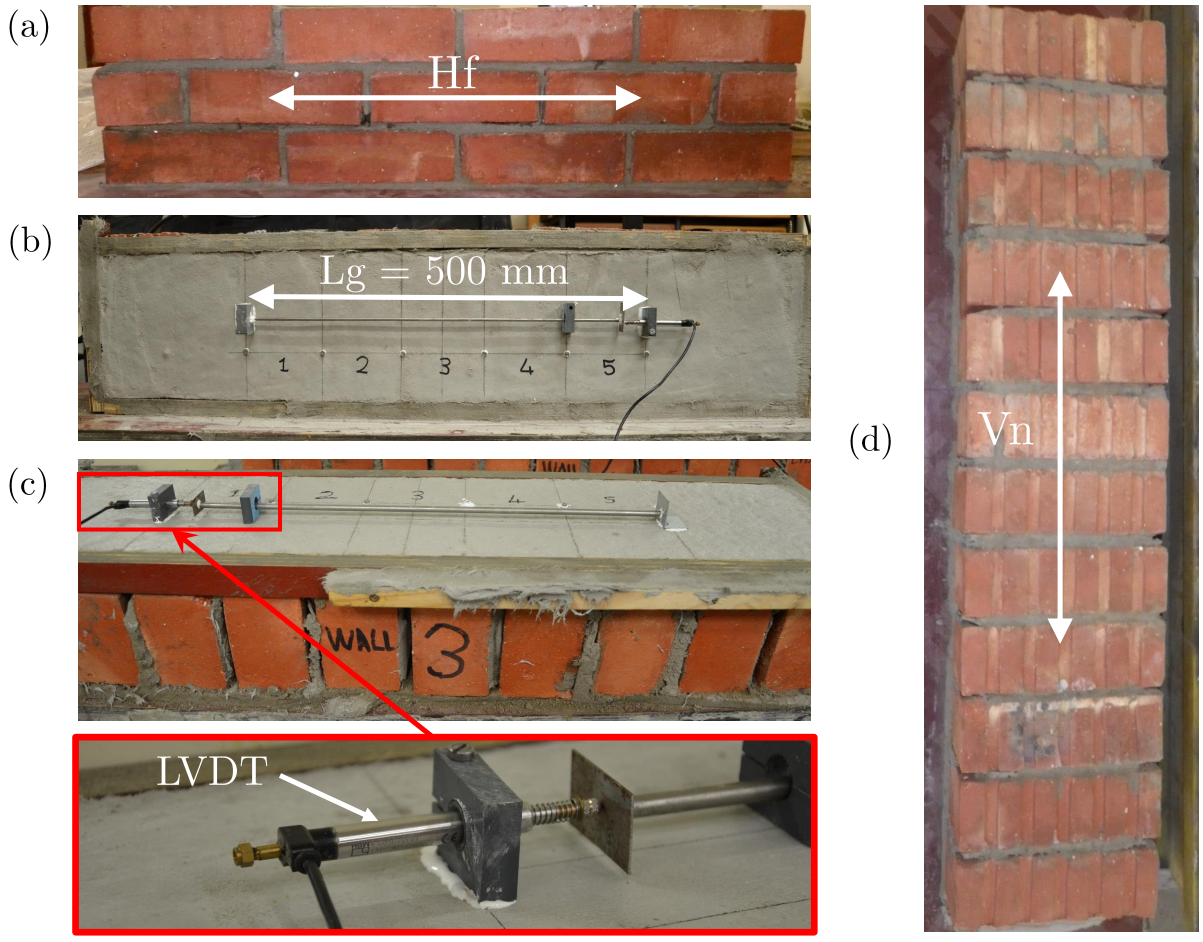

Figure 3.15: (a) Horizontal restraint from smooth brick face; (b) LVDT's fixed at a gauge length of 500 mm; (c) LVDT detail; (d) Vertical restraint from grooved brick face.

3.3.3 Results and discussion

The shrinkage behaviour of both the free and restrained samples are shown in Figure 3.16. After 56 days the average shrinkage strain of the free specimen was 655 micro strain. This is a relatively low shrinkage compared with those reported by other researchers (Boshoff, 2007). Figure 3.16 shows that the restrained shrinkage at the surface followed the same trend as the free shrinkage, with shrinkage strains between 567.5 and 623.7 micro strains and an average of 594.4 micro strain. The initial decrease (samples expanding) in shrinkage, over the first 4 days, cannot be explained and further research of the early age shrinkage behaviour of sprayed SHCC is advised. Unlike in the case of normal mortars (Chilwesa, 2012; Beushausen and Chilwesa, 2013), no cracking or debonding was observed on the SHCC.

Cracking prediction models similar to Chilwesa (2012), are out of the scope of this thesis, but further testing and characterising of the time dependant relaxation of sprayed SHCC are advised. Considering that the overlays did not crack and analysing Figure 2.10 that predicts cracking onset, a postulation is made that sprayed SHCC has a high relaxation capacity. The relatively low stiffness of the masonry also decreases the restrained stress.

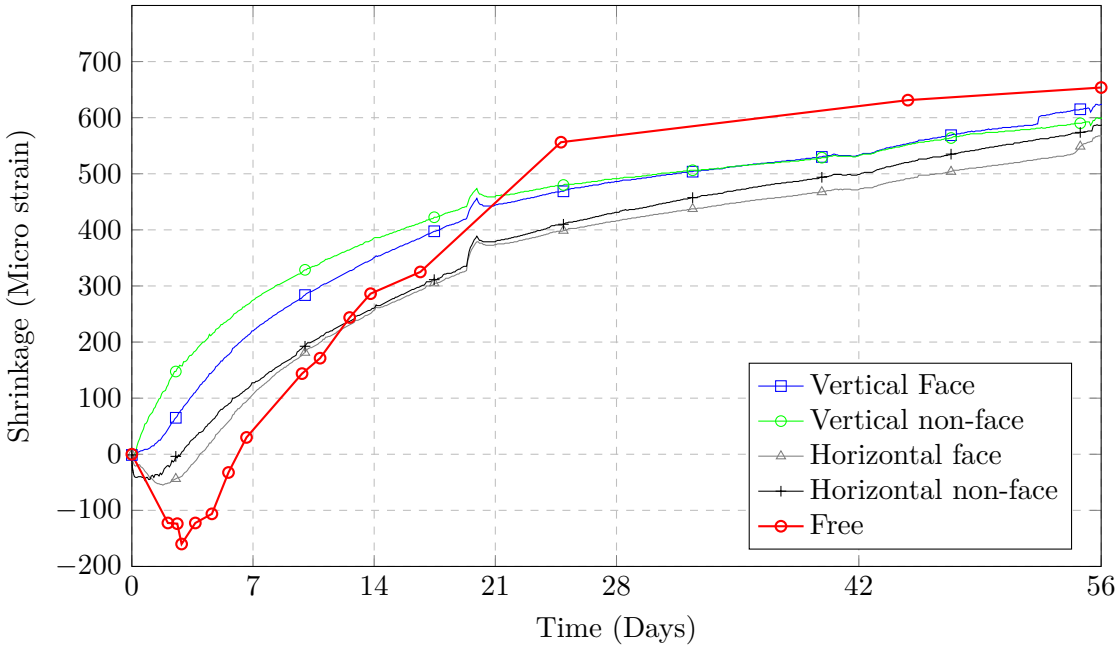

Figure 3.16: Free and restrained shrinkage strain results.

The restrained shrinkage behaviour on samples with dimensions of 1150 mm × 935 mm, can be seen in Figure 3.17. The cracks in the SHCC overlay shown in Figure 3.17 were only visible after wetting the wall with a sprinkler. For a 30 mm overlay thickness, the average vertical crack spacing was 33 mm, while for a 15 mm overlay thickness, the the average vertical crack spacing was 44 mm. Cracks primarily formed in the vertical direction, with few horizontal cracks. Cracking at the vertical edges also decreased, with a 50-100 mm boundary forming that can be seen in Figure 3.17.

Some of the cracks were marked with a pencil (while the wall was wet and cracks pattern visible) to be later inspected with a microscope. The marked cracks were photographed through a microscope with a zoom factor of 300. Figure 3.18a shows a crack width smaller than 10 micro meters (μm), while Figure 3.18b shows no crack, and only the pencil line can be seen. The scale on the left in Figures 3.18a & 3.18b is 1 mm per line (total figure height is 4 mm). All cracks were most likely less than 10 μm wide, with no larger crack observed.

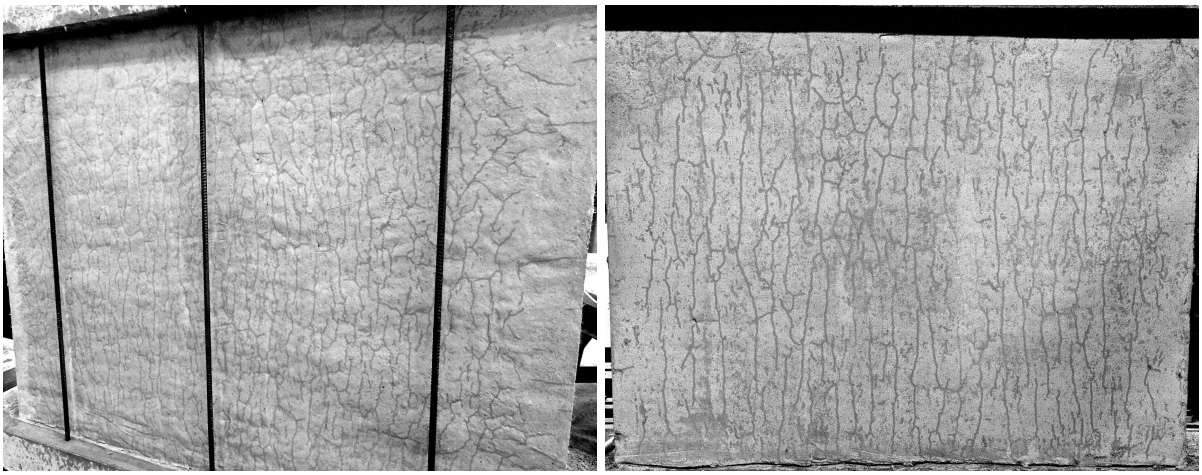

(a) (b)

Figure 3.17: (a) Crack pattern of 30 mm SHCC overlay; (b) Crack pattern of 15 mm SHCC overlay.

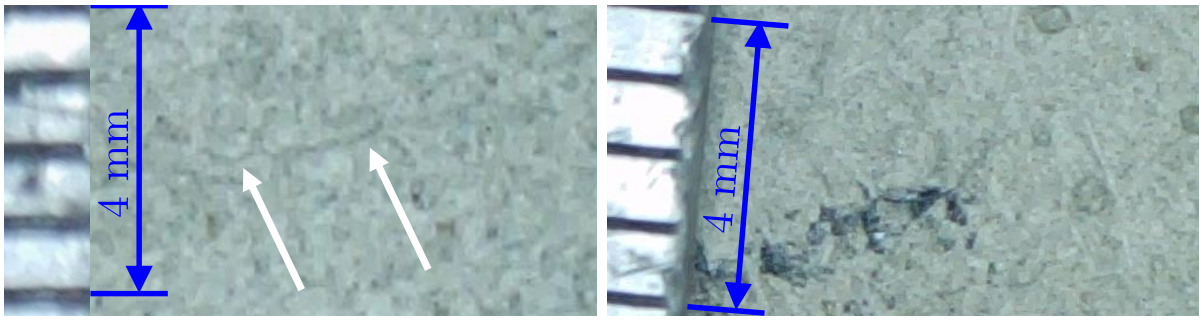

(a) (b)

Figure 3.18: (a) Crack with width $< 10\mu m$; (b) No visible crack.

3.4 Concluding summary

From the material development process, testing and results presented in Chapter 3, the following conclusions can be drawn:

1. SHCC can successfully be applied to masonry through shotcrete, by replacing a small amount of cement with CAC, that leads to the desired viscosity development rate. With the correct rest time, small to no run-off of the SHCC was achieved with strong adhesion to the masonry. Spraying of SHCC can be a successful procedure to apply overlays to masonry substrates with acceptable, trowelled finishes and sufficient range in thickness (10-60mm).

2. The mechanical properties of sprayed SHCC was lower than those of the cast specimens, with a 26.1% and 32.1% decrease in ultimate tensile strength and strain capacity respectively. However, the 2.26% strain and 2.20 MPa strength of the sprayed SHCC is considered sufficient for retrofitting application.

3. Restrained shrinkage is not detrimental to sprayed SHCC overlays on masonry tested in this project. The relatively low free shrinkage values and high relaxation potential combined with high tensile strain capacity hold potential for highly favourable composite behaviour of a masonry wall with a bonded SHCC overlay. No debonding or localized cracking was observed. Cracks with a width of 10 μm and smaller, are insignificant and possibly limited to the surface.

Chapter 4

Experimental design and program

4.1 Introduction

The aim of the experimental program is to determine and accurately predict the performance of bonded SHCC overlays under shear stresses. An important objective of this research was to pursue SHCC overlay preparation, application and overlay thicknesses that are practical and easily implemented in practice.

The experimental phase is the procedure of executing standardized test methods and measuring all the required data in order to derive and identify the characteristic material properties of normal mortar, masonry units, mortar-masonry interface and masonry-SHCC interface. In order to quantify the strength and ductility enhancement that SHCC brings about, additional non-standardised tests were performed.

Reported in this chapter is a notation for all specimens tested and the tests and equipment specifications for the determination of the compressive strength, shear bond strength of mortar bonded bricks, shear bond strength of SHCC bonded to brick, shear strength and fracture properties of SHCC overlays and lastly validation tests of large Shear Wall Specimens (SWS).

4.2 Specimen notation

All specimens are identified and referred to with a code according to the test, masonry- and overlay thickness. These variables are listed in Table 4.1 with the corresponding code.

The notion format used in this thesis exists of these codes followed by the specimen number, for similar specimens tested. For example, the specimen code SW-110-30-2 indicates a masonry shear wall specimen, with a single leaf thickness (110 mm), a SHCC overlay of 30 mm and is the second (2) specimen in the range. Where the last number is ignored, the specimen group is referred to and averaged values are provided.

Table 4.1: Notation used to identify specimens in this study.

	Discription	Code
Test	Triplet test at 0 MPa confinement pressure	T0
	Triplet test at 0.3 MPa confinement pressure	T03
	Triplet test at 0.6 MPa confinement pressure	T06
	Modified Triplet shear test on 9 brick specimen	MT
	Shear Wall test	SW
Masonry thickness	Single brick leaf (110 mm)	110
	Double brick leaves (220 mm)	220
SHCC overlay thickness	No overlay (0 mm)	0
	15 mm	15
	20 mm	20
	30 mm	30

4.3 Characterising tests

Material characterisation tests were performed as an important step towards developing design tools for overlay retrofitting systems and computationally modelling the composite system in future research. The results from the characterisation test were also used during the validation tests of large SW specimens.

4.3.1 Mortar and Masonry compressive strength

A typical mortar mix, with class I specifications from SANS 10164-1 (1989) were used. The mix proportions were determined by trial and error using the mix guidelines provided in SANS 10164-1 (1989). The final mix weight proportions are provided in Table 4.2. The mortar mix has a water-cement ratio of 0.75 and the same cement, as for the SHCC mixture discussed in Section 3.2.4, was used.

All of the specimens constructed and documented in this thesis, made use of the same mortar mix proportions provided in Table 4.2. The mortar compressive strength was measured with at least 3 specimens for every mix made. The compressive strength tests were conducted according to the specifications set out by ASTM C109 (2010). The tests were performed using a 250 kN Zwick MTM. Mortar cubes of 50 mm were crushed at a loading rate of 60 kN/min. The peak compressive force value is converted to the mortar compressive strength, f_{mu}, by deviding the peak force by the contact area of the specimen.

Table 4.2: Mortar mix weight proportions.

Water	Cement	Sand
1	1.33	6

The clay bricks used for all of the specimens constructed and documented in this thesis were of the same batch from a single supplier. The bricks have dimensions of $222\pm2\times105\pm2\times70\pm2$ mm. The bricks have a facing side that is smooth and a non-facing side that contains five, 5 mm deep and 12 mm wide grooves, that are shown in Figure 4.1. The brick type is a typical brick used in URM walls construction. The bricks were wetted 24 hours prior to building specimens, to ensure that the initial absorption rate of the bricks are below 1.8 kg/m$^2\cdot$ min as specified by SANS 10249 (2012). The brick compressive strength was measured on six bricks. The compressive tests were performed according to the specifications set out by BS EN 772-1 (2011). The tests were performed using a 2 MN Instron MTM. The bricks were crushed at a loading rate of 300 kN/min. The compressive strength of the bricks, f_{bu}, was determined similarly to that of the mortar strength, by dividing by the contact area of the specimen.

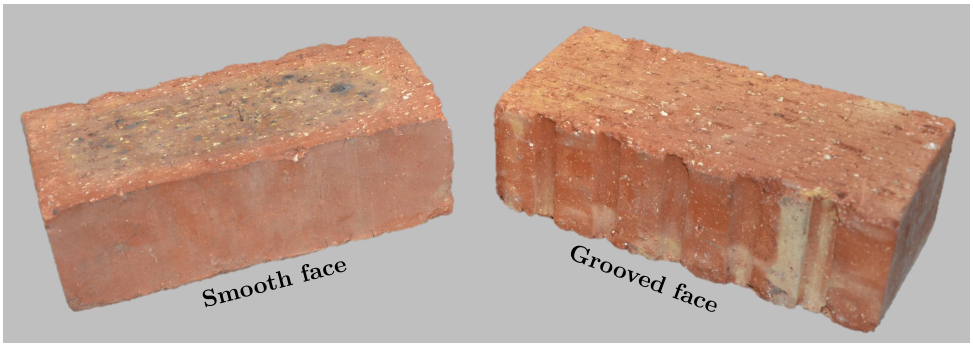

Figure 4.1: Clay burned bricks used throughout research.

4.3.2 Shear strength of brick-mortar bond

4.3.2.1 Introduction

The triplet shear test comprises of three bricks bonded together with two mortar layers loaded in such a manner that the two mortar joints fail in shear. Measurements during the test provide information about the shear strength of a brick-mortar joint.

The triplet shear test is executed according to the specifications set out by BS EN 1052-3 (2002). The triplet shear test was performed on a single type of specimen with no intentional variables. The test was performed at three confinement pressures, 0 MPa, 0.3 MPa and 0.6 MPa, to determine the initial shear strength and the internal friction angle of bed joints in masonry. The specimen notation is T0-110-0, T0.3-110-0 and T0.6-110-0 respectively.

It is important to remember that masonry has a Coulomb friction behaviour under shear load, where the shear strength of the bed joint is proportional to the confinement pressure as described in Equation 2.1.

4.3.2.2 Triplet shear specimen

The triplet shear specimen consists of three bricks joint with two, 12 mm thick, mortar joints as shown in Figure 4.2b, leading to a total dimension of $(h \times b \times d)$ $222 \pm 2 \times 234 \pm 4 \times 70 \pm 2$ mm. The specimens were constructed under laboratory conditions and to the specifications provided in BS EN 1052-3 (2002). The specimens were left unsealed on all surfaces and stored at $24 \pm 2\ ^{\circ}C$ and relative humidity of $65 \pm 5\%$ until the day of testing. The stored specimens can be seen in Figure A.4, in Appendix A.

4.3.2.3 Testing machine and set-up

The test set-up consisted of the two outside bricks supported on steel bearing plates that are on roller supports, and the central brick pushed through by a 2 MN Instron MTM. Steel bearing plates with same total dimensions of the bearing face of the bricks transferred the shear force into the specimen, as shown in Figure 4.2b. The bond shear stress, f_{mb} (where subscript mb refers to mortar-brick) between the brick and both mortar is assumed to be uniformly distributed over the contact areas (A_{mb}) and is equal to the shear force (F_v) in the vertical direction divided by A_{mb}.

To test the triplet specimen at a constant confinement (lateral) pressure of 0.3 MPa and 0.6 MPa, a coil spring was used. The pressure was created by post tensioning the coil spring with a hydraulic jack as shown in Figure 4.3. The pressure was monitored with a Load Cell (LC). When the correct pressure was reached (0.3 or 0.6 MPa) the nuts indicated in Figure 4.3 were tightened and the hydraulic jack was released. This was done to ensure that the jack loosing pressure over time, would not influence the confinement pressure, as all the force would now be

in the spring and rods. The spring was used in order to keep the confinement (normal) force constant, avoiding dilatancy-induced pressure increase when only using rods (Van Zijl, 2004).

The load was applied with a MTM actuator head displacement controlled rate of 0.5 mm/min. This loading rate was within the testing rates of 0.1(N/mm^2)/min and 0.4 (N/mm^2)/min prescribed by BS EN 1052-3 (2002).

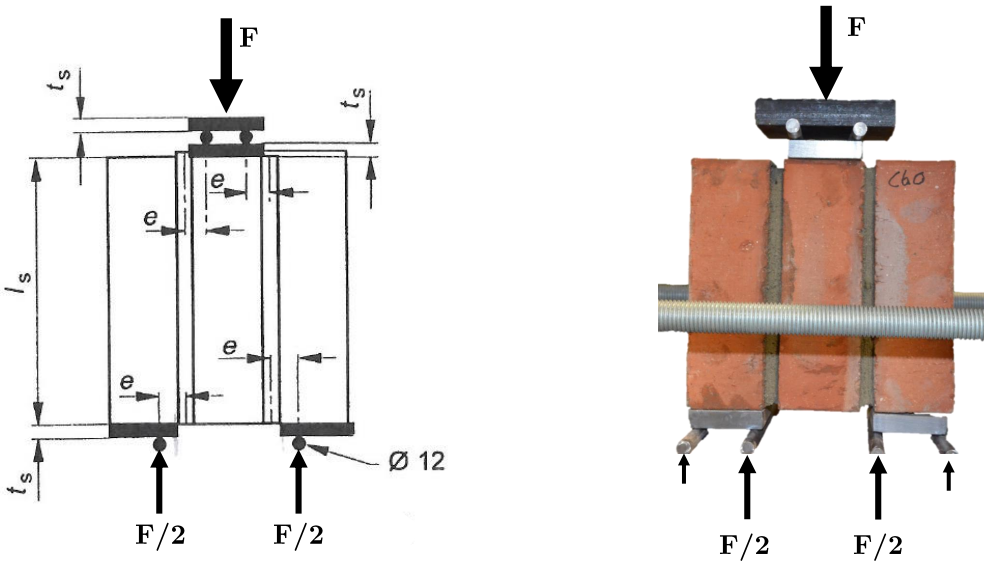

(a) (b)

Figure 4.2: (a) Triplet shear setup as per BS EN 1052-3 (2002); (b) Triplet shear setup.

.

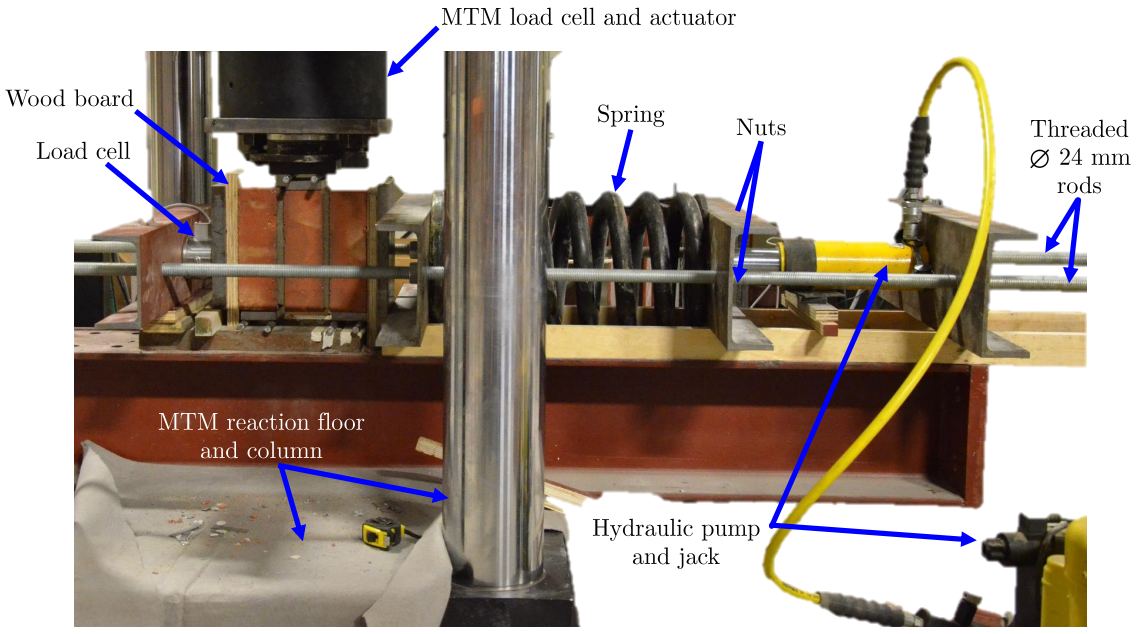

Figure 4.3: Triplet shear test setup, for tests performed with a confinement stress of 0.3 MPa and 0.6 MPa.

4.3.3 SHCC-brick shear bond strength

The SHCC overlay shear bond strength was also determined with the triplet shear test described in the Section 4.3.2, as in the case of Dehghani et al. (2015) and Bruedern et al. (2009). Bond failure is a typically brittle failure mode which is undesirable and abrupt. In addition to overall increase in shear resistance, the development of multiple cracks in the SHCC overlay is believed to increase the ductility of the retrofitted wall. From preliminary tests it was found that the transition between bond and shear failure in the SHCC overlay was more or less at an overlay thickness of 10 mm for a single leaf triplet specimen as described in Section 4.3.2.2. Therefore, to evaluate the overlay bond strength, an SHCC overlay with a thickness of 30 mm, i.e. significantly larger than 10 mm was selected, to ensure that the desired failure mechanism would occur.

At an age of 7 days each triplet shear specimen was inserted into a wooden frame as shown in step 1 of Figure 4.4, and an SHCC layer was sprayed onto both sides of the specimen (step 2) and trowelled flat to a thickness of 30 mm. The wooden frame was removed and the specimens left to harden (step 3) for 24 hours. The specimens were then wrapped in plastic foil (see Figure A.4 for specimen storage) and kept in the same conditions, ($24 \pm 2\ ^{\circ}C$ and R_H of $65 \pm 5\%$) for a further 13 days.

The standard triplet shear test procedure described in Section 4.3.2.3 was followed. It is important to ensure that the bearing plates only push on the bricks and not on the overlay. This is done by grinding the top and bottom surfaces of the bricks clean, where the SHCC overlay accidentally protruded. The test was performed without confinement pressure, as there is no method to determine the stress distribution between the overlay and the bricks. Some of the confinement pressure would thus be absorbed by the overlay, causing lower shear strength in the mortar-brick bond. This phenomenon is further elaborated in the results discussion in Section 5.2.3.

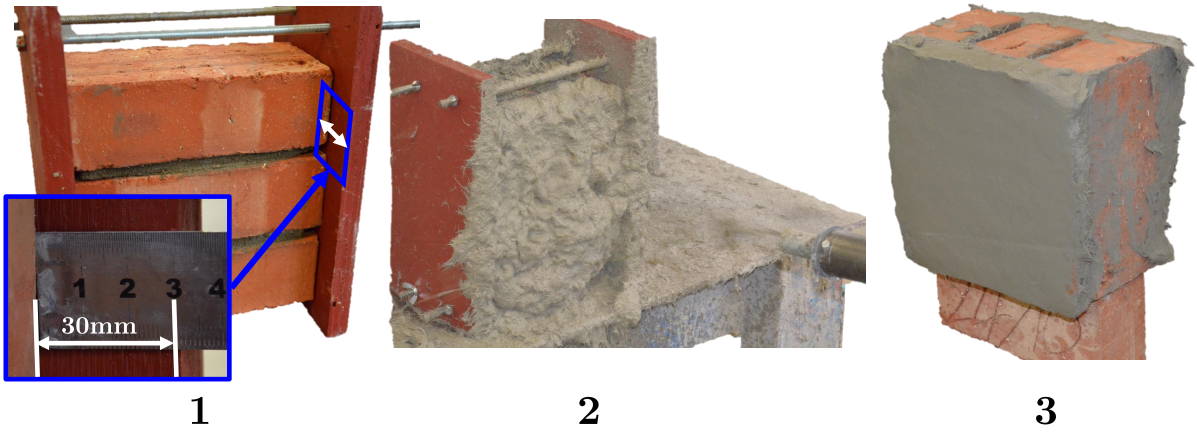

Figure 4.4: SHCC bond strength specimen preparation.

4.3.4 SHCC overlay shear strength

The shear strength and ductility enhancement of a bonded SHCC overlay on masonry was evaluated with a modified triplet shear test. As there is no standard test to determine the shear strength of bonded overlays on masonry, the best possible test method was researched. Dehghani et al. (2015) and Bruedern et al. (2009) used the standard triplet shear test (BS EN 1052-3 (2002)) with SHCC overlay thickness's of 5 mm, 10 mm and 10 mm, 20 mm respectively. The 20 mm overlays tested by Bruedern et al. failed in bond, while the 10 mm overlay showed shear failure through the overlay. A 5 mm overlay is considered as too thin for regular retrofitting and accurate testing. Initial testing, using a 10 mm overlay, in the same manner as the bond strength and researchers mentioned above, yielded that de-bonding still occurred and shear failure through the overlay was not ensured in each test. Instead of testing a thinner overlay, to increase the SHCC shear-area to bond-area ratio, the bond area was increased. Instead of using three single bricks, three sections of three bricks each were used. The rest of the setup was similar to the standard test described in BS EN 1052-3 and Section 4.3.2.3, with the sides being supported and the centre part pushed through with two shear planes being created as shown in Figure 4.5. The dimensions for e and l_s remained unchanged (e & l_s as per definition in Figure 4.2a). The reduction of the thickness to area ratio of the overlay ensured cracking in the overlay and thus leading to a ductile failure, instead of brittle debonding.

The base displacement was measured using four LVDT's in each inside corner of the shear planes, placed at the same distance away from the specimen. The LVDT's measured on a steel plate that was glued to the underside of the brick. For the SHCC specimen, it was ensured that the steel plates did not touch the overlay and only measured the brick displacement. The average base displacement versus the load was later used to assess the ductility and energy dissipation. As for the shear bond test, no confinement pressure was applied.

Two different specimen types were tested. Control specimens without a overlay (MT-110-0) to evaluate the test and compare with the standard triplet test results (T0-110-0) and specimens with a 10 mm SHCC overlay sprayed onto both sides (MT-110-20) to evaluate the shear strength and ductility enhancement.

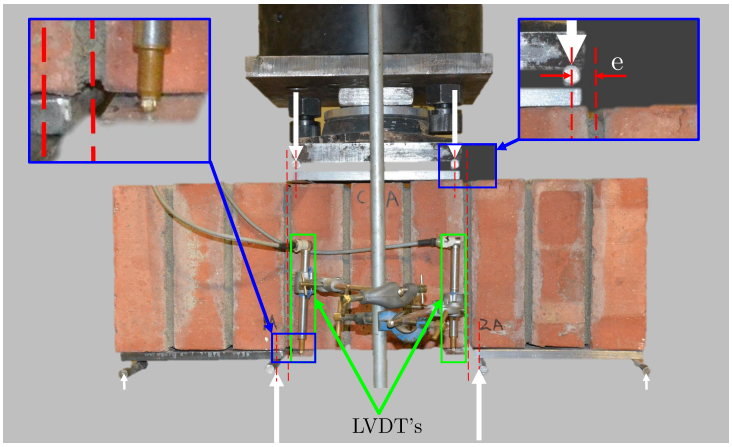

Figure 4.5: Modified shear strength test setup.

4.4 Large scale validation and performance testing

4.4.1 Introduction

URM SW tests were used in this research as a final procedure to determine the SHCC overlay behaviour. As discussed in Section 2.7.2, there is no standard test method that incorporates confinement pressure during masonry shear testing. Keeping in mind the four outcomes of the test method described in Section 2.7.2, it was opted to build a test set-up similar to a combination of test methods 3 and 5 described in Section 2.7.2 and shown in Figures 2.13c and 2.13e.

The SW test comprises of a typical structural URM wall element, of full scale size, loaded vertically and horizontally to fail the wall in diagonal shear. An advantage of this SW test is simulating the vertical pressure due to self-weight of the structure, while applying the shear load over the whole top surface, similar to a SW element in a URM building. The disadvantages of this SW test include the manufacturing of the test frame and full scale wall specimens that are heavy and time consuming to produce and test.

The SW test variables are the thickness of the wall (single and double leaf) and the SHCC overlay thickness.

4.4.2 Shear wall specimen

The SW specimens are unreinforced masonry walls built between two concrete beams, with bricks and mortar as described in Section 4.3.1. The SWS was 5 bricks in length and 11 bricks in height, leading to a dimension of 1150±5 × 935±5 × t±2 mm, as shown in Figure 4.6. The thickness (t) was 105 mm and 230 mm for single and double leave walls respectively. The dimensions were determined from the following factors; dimensions similar to walls between window openings in URM buildings, dimensions achievable with standard bricks, minimizing half bricks and dimensions similar to previous studies conducted by other researchers. The aspect ratio (l/h) of 1.2 was used to favour the shear force action, over the overturning moment created by the shear force.

The top and bottom concrete beam dimensions and reinforcement bars (green) is shown in Figure 4.7. All the reinforcement was high tensile (f_y = 450 MPa) steel with a nominal bar diameter of 12 mm (locally referred to as Y12 bars). High strength, class 8.8 (f_y = 800 MPa), steel bolts with 5 mm thick, 70 × 70 mm steel plates (blue) for additional shear and tensile capacity was cast into the concrete. The beams were made from high strength (65+ MPa) Self-Compacting-Concrete (SCC) and cast in wooden moulds. The beam moulds were designed and constructed from 22 mm thick shutterply wood and the contact surfaces were finished with a moisture barrier paint to ensure repetitive use. The moulds were assembled with 8 × 40 mm screws at a maximum spacing of 120 mm. The bolts and void formers were positioned, with a tolerance of 0.5 mm, by suspending it from the top, with the bolts pointing upwards. A 22 mm

deep, 1200 mm long (L) and 240 mm wide (B) (shown in green on Figure 4.8) groove was created in the beam where the wall was later constructed in. The SCC ensured good compaction and the desired smooth, exposed surface (shown in Figure 4.9), where little surface finishing operations could be done. PVC pipe was used to form voids, at positions as indicated on Figure 4.7. The four voids horizontally in-line with the cast in bolts, are to provide additional place for bolted connections to the testing frame, while the six voids on the sides were used to insert rods to handle the SW specimen with the overhead crane. The breadth of the concrete beams used for single leaf walls, was decreased by 120 mm, leading to a total breath of 280 mm and a groove of 120 mm wide. The bolts and bolt-voids, however remained at the same position.

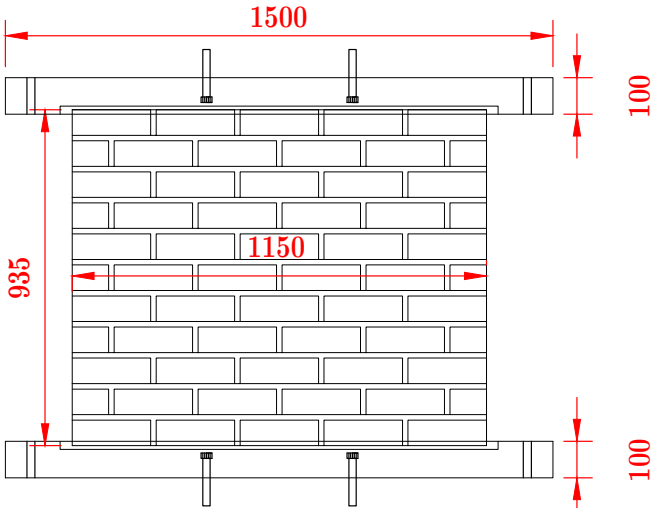

Figure 4.6: Wall specimen dimensions.

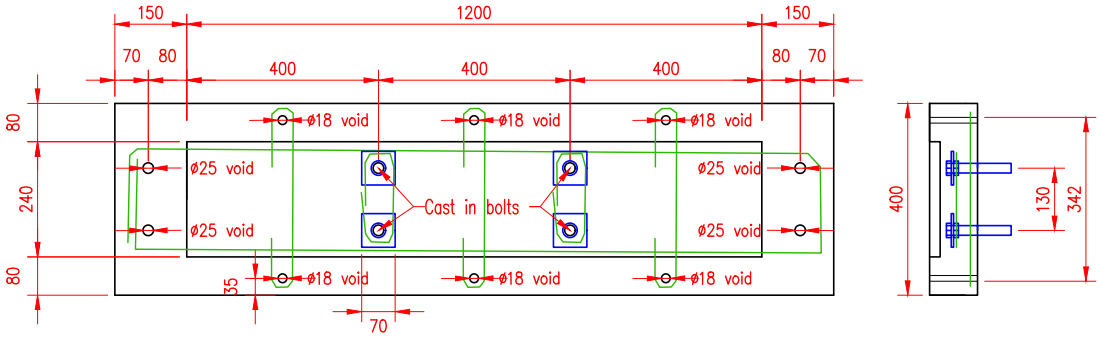

Figure 4.7: Concrete beam drawing.

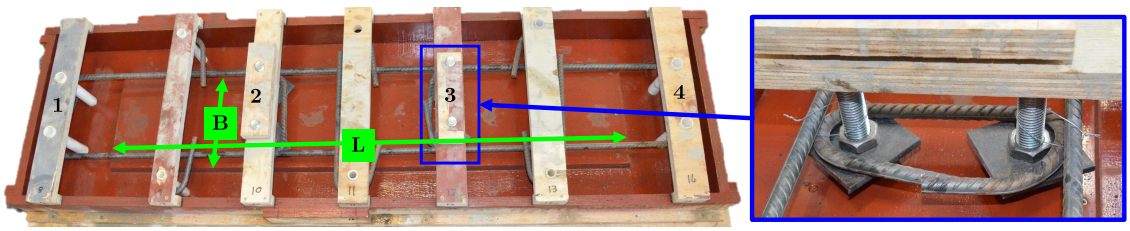

Figure 4.8: Wooden beam moulds with bolts and reinforceing steel used for top and bottom concrete beams.

Figure 4.9: Freshly cast SCC used for top and bottom beams.

After the concrete beams had gained sufficient strength, all of the SWS's were built in a single day by a skilled bricklayer (see Appendix A, Figure A.5 for SWS storage). A stronger mortar ($w/c = 0.4$) was used between the concrete beams and bricks to ensure that failure would occur between the bricks and not at the concrete mortar interface. The same procedure used to produce the triplet SHCC bond specimen, was used to create the overlay on the SWS. A wooden frame as shown in Figure 4.10, was once again used to achieve the desired overlay thickness after which the overlay was finished with a hand trowel. The SHCC in contact with the concrete beams, at the top and bottom, was also removed to ensure that overlay is only in contact with the masonry.

As mentioned in Section 3.3.2, the overlay was sprayed on the smooth side of the bricks and water cured for 7 days after hardening, by wetting the overlay, daily, with a sprinkler. All the SW specimens were stored at indoor conditions.

(a) (b) (c)

Figure 4.10: (a) Sprayed surface finish; (b) SHCC trowelled flat to the required thickness (15 mm or 30 mm); (c) Finished SHCC overlay, after hand trowelled.

4.4.3 Testing machine and rig

The testing machine used for the SW test is an Instron with a maximum capacity of 500 kN. The standard loading frame used by the machine is an adjustable meccano set. The loading rig had to be planned out carefully to use available structural steel as far as possible and minimize adjustments. The 500 mm thick strong laboratory floor has holes spaced at 920 mm, through which the frame can be post tensioned. The final testing frame and setup, with a SW specimen in place, can be seen in Figure 4.11. This figure refers to photographs that are focused on the lateral - (blue frames- (c) and (h)), vertical support (blue frame- (i)) of the loading beam and a photograph focused on the SW specimen (green frame - (l)), respectively in Figures 4.12a, 4.12b, 4.14 and 4.15.

The test setup was built from salvaged structural steel and the available meccano set elements. Care was taken to ensure that no structural failure would occur if the Instron was testing at it's maximum capacity (500 kN). The design drawing is shown in Figure 4.13.

Lateral support frames were constructed as a safety precaution, to ensure that no out-of-plane movement or failure of the SWS could occur. This is of critical importance as the load spreader beam is bolted to the top of the specimen and the head/load-cell of the Instron. If the wall was to fall over, the 400 kg beam and 500 kg wall would cause significant damage to the Instron as it is not designed to take shear forces. Vertical support at the head of the Instron and under the beam at the far end was also provided. A 5 mm clear spacing was left between the load spreader beam and vertical roller support, to provide free vertical movement and only provide support at accidental failure. The lateral support was provided by rollers connected to the lateral support frames as shown in Figures 4.12a and 4.12b, which provide free movement in the in-plane direction of the wall.

The SWS is installed, by lowering and aligning the bolts that are cast into the bottom concrete beam, into the beam on the ground using the overhead crane. The top load spreader beam, with the springs attached, is lowered onto the beam, once again through precision drilled holes. Four more bolts are then added through the voids in the concrete. This is to ensure that the shear force is evenly distributed into the concrete beams. The top load spreader beam is bolted to the Instron, using 4 bolts, through which the tension force is transferred ((a) in Figure 4.15). The bottom steel beam ((j) in Figure 4.11) is bolted to the column to ensure a closed system. It is also connected to the strong floor with two spreader beams ((b) in Figure 4.15), on either side of the wall, running perpendicular to the bottom beam that the wall is bolted to.

Two additional ground beams, parallel to the beam which the wall is connected to, are used to support the vertical rods. The rods are used to apply a vertical load, simulating the self-weight of the structure. Each vertical rod goes through a drilled hole in a short channel and a LC placed under the channel. The rod passes through the LC as seen in 4.16b and is fixed below with a washer and nut. A 200 kN LC is used to measure the axial force in each rod. This is done to ensure an accurate force reading within the rod, to calculate the vertical pressure subjected to the wall. The channel, which supports the LC, is supported on either side by the parallel beams, which are connected to the floor through the spreader beams.

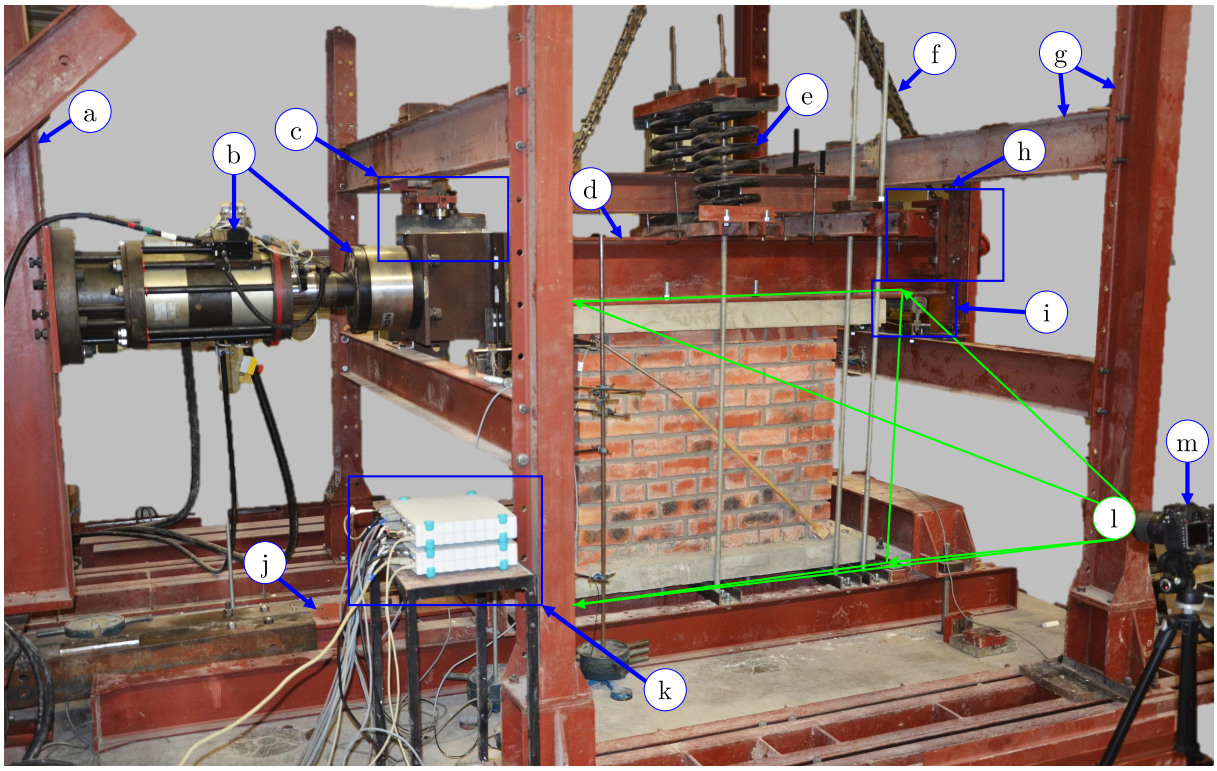

Figure 4.11: The manufactured SW test setup assembled with a wall specimen in place; (a) Instron A-frame column support; (b) Instron hydraulic actuator with 500kN LC attached; (c) Lateral support of Instron, see Figure 4.12a for detail; (d) Shear force spreader beam; (e) Coil springs; (f) Overhead crane chain attachments; (g) Lateral support frame; (h) Lateral support of shear force spreader beam, see Figure 4.12b for detail; (i) Vertical support roller, see Figure 4.14 for detail; (j) Bottom steel beam, that specimen connects to. (k) Spider 8 data acquisition system; (l) SWS and LVDT's positions, see Figure 4.15; (m) Digital camera.

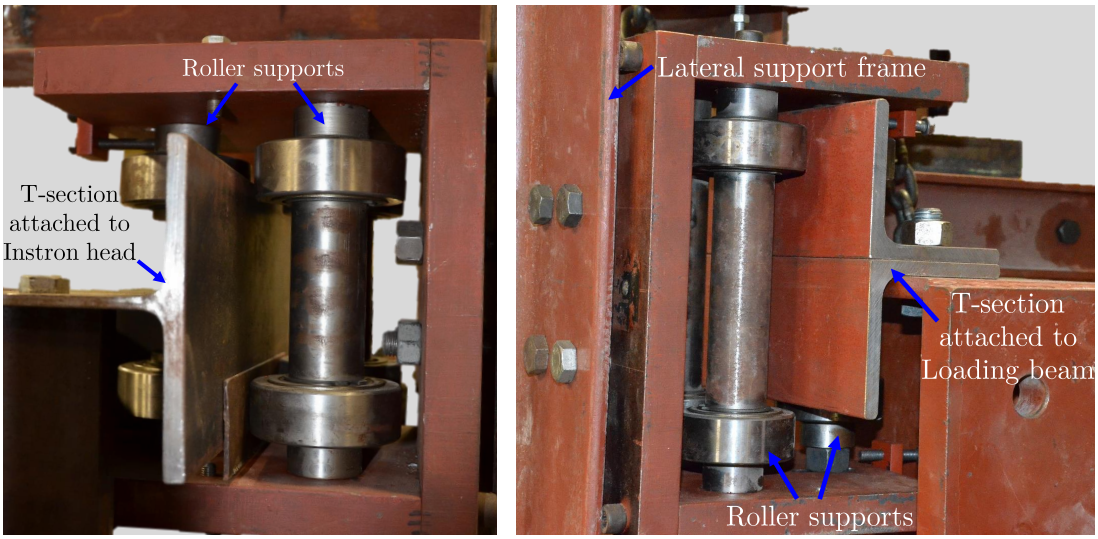

(a) (b)

Figure 4.12: Lateral support, through roller supports, at (a) Instron head and (b) Shear force spreader beam end.

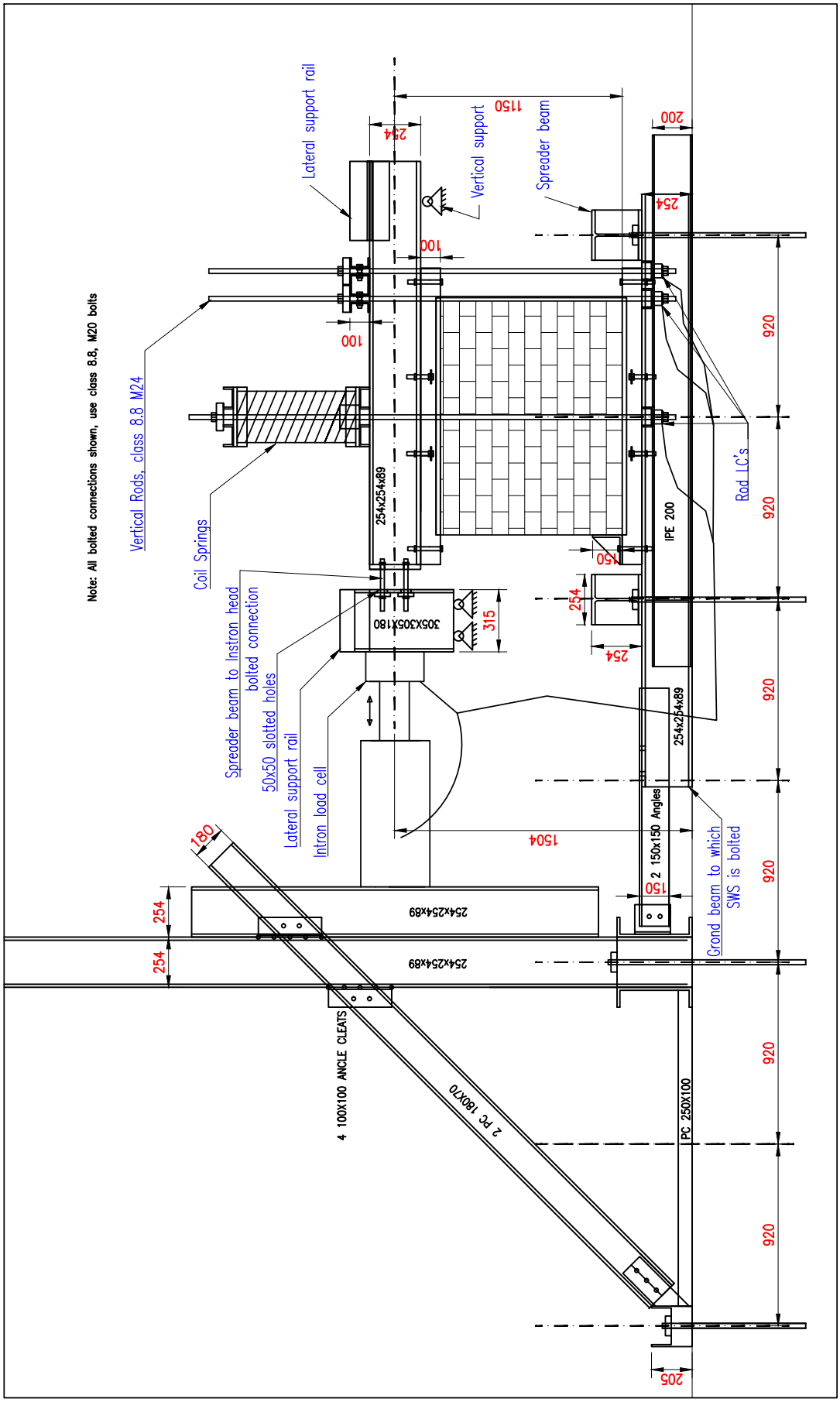

Figure 4.13: Test rig drawing.

Figure 4.14: Close-up view of bottom roller support at the end of the loading beam.

The positions of the LVDT's used can be seen in Figure 4.15 (indicated with red frames). All of the measurements were relative to the floor, with each LVDT positioned in place using clamps and frames.

The horizontal top 100 mm LVDT is positioned on a frame connected to the middle of the top brick. The frame was connected with two screws in drilled holes. This measurement is a crucial reading during the test and is used to obtain the horizontal shear deformation of the wall. Care should therefore be taken to ensure proper alignment of the LVDT in the in-plane direction of the wall, and that there is no movement thereof.

The two vertical 50 mm LVDT's (left and right of SWS) are positioned on a smooth perspex surface, underneath the top concrete beam, 75 mm from the edge as shown in Figure 4.16a. The smooth surfaces are provided to ensure that free movement perpendicular to the LVDT is possible, while only measuring the vertical displacement of each top corner.

The horizontal bottom 10 mm LVDT was positioned on the bottom concrete beam in the in-plane direction similar to the horizontal top LVDT. This measurement was used to detect the slippage in the bottom bolts and ground beam, to calculate the deformation of the wall using the relative movement at the top to that of the bottom. It was not possible to position the LVDT or a frame on the bottom brick, as there was a support ((c) in Figure 4.15), however as there was no sliding shear failure between the bottom row of brick and the concrete beam, the beam movement is assumed to be the same as the corner bricks.

In addition to the horizontal and vertical measurements, two 100 mm LVDT's were fitted diagonally to the front and back side of the SW specimen to measure the diagonal shear deformation between the two corners (indicated by $\star$). The plastic LVDT supports and wooden frames were connected to the specimen, using the same epoxy glue as described in Section 3.3.1. For the SHCC overlay specimens, they were glued to the surface of the overlays.

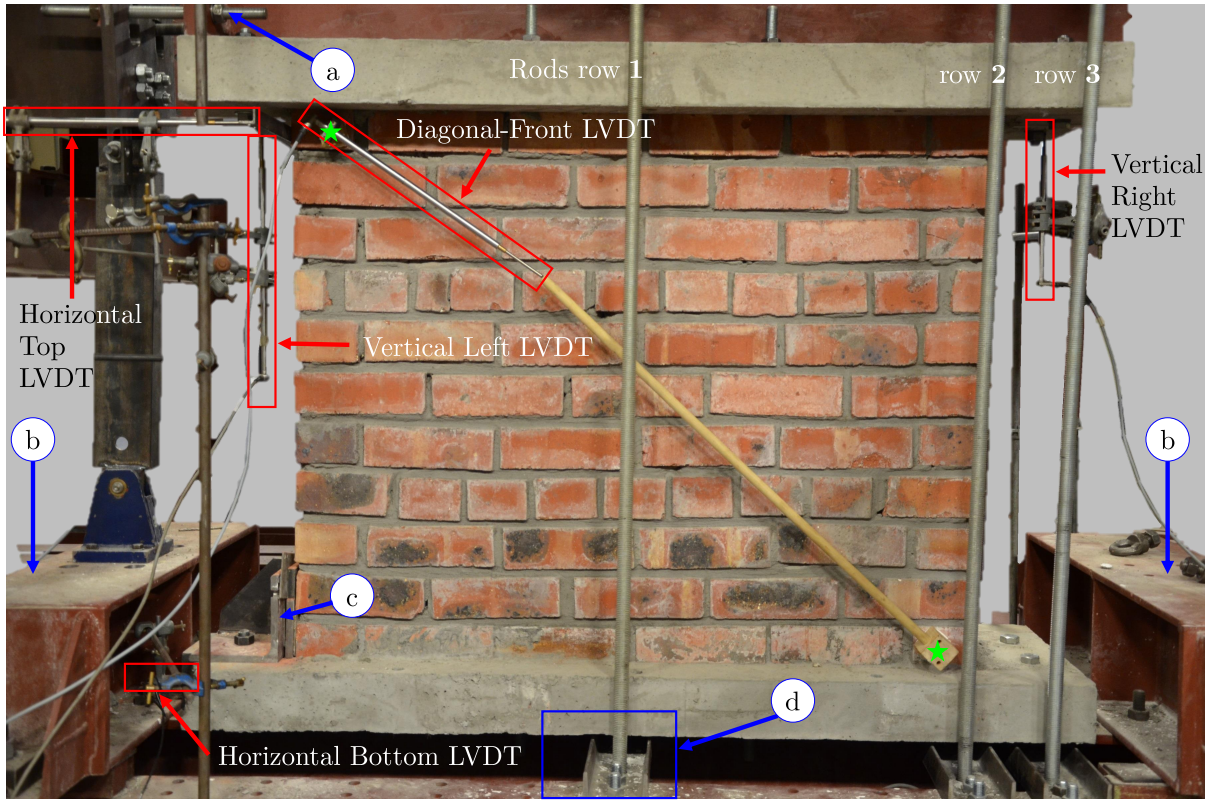

Figure 4.15: Close up view of the SWS inserted into the testing rig, with LVDT's in place and indicated in the red boxes, detail of the vertical LVDT's is shown in Figure 4.16a. Mark:(a) Bolt connection between Instron and loading beam; (b) Transfer beams bolted to bottom beam and strong laboratory floor; (c) Angle section foot stop; (d) Vertical rod, bottom connection to parallel beam, Figure 4.16b shows the detail from below.

(a) (b)

Figure 4.16: Close up views of: (a) Vertical LVDT positioned underneath top concrete beam, sliding on perspex; (b) External LC assembly with the vertical rod passing through the LC, providing an accurate internal rod force reading.

4.4.4 Loading state and boundary conditions

The specimen inserted in the SW test rig is subjected to complex stress states as a result of the shear and vertical compression forces. The shear force induced by the Instron is a tension force at the spreader beam end. The shear force is evenly distributed into the concrete beam through the four rows of two bolts, that connect to the masonry with a strong mortar layer.

A superimposed gravity load was applied to the specimen using two external post-tensioning rods. Coil springs were used with the post-tensioning rods to avoid increment in the post-tensioning force due to the increment in the specimen height caused by flexural cracks opening and dilatancy behaviour of masonry. Two additional rows of rods were used in a fixed configuration, where an increase in rotation/height will result in a increase in normal force. This configuration was used to ensure that diagonal cracks due to shear would occur. Without this additional proportional increasing normal force, the specimen would fail in flexure/rocking, leading to horizontal cracking at the bottom. This is a function of the aspect ratio and vertical compression to shear strength. The position of the rods was determined such that the resultant of the three rods work in at a lever arm equal to the height of the shear force (1150 mm). This is elaborated in Section 5.4.2.1.

As the SW test is not a standardized test, no specifications exist for the vertical normal force and the control system for the shear force. From literature and calculations of vertical pressure in typical URM walls, a vertical pressure of 0.35 MPa was decided on. Higher constant vertical pressures are also not possible with the spring mechanism used in this research. The shear force was applied by a displacement controlled action of the Instron head, at a rate of 2 mm/min.

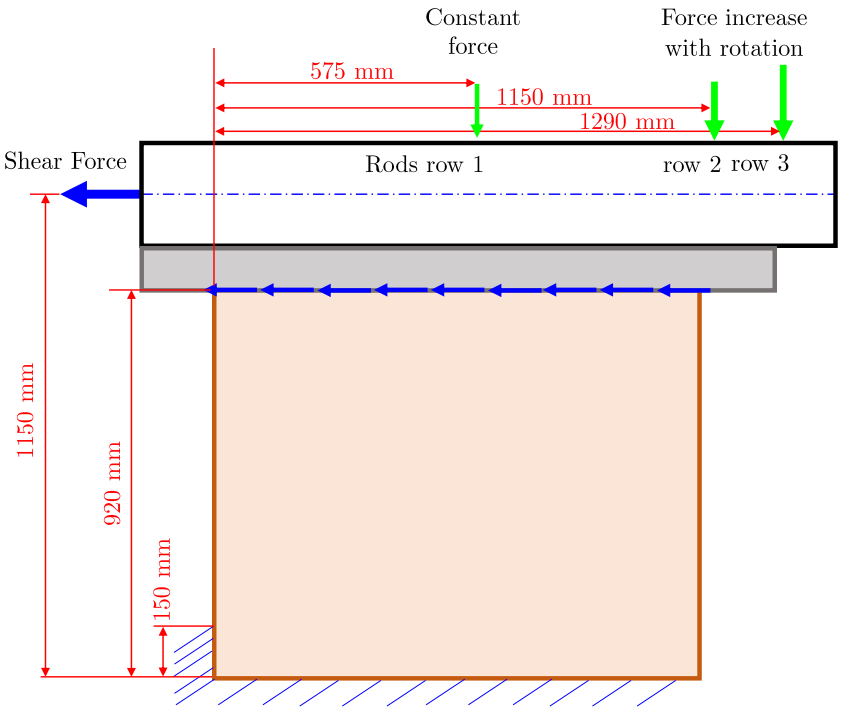

Figure 4.17: Free body diagram of SW test.

4.4.5 Data collection

All of the test data was collected using a Computer and Spider 8 data acquisition system from HBM. Data form the LVDT's and LC's were collected at a sampling rate of 5 Hz. The Instron's load and displacement was also connected to this system. Cracking was also documented with a high resolution 16 mega pixels digital camera at a rate of 12 photographs per minute.

Chapter 5

Results and Discussion

5.1 Introduction

The results of the tests described in Chapter 4 are presented and discussed here. The results are presented and discussed in the same order in which the test methods were introduced in Chapter 4 and include the characteristic material properties of normal mortar, masonry units, mortar-masonry interface and masonry-SHCC interface. The strength and ductility enhancement that SHCC brings about is also quantified from the additional non-standardised tests that were performed. This chapter will make use of the notation specified in Section 4.2 and the number of specimen tested can be found in Table 4.1. Lastly, a mathematical performance prediction model for the design of bonded SHCC overlays is presented.

5.2 Characterising test results

5.2.1 Compressive strength

As described in Section 4.3.1, the compressive strength of the mortar was determined from 50 mm cubes. The mean cube compressive strength of the mortar specimens are listed in Table 5.1, also indicating the associated Coefficient of Variance (CoV) of the different tests for each result. The compressive strength was used to compare strengths and also to identify batch inconsistencies. The test age of specimens made from mortar of the batches used to build the triplets (T0-06) and modified triplet specimens (MT) was 21 days, being the same test age as the corresponding triplet specimens. The mortar specimens from the SWS were tested at the age of 28 days.

The data in Table 5.1 indicate that the mortar complied with a class I specification ($f_{cm} >$ 14.5 MPa) according to SANS 10164-1 (1989) Table 1. There was also sufficient consistency between the different batches of mortar, with the CoV around 10%. The reason for the stronger mortar of the triplet and modified triplet specimen as opposed to the SWS, can possibly be ascribed to the batch size and mixing procedure. Additional water was added by the brick layer to achieve the desired workability. The small difference and consistency through the same tests

were deemed satisfactory.

Table 5.1: Mortar cube compressive strength (f_{cm}) results.

Specimen	Age (days)	no samples	f_{cm}	CoV (%)
T0-06,MT	21	30	24.33	11.5
SWS	28	9	20.23	9.3

The compressive strength of the individual bricks (f_{bu}) was measured according to the test procedure specified in Section 4.3.1. Six randomly selected bricks were tested and an average f_{bu} of 44.5 MPa with a CoV of 10.5% was found. These values are typical for bricks used in URM and falls within the specifications set out in SANS 10164-1 (1989) Table 3.

5.2.2 Shear strength of brick-mortar bond

The shear strength of the brick-mortar bond (f_{mb}) was determined according to the triplet test method stipulated in Section 4.3.2. Six specimens were tested at each confinement pressure (T0,T03,T06) respectively. The results are presented in Figure 5.1, with each point being the calculated shear stress and corresponding confinement pressure. The shear force versus MTM head displacement graphs for specimens T0-110-0, T03-110-0 and T06-110-0 from which the maximum stresses were determined, can be found in Appendix B, Figure B.1a to B.3f. The residual friction coefficient (θ_R) was calculated by dividing the post peak resistance with the corresponding confinement pressure of specimens T03-110-0 and T06-110-0 which is presented in Figure 5.1.

The average initial shear bond strength (ϕ) (determined from specimens T0-110-0) is 0.277 MPa with a CoV of 81.4%. For specimens T03-110-0, f_{mb} is equal to 0.61 MPa with a CoV of 12.0% and for specimens T06-110-0, f_{mb} is equal to 0.93 MPa with a CoV of 18.9%. The friction coefficient is 1.08, calculated from a linear trend line, with a correlation coefficient (R^2) of 0.75. The large CoV (81.4%) for the initial shear bond strength indicates the variability in masonry performance prediction. The shear area for these specimens are however relatively small, compared to a wall where the average of a row of bricks would sum to the shear strength, decreasing variability.

The shear strength of the mortar and masonry used in this research is thus as follows:

$$f_{mb} = 0.277 + 1.08 \cdot g_A \tag{5.1}$$

Where, f_{mb} is a tested average and not the characteristic shear strength (f_v) as in Equation 2.1.

The average residual friction coefficient (θ_{R03}) for specimens T03-110-0 is 0.916 with a CoV of 5.68% and for specimens T06-110-0, θ_{R06} is equal to 0.893 with a CoV of 6.97% . The average residual friction coefficient is 0.896, calculated from a linear trend line (dashed line in Figure 5.1)

with a y-intercept of zero (no friction at zero confinement pressure), with a correlation coefficient (R^2) of 0.95.

The residual (frictional) shear strength of the mortar and masonry used in this research is thus as follows:

$$f_R = 0.896 \cdot g_A \tag{5.2}$$

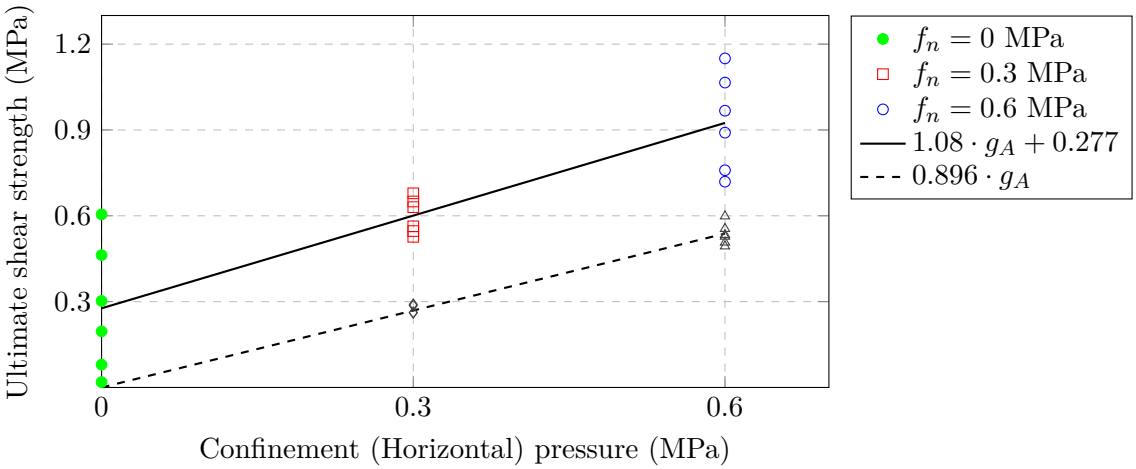

Figure 5.1: Triplet mortar-brick shear results

The different failure modes, for the specimen tested at different confinement pressures are shown in Figures 5.2 and 5.3. Specimens T0-110-0, shown in Figure 5.3a failed on a single bed joint, while specimens T03-110-0 and T06-110-0, shown in Figures 5.3b and 5.3b) failed at both mortar joints. In some cases (eg. T06-110-0-5) both mortar joints failed simultaneously, leading to higher shear forces, while in other cases (eg. T06-110-0-1) the one side failed, followed by a drop in force and then an increase up to a second failure of the other side. This is visible in Figure 5.2. This variation in failure modes enlarges the variability in the results, especially at no confinement pressure. Shear failures through the mortar were also observed where confinement pressures were applied as shown in Figure 5.3c.

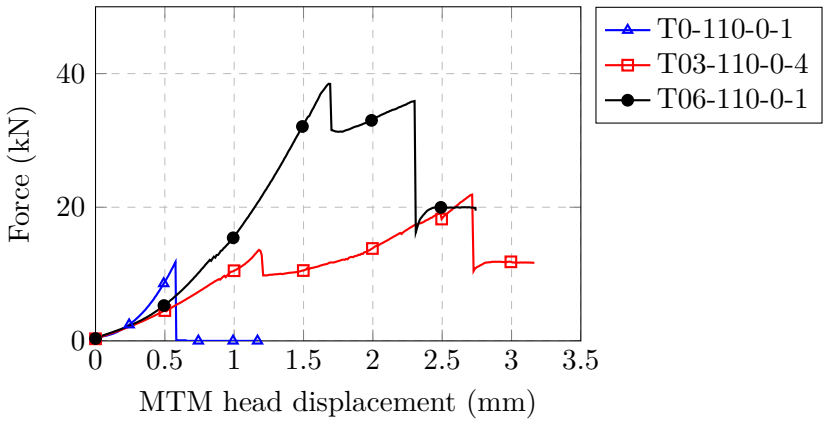

Figure 5.2: Typical triplet response at different confinement pressures

(a) (b) (c)

Figure 5.3: Failure modes for different confinement pressures, (a) 0 MPa (T0-110-0-1) (b) 0.3 MPa (T03-110-0-4) (c) 0.6 MPa (T06-110-0-3)

5.2.3 SHCC-brick shear bond strength

5.2.3.1 General

The SHCC-brick shear bond strength ($f_{\tau-SHCC}$) tests were conducted on five specimen according to the specifications described in Section 4.3.3. This important parameter controls the overlay thickness that should be applied to a certain area. As a ductile failure through the overlay is required, the shear strength (V_{SHCC}) of the cross-sectional area of bonded SHCC overlay needs to be less than the bond strength of either side of the shear failure of the overlay. This expressed as follow:

$$V_{SHCC} < A_{SHCC} \cdot f_{\tau SHCC} \cdot RF_b \tag{5.3}$$

Where

V_{SHCC}	is the shear strength of the cross-sectional area under consideration, (N)
A_{SHCC}	is the bonded area of the overlay on a single side of the shear plane, (mm^2)
$f_{\tau SHCC}$	is the bond shear strength between the brick and SHCC, (MPa)
RF_b	is the Reduction Factor for the bond, which accounts for the decreased area due to localized de-bonding

5.2.3.2 Stress on the bond interface

The bond shear strength of the SHCC was calculated by dividing the peak shear force by the SHCC bond area in contact with the two faces of the central brick. The area to which the SHCC bonded was 2 $\times$ 222 $\times$ 70, where the factor 2 accounts for the overlay on both sides. At the peak resistance, the mortar bond was already impaired and all the force was assumed to be resisted by the overlay. This can be seen in Figure 5.4, where the mortar bond of TO-110-0-1

failed at 1.2 mm and the specimens (T0-110-60) with an overlay only failed at around 2 mm MTM head displacement.

The peak resistance is not purely resisted by the overlay, as there is still friction between the mortar bed joints and bricks. This friction force was zero for specimens T0-110-0, as a result it simply fell apart after peak load was reached, but for specimens T0-110-60, there was a friction force of $f_R \times A_{mb}$, where f_R was determined to be $0.896 \cdot g_A$ in Section 5.2.2. This force comes from the confinement that the overlays provide and the restraining of the mortar joints to enlarge during dilatation behaviour as described by Van Zijl (2004). The normal confinement pressure g_A is however unknown at ultimate failure of specimens T0-110-60. As this additional strength effect comes about only after the SHCC overlay was added, and that the SHCC will have to resist the tension force from the dilatation, it is assumed that the total peak load is resisted by the bond area. Further Finite Element (FE) analysis need to be conducted to more accurately determine the pure bond strength.

5.2.3.3 Results

The SHCC bond shear strength results are presented in Figure 5.4 and Table 5.2, where the shear forces are plotted against MTM head displacement and the calculated bond strength values for each specimen are presented respectively.

The brittle bond failure is observed in Figure 5.4 where a sudden drop after peak force is observed for all specimen tested. The average SHCC bond strength was calculated as 2.30 MPa with a CoV of 29.32%. This is considered to be a significant bond resistance, whereby the composite resistance can be significantly increased.

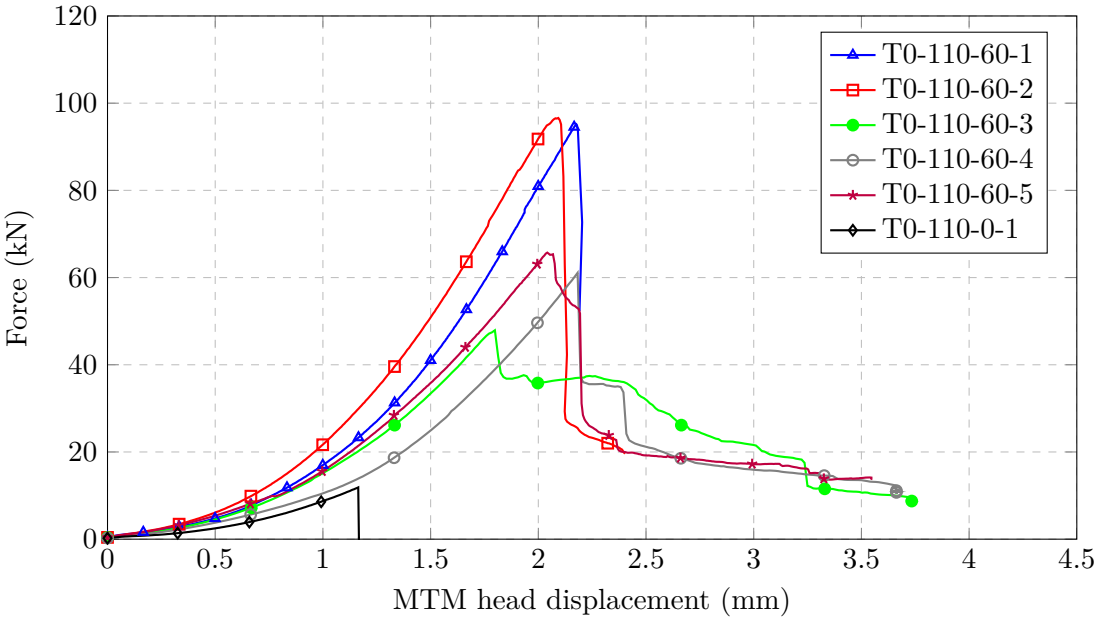

Figure 5.4: SHCC bond shear strength test results

Table 5.2: SHCC bond shear stress calculated.

Sample	Bond strength (MPa)	Comments
T0-110-60-1	2.978	Debond-smooth face
T0-110-60-2	3.022	Debond- both sides
T0-110-60-3	1.507	Masonry failure through shear keys
T0-110-60-4	1.917	Debond-smooth face
T0-110-60-5	2.061	Debond-smooth face
Average	2.30	
CoV (%)	29.32	

The failure modes can be seen in Figure 5.5. The smooth face of the bricks debonded, while the grooved side of the brick showed shear failure through the grooves of the brick. This additional mechanical interlock provided a stronger bond on the grooved side and the typical failure that was observed was a failure where a rotation towards the smooth face, would de-bond the whole overlay on the smooth face, as shown in Figure 5.5a (Specimen T0-110-60-1), while shear failure through the brick occurred on the grooved side, as shown in Figure 5.5b (Specimen T0-110-60-2). Combination of failure surfaces was also observed and shown in Figure 5.5c (Specimen T0-110-60-5). The failure patterns for Specimen T0-110-60-2,3&4 can be seen in Figure A.7.

(a) T0-110-60-1 (b) T0-110-60-2 (c) T0-110-60-5

Figure 5.5: SHCC shear bond test failure mechanisms:(a) Bond failure on smooth face of brick; (b) Shear failure through ribbed face of brick; (c) Combination of failure surfaces.

5.2.4 SHCC overlay shear strength

5.2.4.1 General

The shear strength (f_{SHCC}) and ductility enhancement of a bonded SHCC overlay on masonry were evaluated with the modified triplet shear test described in Section 4.3.4. Ten MT specimens were tested, five of which had a 10 mm SHCC overlay on both sides (MT-110-20) and five control specimens (MT-110-0) with no overlay. The average bottom displacement of the central group of bricks being pushed through was used to evaluate the ductility enhancement that SHCC brings about.

Specimen MT-110-0-2, MT-110-20-2, and MT-110-20-3 failed in bending through the centre due to inperfections in the specimen dimensions. The above mentioned specimen was supported only at the far outer edges, and the test behaved similar to a 4 point bending test. These results were thus not included, but the failed specimens are shown Figure A.6, in Appendix A.

5.2.4.2 Test validation

The initial shear strength (ϕ) results for specimens MT-110-0 is shown in Table 5.3, where the average was 0.225 MPa with a CoV of 82.5%. This is in reasonable agreement with the results from specimens T0-110-0 presented in Figure 5.1, where an average of 0.277 MPa with a CoV of 81.4% was determined. The failure mode was similar for the two test methods, with a single mortar-brick bond failure on one of the shear planes. The test method was thus deemed satisfactory for determining the additional shear strength and ductility that SHCC brings about.

Table 5.3: Modified Triplet shear test results for specimens MT-110-0.

Specimen	Peak shear force (kN)	Mortar shear strength (MPa)
MT-110-0-1	5.01	0.126
MT-110-0-3	17.42	0.438
MT-110-0-4	0.93	0.023
MT-110-0-5	12.43	0.313
Average	8.95	0.225
CoV (%)	82.5	

5.2.4.3 Shear stress calculation

The shear stress in the SHCC was calculated by dividing the peak resistance by the cross-section area of the overlay across the shear planes. As for the bond strength calculation presented in Section 5.2.3.2, it was assumed that the mortar resistance would have been lost at the peak

resistance displacement. This assumption is supported by Figure 5.6, where the average base displacement for specimens MT-110-0 was around 0.6 mm, while peak resistance for specimens MT-110-20 was only reached at displacements larger than 1.3 mm.

The cross sectional area was determined as an averaged thickness value from measurements (taken to an accuracy of 0.5 mm.) after failure, multiplied by the actual overlay height.

5.2.4.4 Results

The SHCC shear strength results are presented in Table 5.4 and Figure 5.6, where the shear forces are presented against average base displacement and the calculated SHCC shear stress values for each specimen are presented respectively. The displacement of each of the four LVDT's together with the average is shown in Figure C.1. The average base displacement, when the shear force decreased to 9.0 kN after the peak load, where 9 kN corresponds to 0.225 MPa for mortar brick bond strength of specimen MT-110-0, was also listed in Table 5.4.

The average ultimate shear force for specimens MT-110-20 was 5.2 times that of the control specimens (MT-110-0). An average shear stress of 5.06 MPa was calculated, which is in reasonable agreement with the findings by Van Zijl (2007) that the shear capacity of SHCC is roughly 1.5 times that of the tensile strength. Recall that the average tensile strength of the SHCC developed here is 2.19 MPa (sprayed) and 2.62 MPa (cast) - Table 3.3. The 1 to 1.5 MPa over strength of the SHCC can be ascribed to the friction in the failed mortar bed joints. The stress in the SHCC is thus not 5.06 MPa, but it however has the effect of 5.06 MPa by adding confining pressure for friction forces to exist.

The ductility increased significantly, as can be seen by the gradual loss in post-peak resistance with increased shearing displacement of the central set of bricks. The post peak displacement at 9.0 kN for specimens MT-110-20 was on average 6.4 times more than the average displacement at 9 kN for specimens MT-110-0.

Table 5.4: Modified triplet shear test results with calculated SHCC stresses.

Specimen	Peak shear force (kN)	SHCC shear stress (MPa)	Displacement at 9.0 kN
MT-110-20-1	37.74	4.13	4.61
MT-110-20-3	50.29	5.51	3.93
MT-110-20-5	50.60	5.54	2.99
Average	46.21	5.06	3.84
CoV (%)	15.88		21.17

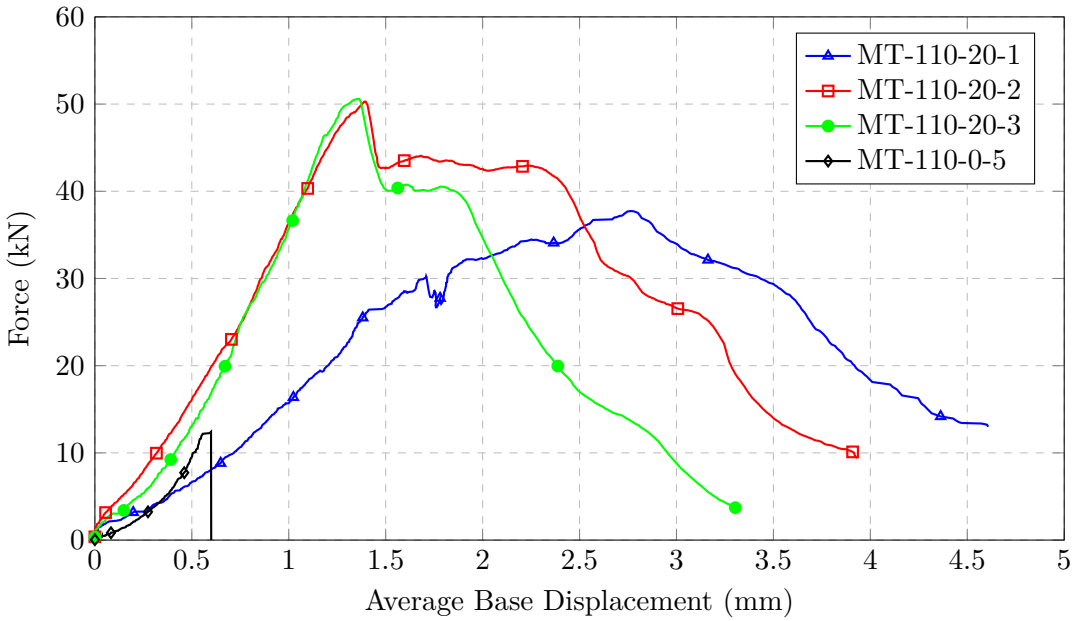

Figure 5.6: Modified triplet shear force displacement test results.

5.2.4.5 Failure mechanism and crack pattern

The MT-110-20 specimens showed a ductile post peak response, due to the multiple fine cracking phenomenon explained in Section 3.2.3. After the initial crack formed, localized debonding occurred around the crack region followed by the next crack through the SHCC. This process continued until a localization crack formed.

Failed specimens MT-110-20-1, 3 and 5 is shown in Figure 5.7, with the multiple cracking visible in the zoomed photo of Figure 5.7a. Flexural cracks in the centre at the bottom were also observed, but the ultimate failure was a shear failure. A postulation is that the different force displacement response in Figure 5.6 of Specimen MT-110-20-1 compared to MT-110-20-3 and 5 is from this initial bending deflection.

The failures differed on the smooth face from that on the grooved face of the bricks. The SHCC on the smooth face showed a debonding and crack kinking behaviour as described by Stander (2007), with a wider cracked area and number of cracks forming. The final localized crack on this face formed away from the shear plane. The grooved bond had a more localized failure pattern around the mortar shear plane. The final localized crack was more vertical and closer to the shear plane, as shown in Figure 5.7b and 5.7c, where the grooved face corresponds to label '3A' and '5A' and label '3B' and '5B' to the smooth face.

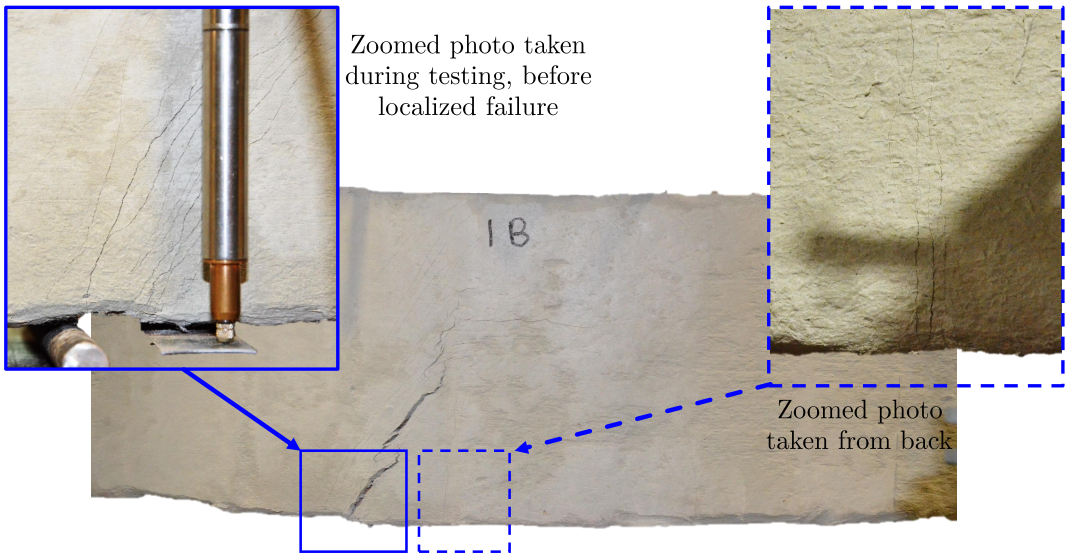

(a) MT-110-20-1.

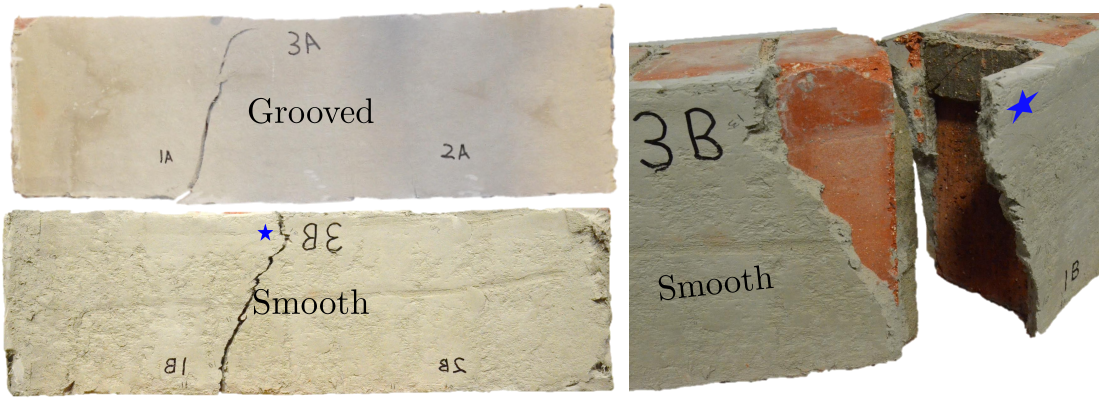

(b) MT-110-20-3.

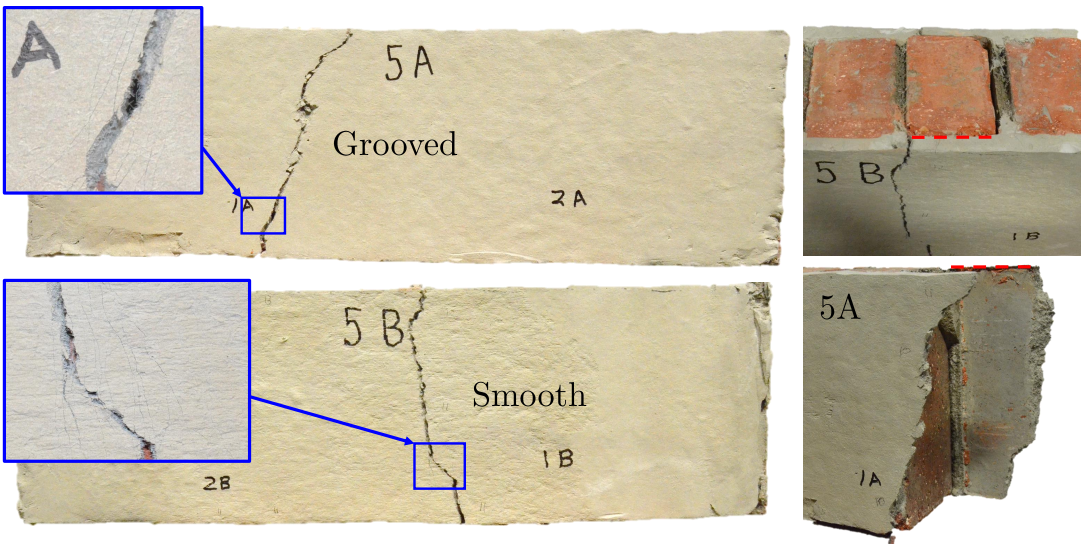

(c) MT-110-20-5.

Figure 5.7: Failed MT shear specimen with 10mm overlay on both sides.

5.2.5 Summary and concluding remarks

From the characterising test results presented in this section the following conclusions are drawn:

- The average compressive strength of the solid clay bricks used is 44.5 MPa, while the mortar has a class I specification and an average compressive strength of 24.3 MPa for the specimens elaborated in this section.
- From the standard triplet test results, the initial shear bond strength of the mortar joint was determined to be 0.277 MPa, with a friction coefficient of 1.08. Using the same test, the shear bond strength of the SHCC overlay was determined to be 2.30 MPa for the materials tested.
- In a modified triplet test with larger specimens and 10 mm thick bonded SHCC overlays on both faces, multiple shear cracking formed in the overlays, leading to ductile shearing response of these specimens. The MT specimens with an overlay, showed an ultimate resistance increase of 5.2 times, compared to the control specimen, with the SHCC having an effective shear strength of 5.06 MPa. A significant (6.4 times) increase in post-peak ductility was evident for all specimens with overlays, compared with the control specimens.

The SHCC overlay material and shotcrete overlay strategy is shown to significantly enhance the mechanical performance of masonry wall parts. The values determined during these tests formed the basis of Section 5.3, for determining test parameters and overlay thicknesses for the SWS.

5.3 Shear wall test results

5.3.1 Introduction

The measurement and analysis of data from URM SW tests conducted under the conditions described in Section 4.4 provide a method for determining SHCC retrofitted SW performance, that is representative of actual multi-storey URM shear walls.

Two single brick SWS, a control specimen without an overlay (SW-110-0-1) and one with a 30 mm overlay (SW-110-30-1) were initially tested under different loading conditions and are shortly discussed, followed by the results of eight specimens tested according to the specifications introduced in Section 4.4. The eight SWS consisted of two single skin (110 mm) walls, one without and one with a 30 mm overlay (SW-110-0-2 and SW-110-30-2) and six double skin (220 mm) walls, three without and three with a 15 mm overlay (SW-220-0 and SW-220-15). Typical results and data are presented, followed by the response and cracking behaviour of each SWS. These results are then summarised and used to produce a performance prediction model for SHCC overlay retrofitting.

5.3.2 Initial test results

5.3.2.1 SW-110-0-1

Specimen SW-110-0-1 was tested at a constant vertical pressure of 0.35 MPa, with no force increase with rotational increase. Three rows of two springs placed at the centre of the wall and 420 mm to either side of the centre was used as shown in Figure D.1. The loading state was cyclic with an incremental displacement of the Instron head to a maximum displacement of $\pm 20\ mm$ as shown in Figure D.4a.

This loading state and boundary conditions caused the wall to fail in flexure on both sides, followed by a sliding and rocking motion on the second row of bricks. The opening of the flexure crack can be seen in Figure D.2, with the vertical displacement over time shown in Figure D.4b. The hysteretic loop of the shear forces versus the absolute top displacement is shown in Figure D.3. The relatively low vertical force with a small lever arm, led to the wall showing a tension failure on the one side, followed by the other side during the reversed load cycle.

The bottom beams of the test rig moved during the test due to bolts slipping into place before carrying there load, resulting in a larger push cycle than pull cycle. This is also visible from the vertical displacement over time shown in Figure D.4b.

In order to fail a SW specimen in diagonal shear, the rotation and rocking failure has to be prohibited. The was done for the SW test on SW-110-30-1 by fixing the end rods, which will thus increase the vertical force and counter the overturning moment. The slippage of the bottom beams was also minimized with additional supports.

5.3.2.2 SW-110-30-1

Specimen SW-110-30-1 was tested under cyclic loading with a 2 mm incremental displacement of the Instron head to a maximum displacement of ± 35 mm as shown in Figure D.9a. The vertical force in the central rods remained constant, while the forces of the end rods increased with the increase in rotation as shown in Figure D.9b. Two 150 mm high foot stops were added on either side (Figure D.5) to stop the wall form siding and transferring the shear force from the wall to the base.

Specimen SW-110-30-1 initially failed in flexure on both sides, between the bottom row of bricks and strong mortar connecting it to the concrete beam as the 30 mm SHCC overlay was only bonded to the wall and not to the base. The wall started to rock with the foot stops stopping sliding, and the shear and vertical force increased with each cycle as shown on the hysteretic loop of the shear forces versus the absolute top displacement in Figure D.8. The bricks at both wall toes started to crush with the rocking and concentrated forces at the corners as shown in Figure D.6. Debonding of the bottom row of bricks from the SHCC occurred during the third last push cycle, and an increase in displacement can be seen in Figure D.8, with no force increase. The debonded specimen can be seen in Figure D.7. The reason for this failure is the concentrated force from the foot stop and little contribution form friction between the base as bottom row, due to the large rotation and rocking.

For a SW to fail in diagonal shear, the stabilizing moment provided by the vertical force, should be higher than the overturning moment, while rocking and flexural cracks should be minimized to distribute the shear force through the wall into the base. With large rotations the stress concentration at the toes simply crushes the bricks and diagonal shear failure did not occur. During cyclic shearing action, both sides fail in flexural, while a single direction static push over test would only show flexure cracks on one side, while keeping the bond for the other side in tact. This bond is important to transfer the shear force from the wall into the base and testing rig, without failing in sliding shear/flexure.

For these reasons the test method described in Section 4.4 was used, where the rotation was minimized by doubling the number of rods and larger moment lever arms for the outer rods. The static push over method was implemented to ensure flexural cracks only exist on a single side. Although cyclic testing is preferred to asses the ductility and post peak failure similar to what is expected in an earthquake, static single direction push over test have previously been used and strength, ductility and failure mechanisms can still be assessed.

5.3.3 Shear Wall test

5.3.3.1 Typical results and interpretation

The typical SWS response during a test according to specifications described in Section 4.4 is introduced. As some of the data is less critical an overview is provided for understanding the SWS behaviour during the test, and not provided for each individual SWS as similar behaviour for all SWS was observed.

The springs connected to the centre row of springs were tensioned before the test to the correct force (14 kN for SW-220), while a right and far right rows of rods were fixed with a nut and tightened to induce a force (9 kN for SW-220) (See Figure 4.15 for positions of the rods). During the test the force in the central rods (Row 1) remained constant, while the force in the fixed right side rods (Rows 2 & 3) increased as shown in Figure 5.8a. The sum of the six rod forces plus the weight of the top beam are the total vertical force applied from which the vertical pressure is calculated by dividing the force with the cross sectional area of the wall. For the vertical LVDTs on the left and right of the wall as shown in Figure 4.15, a positive displacement is recorded when the movement is towards the LVDT and a negative displacement is recorded when the movement is away. The increase in rod forces with a negative (upwards movement of concrete beam) in vertical displacement on the right side of the SW and positive (downwards movement of the concrete beam) vertical displacement on the left is shown in Figure 5.8b.

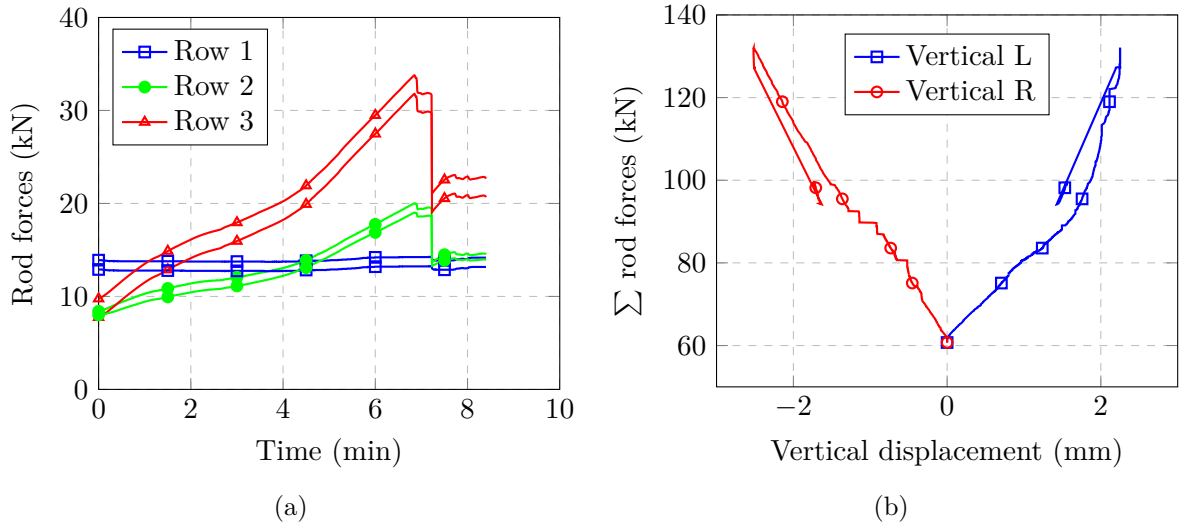

Figure 5.8: (a) Rod forces vs top horizontal shear deformation; (b) Rod forces vs vertical displacement left and right of SWS.

Figure 5.9a shows the sum of the vertical forces applied and the shear force versus test time. The initial vertical force increases slightly as the shear force is applied, up until a flexural crack starts to open, after which the vertical forces increase at the same rate as the shear force. This one to one ratio of vertical to shear force application, after the flexural cracked formed (90-130 kN shear force) is shown in Figure 5.9b where the vertical force in relation to the shear force is presented. This is an important characteristic of this test that is used in Section 5.4.2.1 to

distinguish the resistance by the masonry from that of the SHCC overlay.

The post peak response, where the shear force and vertical force remains relatively constant can be seen in Figure 5.9a. This comes from the friction of the mortar brick interface sliding on the horizontal failure surfaces while the vertical cracks open. The drop in vertical force is from the backwards rotation of the bottom part of the SW after diagonal shear failure.

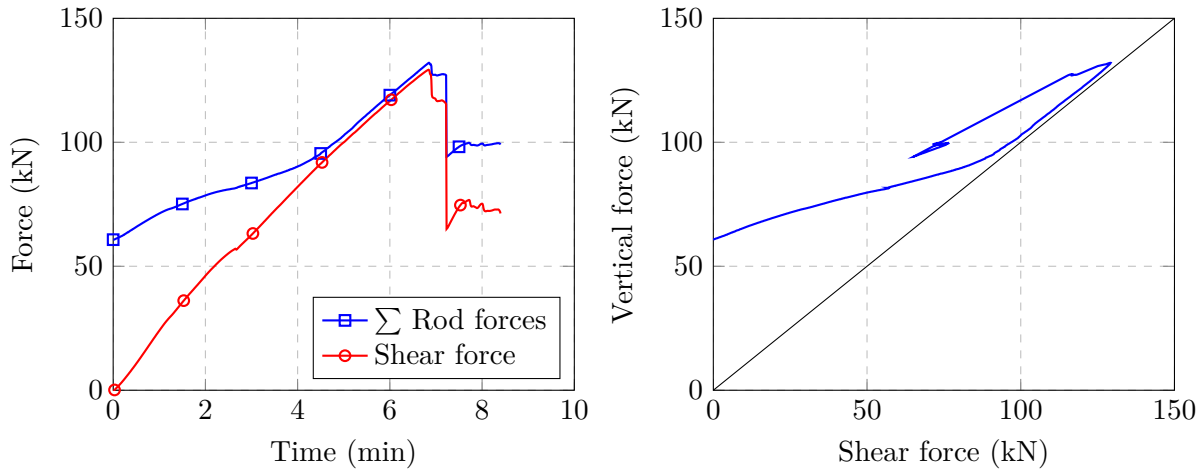

(a) Rod forces vs top horizontal shear deformation.

(b) Shear force versus vertical force.

Figure 5.9: (a) (b) Right of SWS.

The results of all the SW tests are presented followed by a summary in Figure 5.33. In the next two sections to follow a concise description of observed measurements of each SW test is reported and explained. For the Control SW (SW-110-0-1 and SW-220-0), Figures 5.10,5.12,5.14a and 5.16a show the shear force in relation to the absolute top displacement, with the stress also indicated on a secondary vertical axis. (Refer to Section 4.4 for the position of the LVDT's and determination of the absolute top displacement). Figures 5.11a,5.13a,5.15a and 5.17a show the cracked SWS after testing while Figures 5.11b,5.13b,5.15b and 5.17b show the cracks marked out on a drawing. The diagonal shear crack failure occurred in all of the tests.

5.3.3.2 Control SWS

SW-110-0-2

The SW test of SW-110-0-2 tested at an age of 78 days resulted in the shear force (red line) and vertical force (blue line) as shown in Figure 5.10. No flexural cracks formed and thus the vertical force and shear force did not join and follow the one to one ratio as introduced in Figures 5.9a & 5.9b. At a shear force of 60.28 kN and a displacement of 1.146 mm, a localized diagonal shear crack started to form and a drop in load is observed. The shear force increased once again to the same load and stabilized while the crack started to grow and the displacement increased up to 1.721 mm and an ultimate shear force of 62.14 kN (V = 75.58 kN) (corresponding vertical force) was reached. A sudden, localised crack formed with the load decreasing to 49.5 kN and displacement increased with 0.5 mm in 0.4 seconds. Sliding of the horizontal bed joints continued, with a steady decline in resistance due to the friction area decreasing as the vertical cracks open and the bricks slide on the bed joints in the crack path. A friction coefficient of 0.725 was determined from the shear and vertical force at 3 mm displacement.

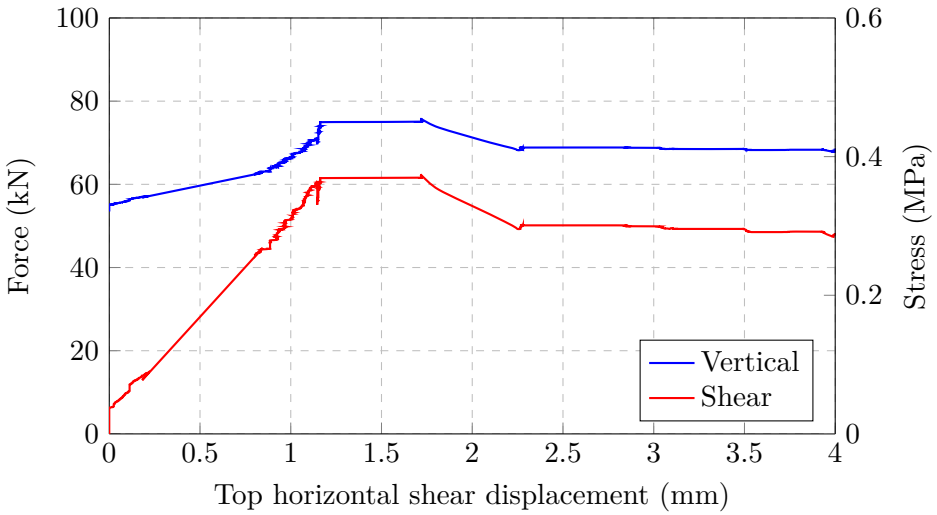

Figure 5.10: SW-110-0-2 shear and vertical force vs shear deformation.

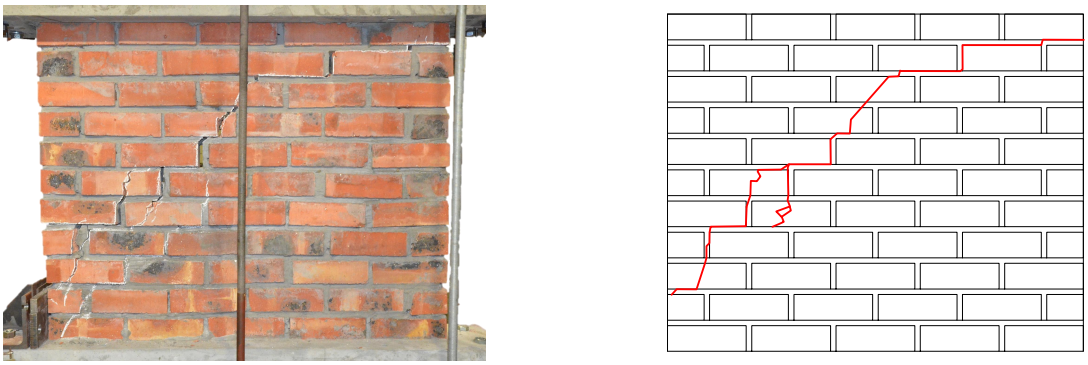

(a) (b)

Figure 5.11: SW-110-0-2 (a) Cracked specimen; (b) Crack pattern documented

SW-220-0-1

The SW test of SW-220-0-1 tested at an age of 84 days resulted in the shear force (red line) and vertical force (blue line) as shown in Figure 5.12. It should however be noted that the horizontal top LVDT malfunctioned during the test, and the Instron head displacement was used for the graphical representation in Figure 5.12. A flexural crack formed at the bottom right corner between the concrete base and bottom row of bricks at a shear force of 50 kN, as shown in Figure 5.13b.

A brittle diagonal shear crack formed at the ultimate shear force of 201.5 kN (V = 229.75 kN). The sudden drop in load is an indication of the brittleness of the failure where the vertical cracks between the bricks opened by 3 mm in 0.6 seconds. This crack opening is shown in Figures A.8a to A.8c. After the crack formed, sliding along the horizontal bed joints commenced until the test was stopped. A friction coefficient of 0.69 was determined from the shear and vertical force at the end of the test.

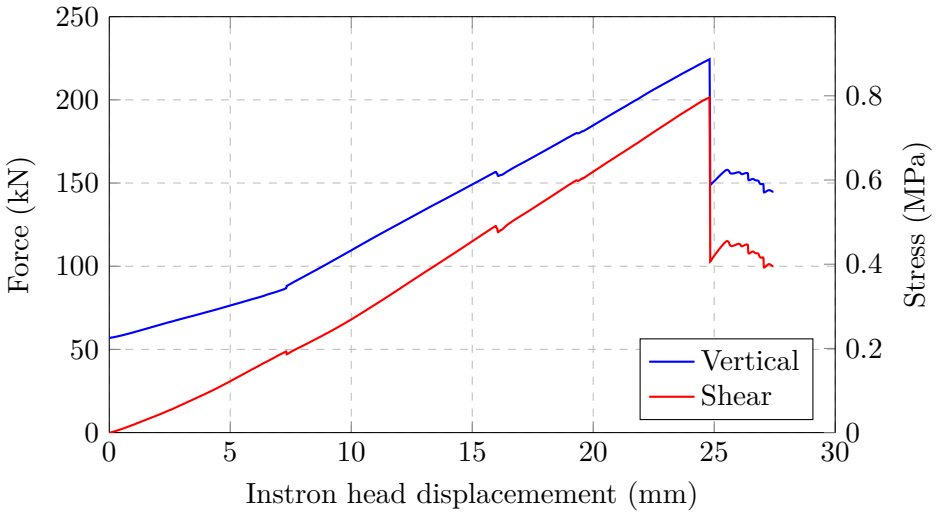

Figure 5.12: SW-220-0-1, shear force vs Instron head displacement

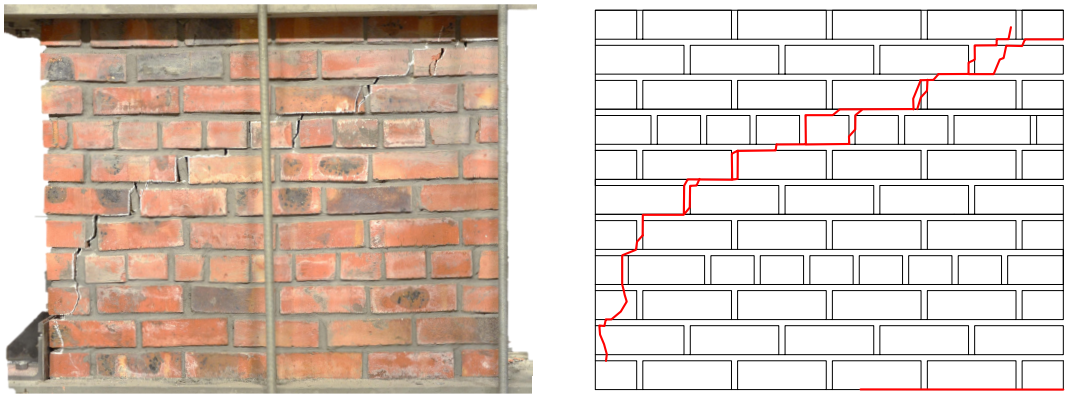

(a) (b)

Figure 5.13: SW-220-0-1 (a)Cracked specimen; (b) Crack pattern documented

SW-220-0-2

The SW test of SW-220-0-2, tested at an age of 85 days, resulted in the shear force (red line) and vertical force (blue line) as shown in Figures 5.14a and 5.14b. A flexural crack formed at the bottom right corner between the first and second row of bricks as shown in Figure 5.15b. A shorter flexural crack with less rotation compared to SW-220-0-1 meant that the wall behaved similar to SW-110-0-2. At a shear force of 127.54 kN and a displacement of 3.21 mm, the primary diagonal shear crack formed (crack running from corner to corner in Figure 5.15b) and a drop in load, with increase in displacement is observed (drop more clear in Figure 5.14b). The crack grew and branched off until a peak shear force of 132.86 kN (V=159.16 kN) at a displacement of 5.394 mm was reached. Sliding of the bed joints commenced followed by an increase in shear force due to rotation and increased vertical force. Secondary branched cracks at the top right side of the wall formed. Pure sliding along the horizontal cracks was not observed and a friction coefficient thus not calculated.

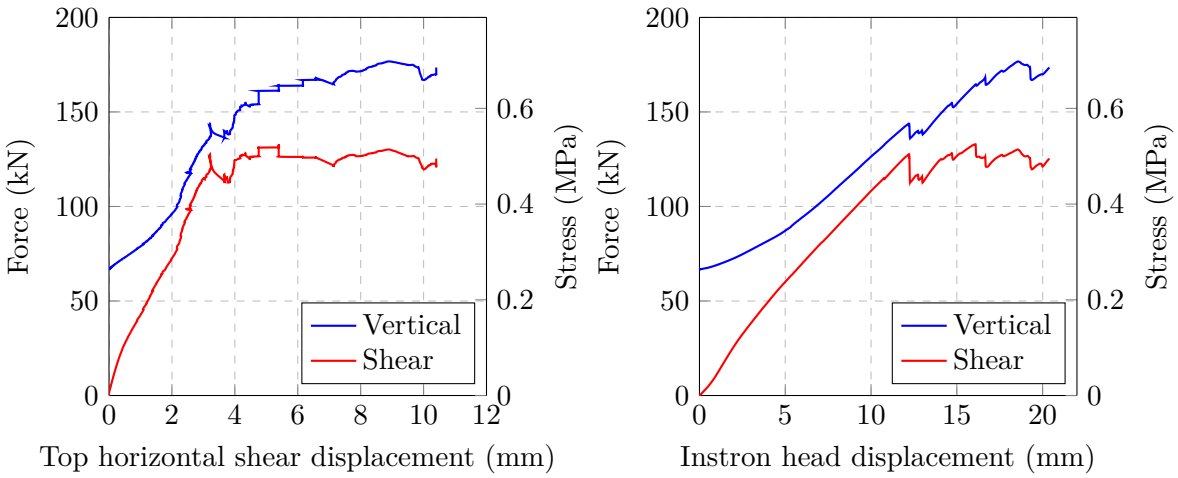

(a) (b)

Figure 5.14: SW-220-0-2, shear force and stress vs (a) Top shear displacement and (b) Instron head displacement

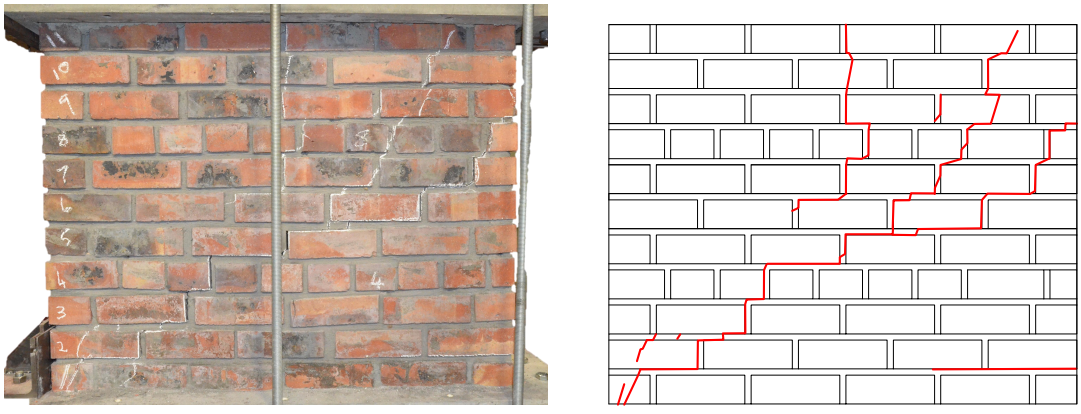

(a) (b)

Figure 5.15: SW-220-0-2 (a) Cracked specimen; (b) Crack pattern documented

SW-220-0-3

The SW test of SW-220-0-3 tested at an age of 148 days resulted in the shear force (red line) and vertical force (blue line) as shown in Figures 5.16a and 5.16b. A flexural crack formed at the bottom right corner between the first and second row of bricks. The crack opening before diagonal shear failure was less than 0.5 mm, which is considered small. At a shear force of 129.24 kN (V=132.05 kN) and a displacement of 5.03 mm, the diagonal shear crack formed and a small drop in load, with increase in displacement observed (drop more clear in Figure 5.16b, where the vertical and shear force lines also part). Sliding along the bed joints commenced for a short period, followed by a sudden drop in resistance and vertical force accompanied by a 2 mm top horizontal displacement. The same response as for SW-220-0-1 was observed with a rapid crack opening and back rotation of the right bottom half. After the crack formed sliding along the horizontal bed joints commenced until the test was stopped. A friction coefficient of 0.71 was determined from the shear and vertical force at the end of the test.

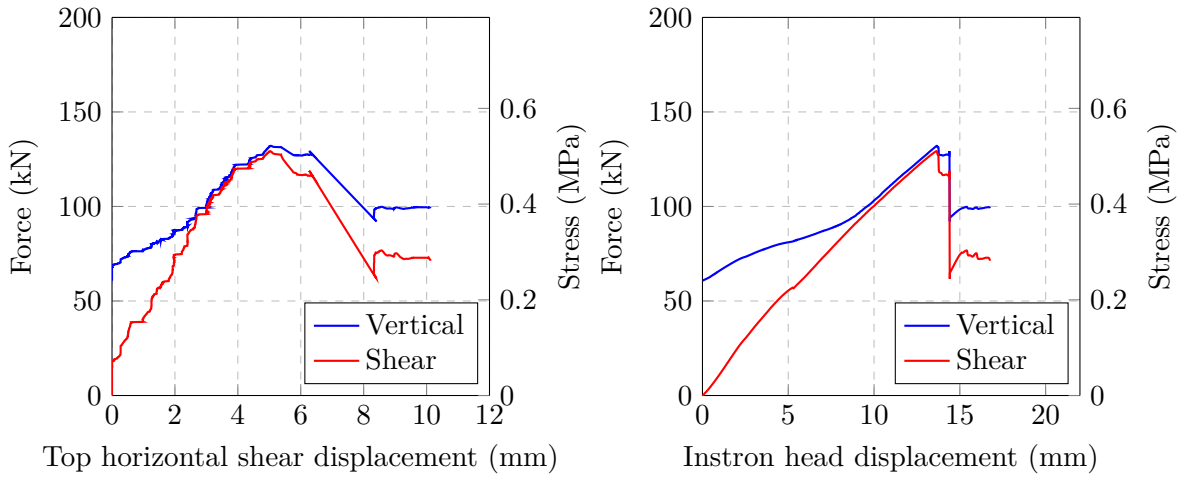

(a) (b)

Figure 5.16: SW-220-0-3, shear force and stress vs (a) Top shear displacement and (b) Instron head displacement.

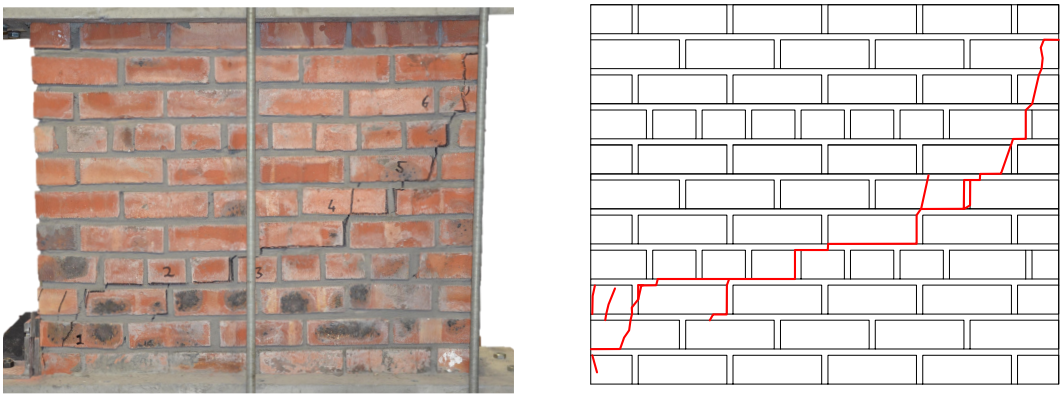

(a) (b)

Figure 5.17: SW-220-0-3 (a) Cracked specimen; (b) Crack pattern documented.

5.3.3.3 SWS with a SHCC overlay

The shear and vertical force against top horizontal displacement for SW-110-30-2 and SW-220-15 are presented in Figures 5.18, 5.21, 5.25 and 5.29 respectively, where plot V1 and S1 (V-Vertical, S-Shear) represent the phase before the SHCC overlay cracked, V2 and S2 the phase during SHCC multiple fine crack forming and V3 and S3 after a localization crack in the SHCC formed and the shear force resisted by mortar bed joint friction. SW-110-30-2 was tested at a masonry age of 80 days with an overlay age of 50 days. The SW tests of SW-220-15 was performed at a masonry age of 142 , 144 and 147 days with an overlay age of 14 days. The effect of the masonry age difference was considered negligible.

SW-110-30-2

The shear and vertical force against top horizontal displacement for SW-110-30-2 is presented in Figure 5.18. During the test a large flexural crack, two thirds the length of the wall, formed at the bottom right corner between the concrete beam and bottom row of bricks. The flexural crack is visible in Figure 5.19a and shown zoomed in Figure A.9. At a shear force of 200.5 kN and a displacement of 10.09 mm, the mortar joint between the top concrete beam and wall cracked and started to slide, leading to increased force on the right top foot stop, which cracked the top beam as shown in Figure 5.20a. The horizontal top LVDT was unfortunately not positioned on a frame, connected to the top brick as shown in Figure 4.15 and was positioned on the top concrete beam. As the mortar between the beam and wall failed and started to slide, the top horizontal displacement measurement was affected and did not measure the wall displacement. At the end of the test the wall slid 15 mm as shown in Figure A.10.

At a shear force of 247.2 kN a fine diagonal shear crack formed through the masonry as shown in Figure 5.19. The shear force continued to increase with the force being resisted by the SHCC overlay and friction in the horizontal bed joints. The force continued to increase and follow the response of line S2 in Figure 5.18, with most of the displacement from the beam crack opening and top beam sliding. The test stopped at a maximum shear force of 289.0 kN as the prescribed Instron head displacement was reached. During close inspection, fine 0.1 mm wide cracks were seen on the overlay surface as shown in Figure 5.20b with a pattern as shown in Figure 5.20a.

The crack patterns at the end of the test on the masonry side is shown in Figure 5.19a, with the image mirrored for easier interpretation. A diagonal stepping crack from corner to corner with crack widths of 0.25-0.75 mm was documented.

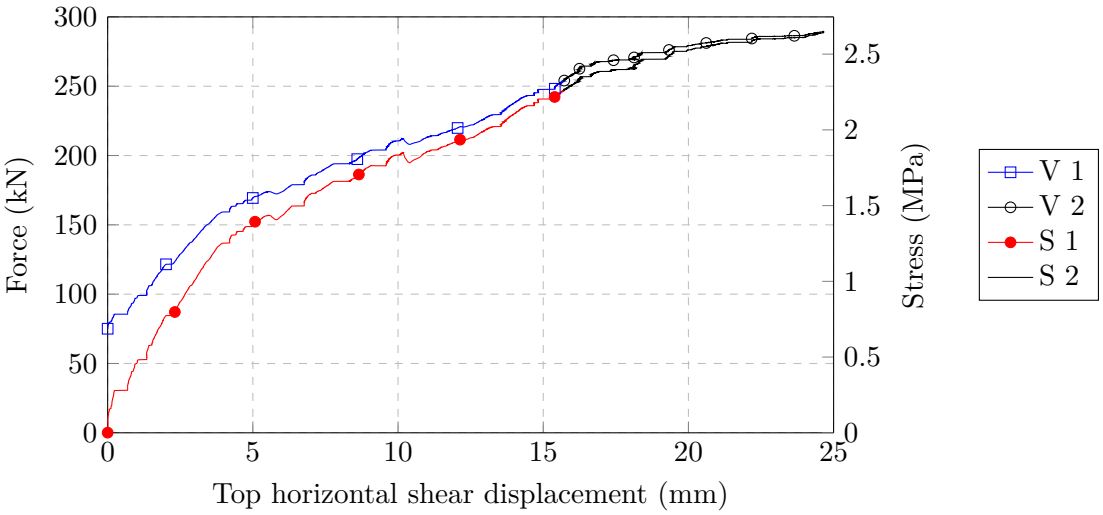

Figure 5.18: SW-110-30-2, Top horizontal shear displacement vs shear force.

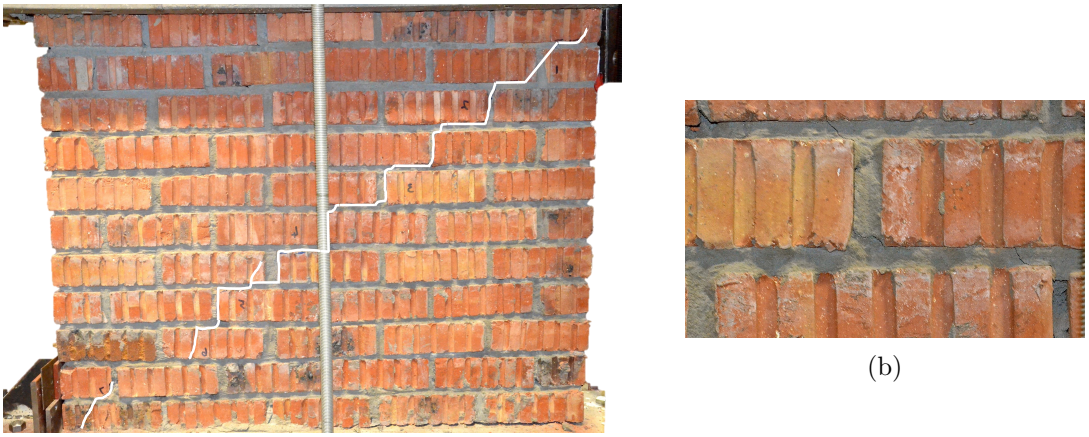

(a) (b)

Figure 5.19: SW-110-30-2 (a) Masonry crack pattern; (b) Focussed on masonry crack initiation.

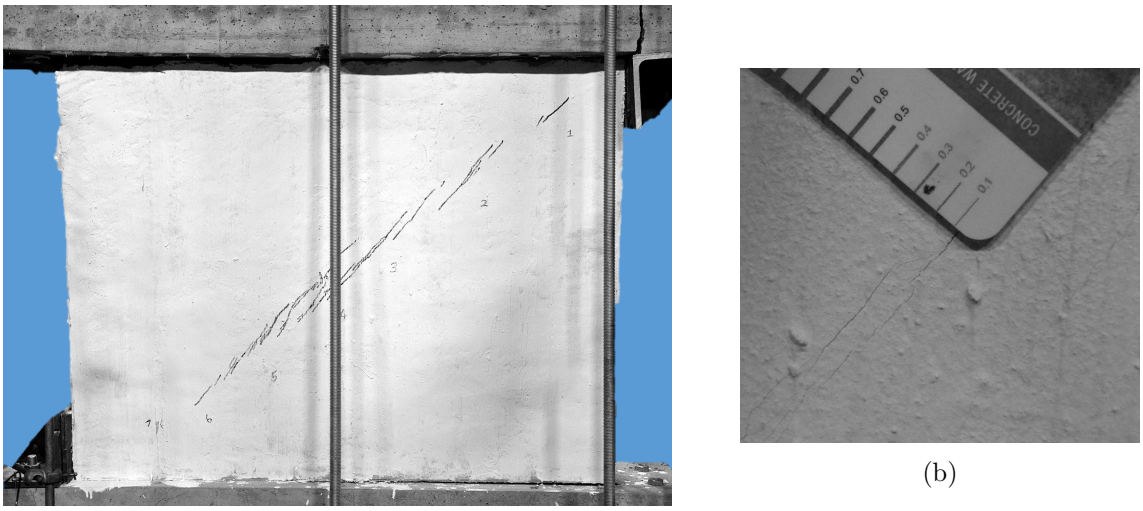

(a) (b)

Figure 5.20: SW-110-30-2 (a)SHCC crack pattern; (b) Focussed on top right box.

SW-220-15-1

The shear and vertical force against top horizontal displacement for SW-220-15-1 is presented in Figure 5.21. A flexural crack, one third of the length of the wall, formed at the bottom right corner between the concrete beam and bottom row of bricks. At a shear force of 246.8 kN (V=269.4 kN) and a displacement of 10.31 mm, a fine diagonal shear crack formed through the masonry as shown in Figure 5.22b. The shear force continued to increase with the force being resisted by the SHCC overlay and friction in the horizontal bed joints. Soon after, at a shear force of 249.74 kN (V=267.87 kN) and a displacement of 10.60 mm, the SHCC overlay started to show multiple fine cracking growing outwards from the diagonal and continued until reaching the peak resistance of 259.82 kN (V=285.22 kN). A localized crack started to form from the centre and growing towards the corners. At a displacement of 14.24 mm the localization crack was fully developed as shown in Figure 5.24a and the bottom corner debonded. This localized debonding of the overlay can be seen in Figures 5.23, where the overlay debonds and slides past the masonry that is restrained by the foot stop. The debonding failure was the onset of a large 10 mm top horizontal displacement and a drop in resistance followed by sliding along the horizontal bed joints until the test was stopped. A friction coefficient of 0.73 was determined from the shear and vertical force at the end of the test. The energy dissipated during the failure of the SHCC (phase 2) is equal to the area under the stress-strain curve. As the stress is a function of force and strain a function of displacement the force displacement graph is used to visually indicate the energy dissipated with the gray area under the shear force in Figure5.21.

The crack patterns at the end of the test on the overlay and masonry side are shown in Figure 5.24a and Figure 5.22a, with the masonry side being mirrored for easier interpretation. The lines parallel to the localized crack in Figure 5.22a show the boundary of the fine cracks that formed, with the fine cracks shown with pencil markings. The overlay localization crack pattern is also shown in blue on Figure 5.22a, with the white lines being the crack pattern through the masonry. The same crack pattern marking scheme is used for other SWS presented next. Unlike the SW-220-0 unreinforced SWS, multiple diagonal cracks with cracks branching out formed through the masonry, adding strength and ductility that the SHCC overlay brings about.

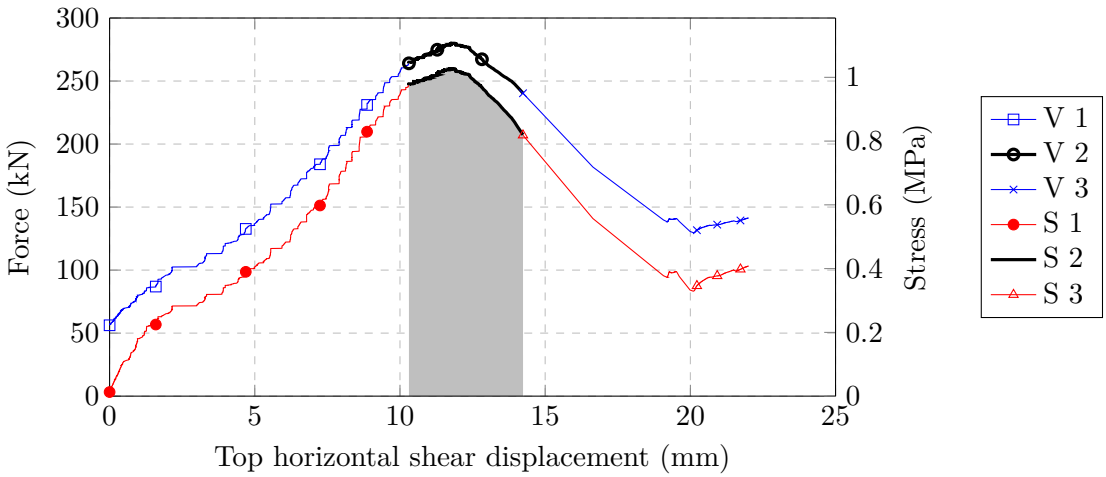

Figure 5.21: SW-220-15-1,Top horizontal shear displacement vs shear force.

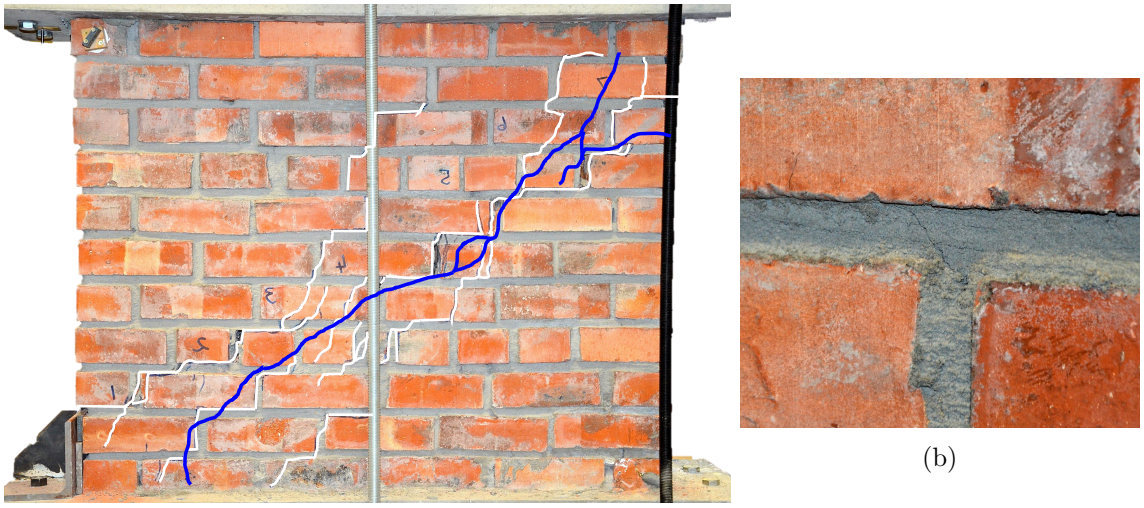

(a) (b)

Figure 5.22: SW-220-15-1 (a) Masonry crack pattern; (b) Focussed on masonry crack initiation.

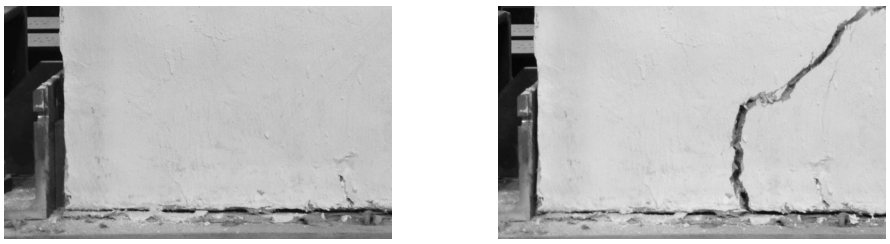

(a) (b)

Figure 5.23: SW-220-15-1 (a) Before debond; (b) After debond.

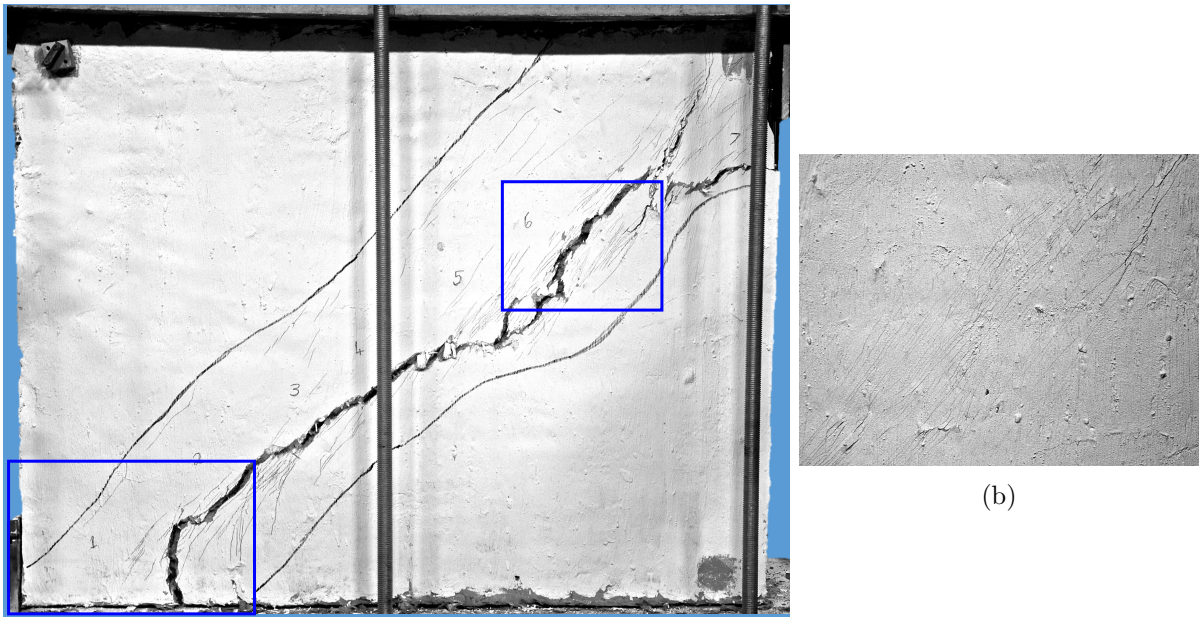

(a) (b)

Figure 5.24: SW-220-15-1 (a) SHCC crack pattern; (b) Focussed on top right box.

SW-220-15-2

The shear and vertical force against top horizontal displacement for SW-220-15-2 is presented in Figure 5.25. A large flexural crack, half the length of the wall, formed at the bottom right corner between the concrete beam and bottom row of bricks as shown in Figure 5.28b. At a shear force of 284.62 kN (V=292.74 kN) and a displacement of 5.41 mm, a diagonal shear crack formed through the masonry. The shear force increased to 286.04 kN with the force being resisted by the SHCC overlay and friction in the horizontal bed joints. At the same point the SHCC overlay started to show multiple fine cracking followed by a localization crack that formed across the diagonal. The localization crack opened rapidly across the diagonal and did not progressively grow as for SW-220-15-1. At a displacement of 5.91 mm the localized crack through the SHCC was formed and the onset of a 6 mm top displacement and drop and resistance followed by sliding along the horizontal bed joints. A second drop followed due to the backwards rotation (closing of flexure crack) of the right bottom side of the wall.

The crack patterns at the end of the test of the overlay and masonry side is shown in Figure 5.26 and Figure 5.28a. The narrower cracking extent of the overlay and single failure path through the masonry led to the less ductile response. Multiple fine cracking through the overlay was however still observed as shown in Figures 5.27.

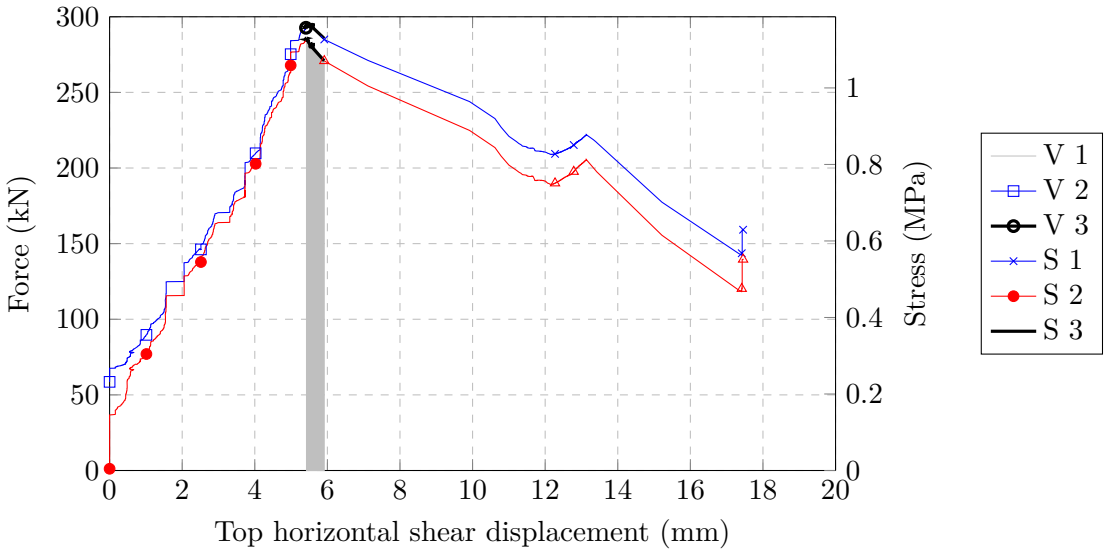

Figure 5.25: SW-220-15-2, Top horizontal shear displacement vs shear force.

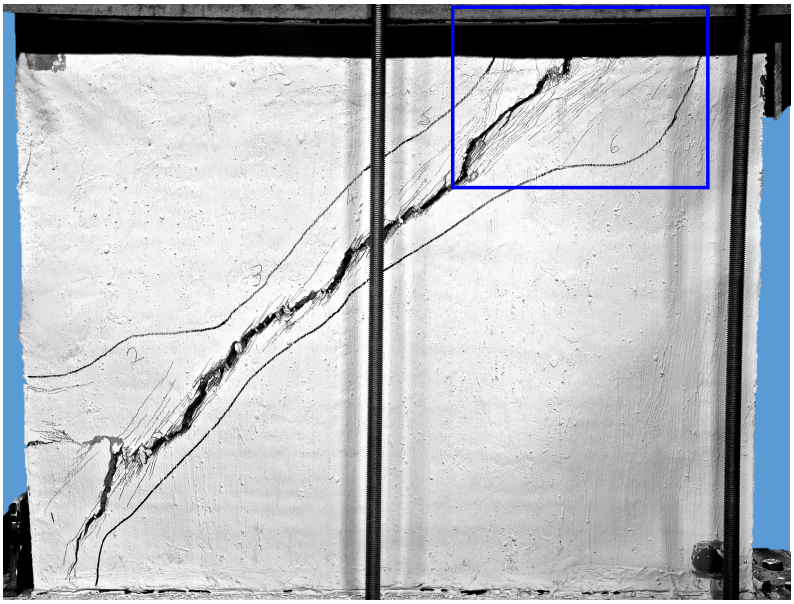

Figure 5.26: SW-220-15-2 cracked pattern with focussed photograph shown in Figure 5.27a.

(a) (b)

Figure 5.27: SW-220-15-2 (a) Focussed with focused box shown in Figure 5.27b ; (b) Multiple cracking around localized crack.

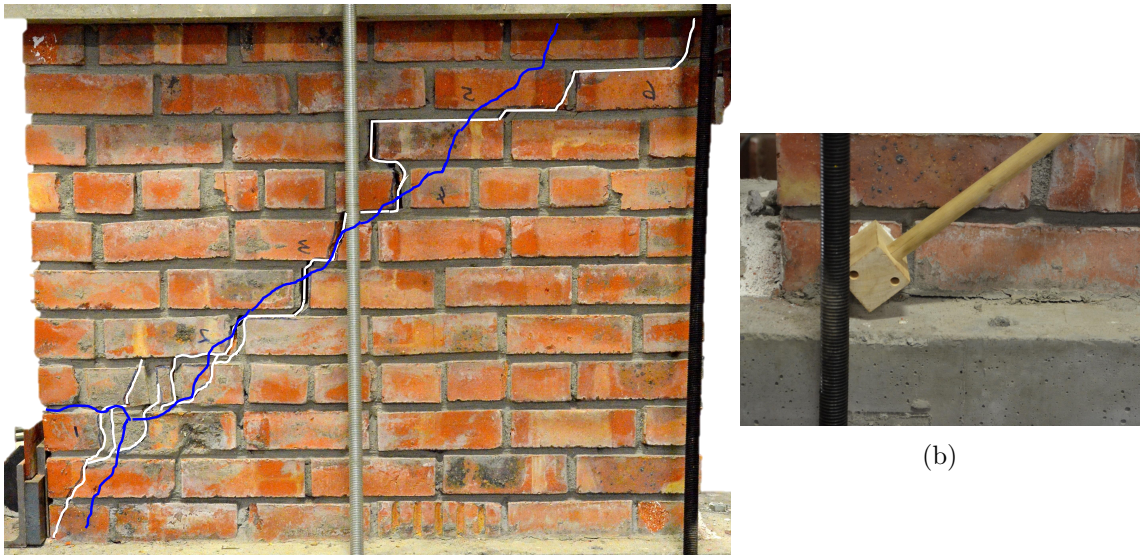

(a) (b)

Figure 5.28: SW-220-15-2 (a) Masonry crack pattern; (b) Focussed on flexure crack.

SW-220-15-3

The shear and vertical force against top horizontal displacement for SW-220-15-3 is presented in Figure 5.29. A small flexure crack, a quarter of the length of the wall, formed at the bottom right corner between the concrete beam and bottom row of bricks. At a shear force of 187.74 kN (V=198.5 kN) and a displacement of 5.71 mm, a fine diagonal shear crack formed through the masonry while the shear force continued to increase, showing similar behaviour as for SW-220-15-1. A secondary crack through the masonry, below the diagonal, formed at the same time, but the crack width grew at a slower pace compared to the primary crack along the diagonal.

The SHCC overlay started to show multiple fine cracking growing outwards from the diagonal and around the secondary masonry crack, until a peak resistance of 238.46 kN (V=250.64 kN) at a displacement of 8.35 mm was reached. A localization crack along the diagonal started to form as shown in Figure 5.31 and grew towards the corners, as the resistance decreased in the post-peak phase. At a displacement of 8.93 mm the localization crack was fully grown as shown in Figure 5.30.

From displacement 9 mm to 10.5 mm stable decrease in resistance is observed that was accompanied by increase in cracking of the SHCC around the second branch masonry crack. A sudden drop in force followed due to both corners showing localized debonding as shown in Figure A.13. Sliding along the horizontal bed joints followed with a decrease in resistance. The vertical and shear force of S3 and V3 can be seen running parallel and slowly diverging, due to the friction area decreasing.

The crack patterns at the end of the test of the overlay and masonry side are shown in Figure 5.30 and Figure 5.32. As in the case of SW-220-15-1, a wide region of multiple fine cracks formed in the SHCC, leading to a ductile response and large energy dissipation compared to SW-220-15-2, with the addition of more cracking paths through the masonry compared to the unreinforced SW-220-0 specimens.

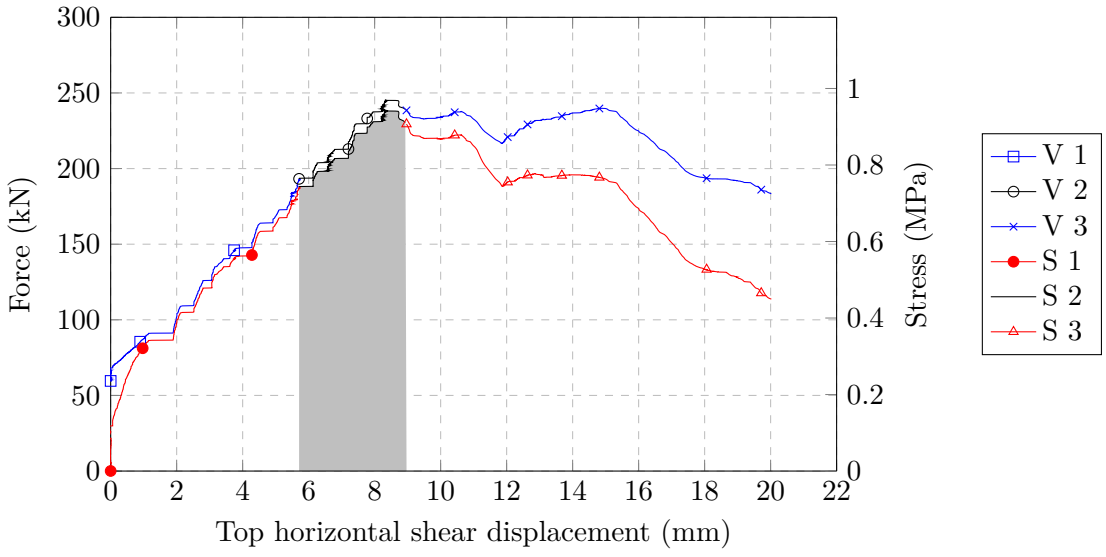

Figure 5.29: SW-220-15-3, Top horizontal shear displacement vs shear force.

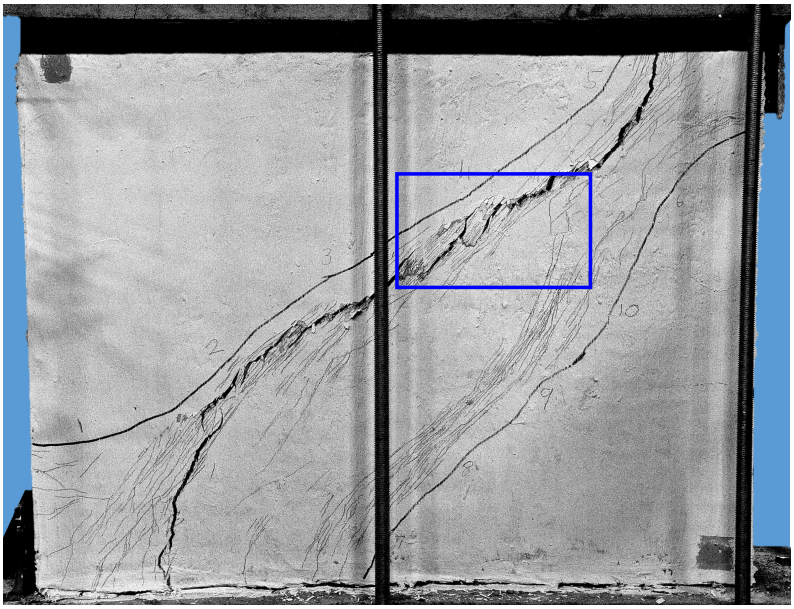

Figure 5.30: SW-220-15-3, Cracked pattern with focussed photograph shown in Figure 5.31 taken before the peak resistance was reached .

Figure 5.31: SW-220-15-3, Localized diagonal shear crack starting to form (before peak resistance was reached).

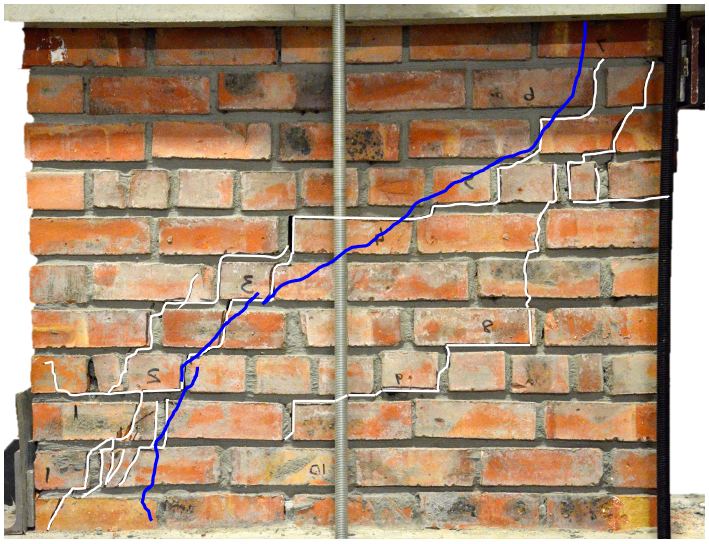

Figure 5.32: SW-220-15-3, Masonry crack pattern.

5.3.3.4 SW summary graph

The strengthening effect of the 30 mm SHCC overlay on the 110 mm thick wall is significant with a peak force of 4.65 times that of the control specimen. The strengthening effect of a thin single side 15 mm overlay is also pronounced, as shown in Figure 5.33. Peak shear and vertical force values during each phase are analysed in the Section 5.4 to distinguish the resistance of the SHCC from that of the masonry.

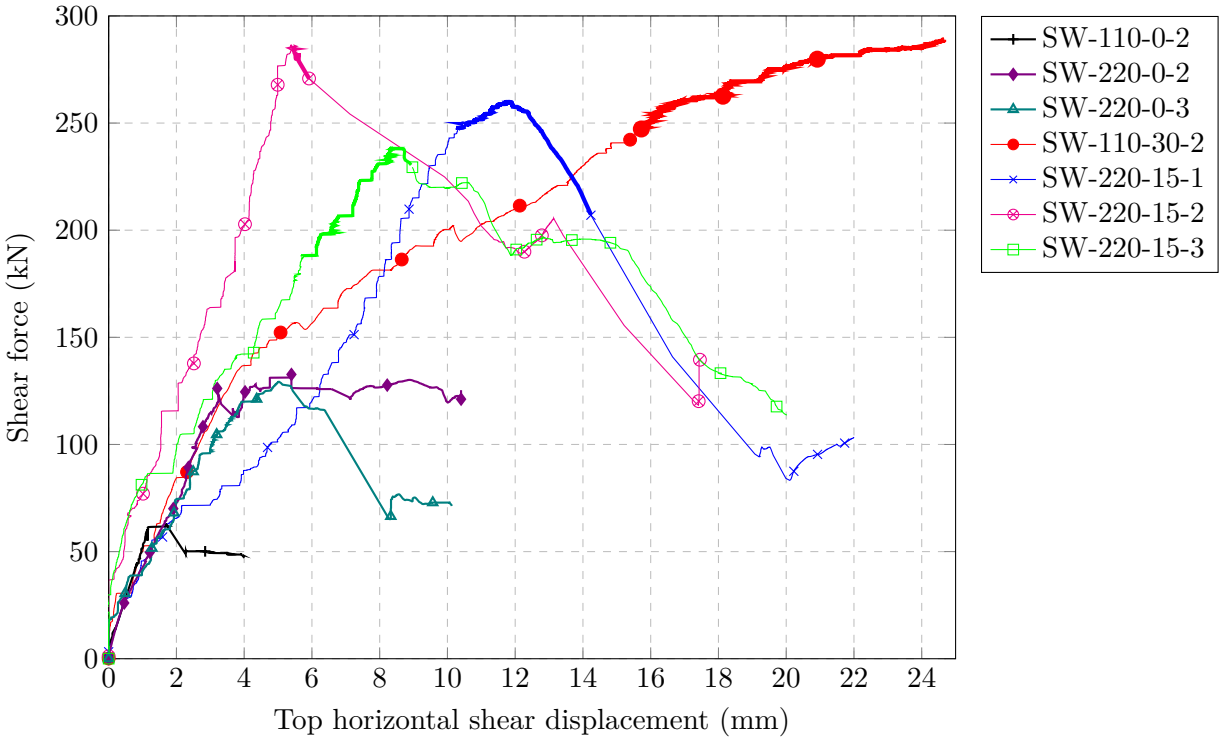

Figure 5.33: Summary graph of all SW tests.

5.4 SW Results comparison

In this section the results of the measured data from Section 5.3 are compared and the SHCC overlay contribution to the shearing resistance is evaluated and summarized.

5.4.1 Control SW test results summarized

The peak shear forces and stresses of the SW tests performed on the control SWS are summarized in Table 5.5 and shown in Figure 5.34. As the vertical force was not constant during the SW tests, the peak shear forces cannot be compared to each other directly, but rather compared to the Coulomb friction model introduced in Section 2.2 and Equation 2.1, as well as the trend lines from the test results. Using the SW-220-0 data points, three trend lines with their corresponding equation and correlation coefficient (R^2) are shown in Figure 5.34. The result from SW-110-0-2 was not used as only a single test was performed and possible differences between the 110 mm and 220 mm wall tests could arise due to their strength difference.

The trend line with a y intercept (initial shear strength) equal to 0.071 MPa and R^2 value of 0.949 is the best fit line. However forcing the y intercept to be 0.15 MPa and 0.2 MPa does not significantly change the R^2 values, as the trend lines intercept between the low number (three) of data points. Triplet results introduced in Section 5.2.2, also encourage a higher initial shear strength.

For the calculation of the strength of the SHCC overlays, it is assumed that the masonry walls behave according to Equation 5.4. This behaviour is in reasonable agreement with SANS 10164-1 (1989), which gives a design formula stated in Equation 2.1. An initial shear strength of 0.35 MPa for a class I mortar stated in SANS 10164-1 (1989) was however not observed in this results of the SW tested in the research.

$$f_v = 0.15 + 0.6775 \cdot g_A \tag{5.4}$$

Where the variables are the same as those introduced in Equation 2.1.

Table 5.5: Control SW shear and vertical force and stress results summarized.

	Force (kN)		Stress (MPa)	
Specimen	Max shear	Vertical	Max shear	Vertical
SW-110-0-2	62.14	75.58	0.600	0.730
SW-220-0-1	201.5	229.75	0.796	0.908
SW-220-0-2	132.86	159.16	0.525	0.629
SW-220-0-3	129.24	132.05	0.511	0.522

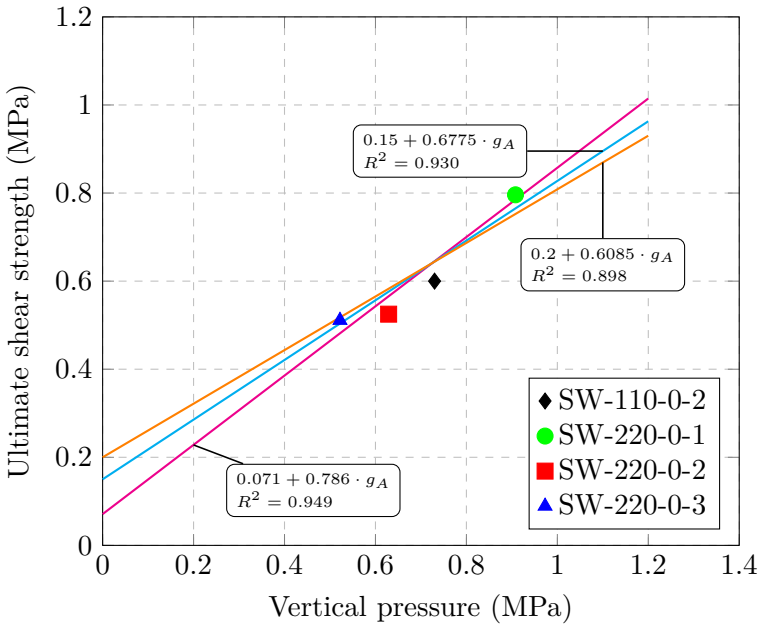

Figure 5.34: Control SW results with trend lines.

5.4.2 SHCC SW test results summarized

The peak shear and vertical forces and stresses during phase 1 and 2 of the results of the SW tests performed on the strengthened SHCC SWS are summarized in Table 5.6 and shown in Figure 5.35. The reader is reminded that phase 1 ends at the force at which the masonry showed diagonal shear cracks, followed by phase 2 which ends when the maximum resistance is reached by the wall (for more detail refer to Section 5.3.3.3). The data points from phase 1 are to the left and below that of phase 2 in Figure 5.35.

Table 5.6: SHCC SW shear and vertical force and stress results summarized.

		Force (kN)		Stress (MPa)	
Specimen	Phase	Max shear	Vertical	Max shear	Vertical
SW-110-0-2	1	247.24	249.36	2.389	2.409
	2	288.98	284.88	2.792	2.752
SW-220-0-1	1	246.80	269.35	0.975	1.065
	2	259.82	285.22	1.027	1.127
SW-220-0-2	1	284.60	297.94	1.125	1.178
	2	286.04	300.67	1.131	1.188
SW-220-0-3	1	187.74	198.50	0.742	0.785
	2	238.46	250.64	0.943	0.991

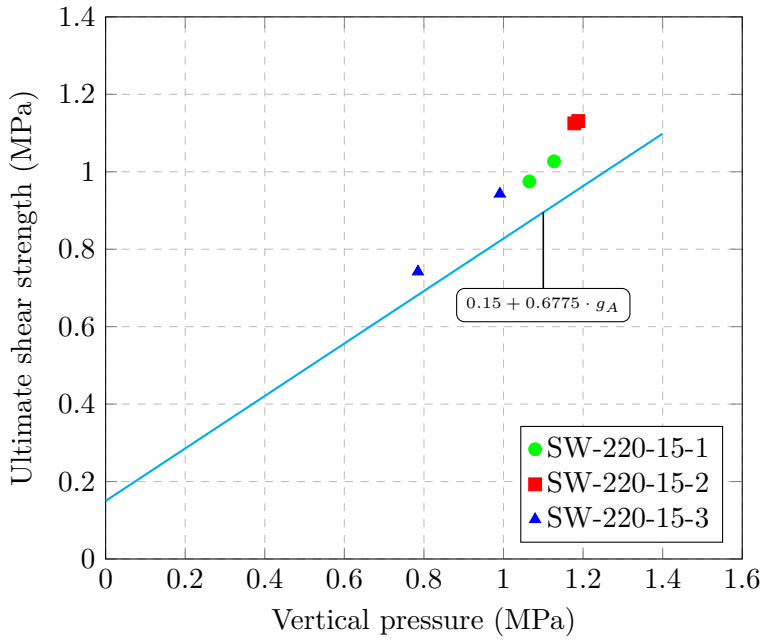

Figure 5.35: SHCC retrofitted SW results with trend lines.

The control SW strength according Equation 5.4 is also shown in Figure 5.35, where it can be observed that all the results from the SHCC SW's are above the line, indicating higher shear strength for the same vertical stress.

5.4.2.1 SHCC resistance contribution calculation

The test and loading configuration dimensions were used to quantify the individual resistance of the masonry and SHCC while acting as a composite. The shear forces were applied at a lever arm of 1150 mm (Figure 4.17) above the bottom left corner, while the equivalent vertical force from the three rows of rods also worked in at a lever arm of 1150 mm to the right of the bottom left corner. This one to one (1:1) shear to vertical load application is also visible in Figure 5.29, where the vertical and shear force lines run parallel at failures.

Considering the SHCC overlay as a continuum (not as a composite), with only a pin support at the left bottom corner, as the overlay was not in contact with the concrete beams and could not go into bending. Then, for equilibrium a vertical force equal to the shear force (when the lever arms are the same as in this case, and own weight of the overlay is ignored) will arise. An increase in shear force will thus lead to the same increase in vertical force. This one to one ratio implies that for the shear force resisted by the SHCC a same magnitude vertical force is required.

Using this characteristic of the test setup, the strength of the masonry and SHCC overlay can be determined by reducing the vertical and shear force with equal amounts (1:1 ratio) until the assumed control SW masonry strength line is intercepted. This process is shown in Figure 5.36 and mathematically expressed in Equations 5.5 to 5.7. Note however that V1,S1 and V2,S2 do

not correspond to phase 1 as 2 as described earlier. V2 and S2 are the peak stresses at phase 1, while V1 and S1 are the normal and shear stress of the masonry at peak resistance corresponding to phase 1. Similarly S4 is the peak force of the composite at ultimate failure (phase 2), while S3 is the friction stress in the masonry at ultimate failure.

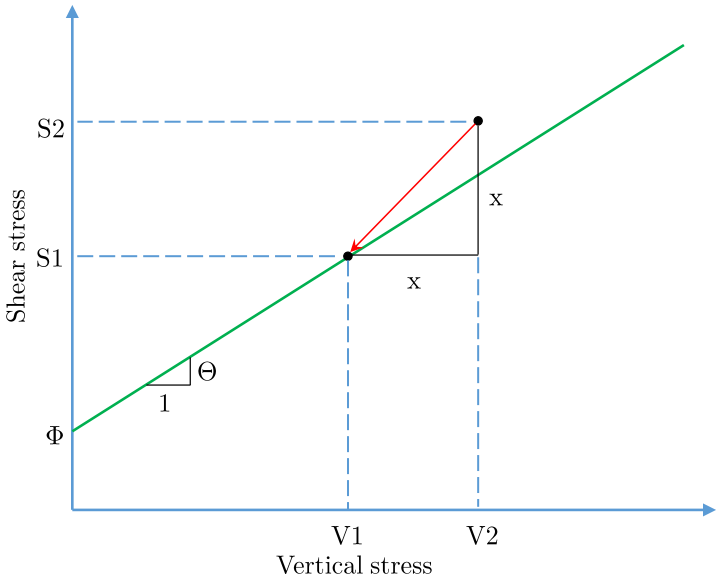

Figure 5.36: Stress contribution calculation.

$$S1 = \phi + \theta \cdot V1 \tag{5.5}$$

$$S1 = S2 - x \tag{5.6}$$

$$V1 = V2 - x \tag{5.7}$$

Substituting Equations 5.6 and 5.7 into 5.5 and solving for x yields:

$$x = \frac{S2 - \theta \cdot V2 - \phi}{1 - \theta} \tag{5.8}$$

Where

$S1$	is the shear strength of the masonry
$S2$	is the combined shear strength of the masonry and SHCC at the point where the masonry wall cracks
$V1$	is the vertical stress at S1
$V2$	is the vertical stress at S2
x	is the SHCC contribution

Using values obtained from the control tests as stated in Equation 5.4 for ϕ and θ, S1 was calculated. S3 was calculated in a similar fashion, but using the average friction coefficient of 0.69 from the control SW tests. The calculated values for S1 and S3 are summarized in Table 5.7 and shown in Figure 5.37.

The stress in the SHCC at the point when the masonry cracked diagonally is also shown under phase 1. The SHCC stress under phase 2 in Table 5.7 is i.t.o the masonry area, to be able to sum the two stresses for the total ultimate resistance/stress (S4). For calculating the 'actual' SHCC stress, the stress contribution from the SHCC in phase 2 was divided by the overlay thickness and multiplied by the wall thickness to convert the stress. An 'effective' SHCC stress was also calculated, by dividing the shear strength increase with the overlay shear area, where the shear strength increase is taken from S1 to S4. For retrofitting S1 would be the existing shear strength of the wall and S4 the retrofitted. As walls have not necessarily failed diagonally before retrofitting, the original strength has to be used and not the cracked state (S3).

An average 'actual' SHCC stress of 7.65 MPa (CoV of 23%) was determined. This is considerably higher than (double) the expected 3.3 ± 0.5 MPa, where the 3.3 MPa comes from the shear strength of SHCC being one and a half times that of its tensile strength (recall that $f_u = 2.2$ MPa was found, as presented in Table 3.3). The 'actual' SHCC stress calculated from the additional force divided by the shear area (1150 ×15 or 30 mm), does not accurately represent the stress, but the only way to represent these results. A postulation is that the additional failure mechanisms that the SHCC brings about, enhances the resistance and the SHCC also provides resistance in tension across the vertical head joints that failed.

Table 5.7: SHCC stresses calculated (all values shown in MPa).

	Phase 1		Phase 2					SHCC stress	
Specimen	S1 *	SHCC Stress	S4 ⊖		S3 †		SHCC ‡	Actual	Effective ◇
SW-110-30-2	0.508	5.642	2.792	=	0.417	+	2.375	7.126	6.852
SW-220-15-1	0.652	4.740	1.027		0.542		0.485	7.116	5.494
SW-220-15-2	0.576	8.052	1.131		0.438		0.693	10.162	8.135
SW-220-15-3	0.554	2.751	0.943		0.520		0.422	6.195	5.691
Average	0.573	5.296						7.650	6.543
Std	0.060	2.199						1.731	1.219
CoV	11%	42%						23%	19%

Notes:
* Masonry shear strength
⊖ Ultimate shear resistance, masonry + SHCC (From Table 5.6)
† Friction stress in cracked masonry joint
‡ SHCC stress i.t.o masonry stress (Masonry area used)
◇ Effective stress equals (S4-S1)/A_{ratio}

The more relevant parameter for the design of overlays is the 'effective' stress, as this captures the strength enhancement that is brought about with the overlay. An average effective stress of 6.543 MPa with a relative low (19%) CoV was determined, showing the potential of SHCC as a retrofitting solution. This effective SHCC shear strength is also in reasonable agreement with the strength of 5.06 MPa determined during the MT tests presented in Section 5.2.4.

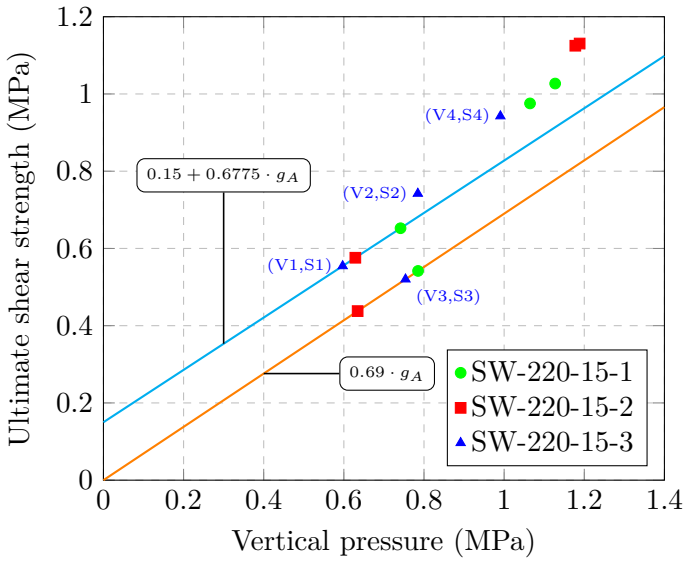

Figure 5.37: Calculated shear stress in the masonry (S1,S3), and masonry with a overlay (S2,S4) against vertical pressure.

5.5 Design model

A proposed design model for the design shear strength of retrofitted clay brick masonry with a SHCC overlay is presented in this section. With any industrial application that depends on a vast number of variables and prerequisites, it is advantageous to have a model that guides the user to a rapid selection with the required characteristics. The model is, however, based on limited data and further refinement with FE analysis and additional tests is encouraged.

From the measured data presented in Figures 5.35 and 5.37, it is apparent that the shear strength increases with a set value, leading to data points being the same distance above the control trend line. It is also generally agreed that masonry shear strength follows a Coulomb friction relation/law.

A novel expression was therefore developed with an increase in initial shear strength determined from the measured data and calculated effective stresses. The presented expression is based on the shear strength equation presented in Equation 2.1, with an additional term to increase the initial shear strength.

$$f_{composite} = \phi + \theta \cdot g_A + f^*_{SHCC} \cdot \frac{t_{SHCC}}{t_{mb}} \tag{5.9}$$

with

$$f^*_{SHCC} = f_u \times F_{vt} - R_{char} \tag{5.10}$$

Where

$f_{composite}$	is the characteristic shear strength of clay masonry with a SHCC overlay
$f_{SHCC}*$	is the effective characteristic shear strength of the SHCC
t_{SHCC}	is the thickness of the SHCC overlay
F_{vt}	is the tension to effective shear stress ratio (constant of 2.97)
R_{char}	is the reduction of F_{vt} from a average to characteristic value with a 95% exceedance probability. (constant of 2.00 MPa)

The use of Equation 5.9 is illustrated in Figure 5.38. Values obtained during the SW tests are used, thus ϕ equals 0.15, θ equals 0.6775, t_{SHCC} and $t_{masonry}$ equal to 15 mm and 220 mm respectively and f_u equals 2.2 MPa. The results from SW-220-15 are also shown. An increased initial shear strength of 0.31 MPa can be seen.

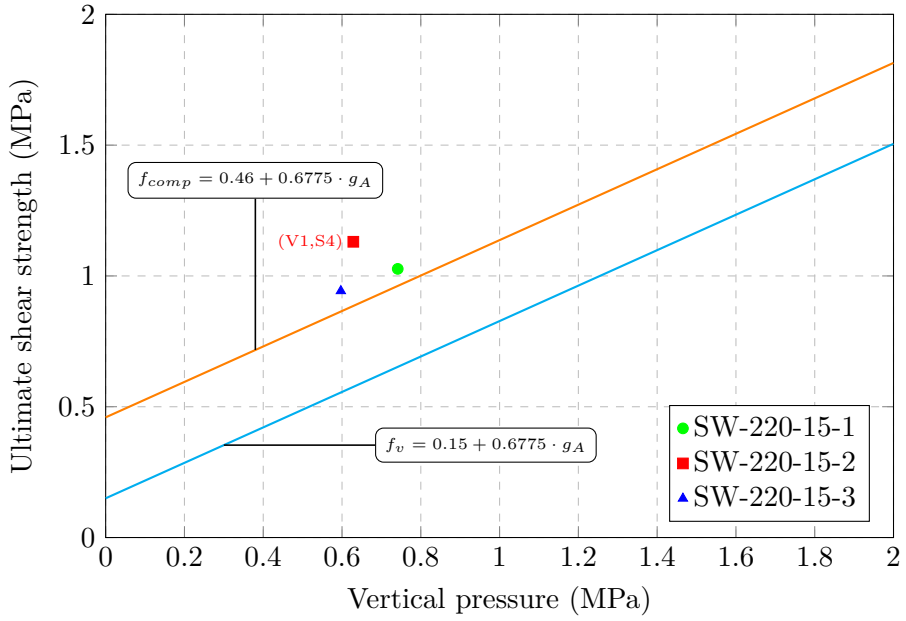

Figure 5.38: Design model prediction illustrated.

5.5.1 Design aid figures for retrofitting of URM walls designed according to SANS 10164-1

Two design aid figures are presented in Figures 5.39 and 5.40 for class I mortar with a width of 110 mm and 220 mm respectively and shear behaviour as stated under Section 4.2.4 of SANS 10164-1 (1989) ($f_v = 0.35 + 0.6 \cdot g_A$). Similar figures can be derived for class II mortar ($f_v = 0.15 + 0.6 \cdot g_A$) using Equations 5.9 and 5.10.

The following conditions have to be satisfied for the shear resistance from Figures 5.39 and 5.40 to be valid:

- Failure through the overlay should occur, and not debonding. Thus the condition in Equation 5.2.3.1 ($V_{SHCC} < A_{SHCC} \cdot f_{\tau SHCC} \cdot RF_b$), has to be satisfied. $f_{\tau SHCC}$ has to be determined experimentally for a specific type of brick. From the research presented in this thesis, RF_b can be assumed as 0.8.
- Shear cracking should be the predicted failure mode of the wall, and not flexural, rocking or toe crushing failures. The aspect ratio of the wall plays an important role in the failure mode and attention should be paid to toe crushing when using weaker bricks or hollow core bricks.
- $f_u \geq 2.2$ MPa. (For f_u values greater than 2.2 MPa, the use of Equations 5.9 and 5.10 to calculate $f_{composite}$ is advised.)
- For other SHCC mixtures, $\varepsilon_u \geq 0.02$ and values for $f_{\tau SHCC}$ should be determined experimentally.

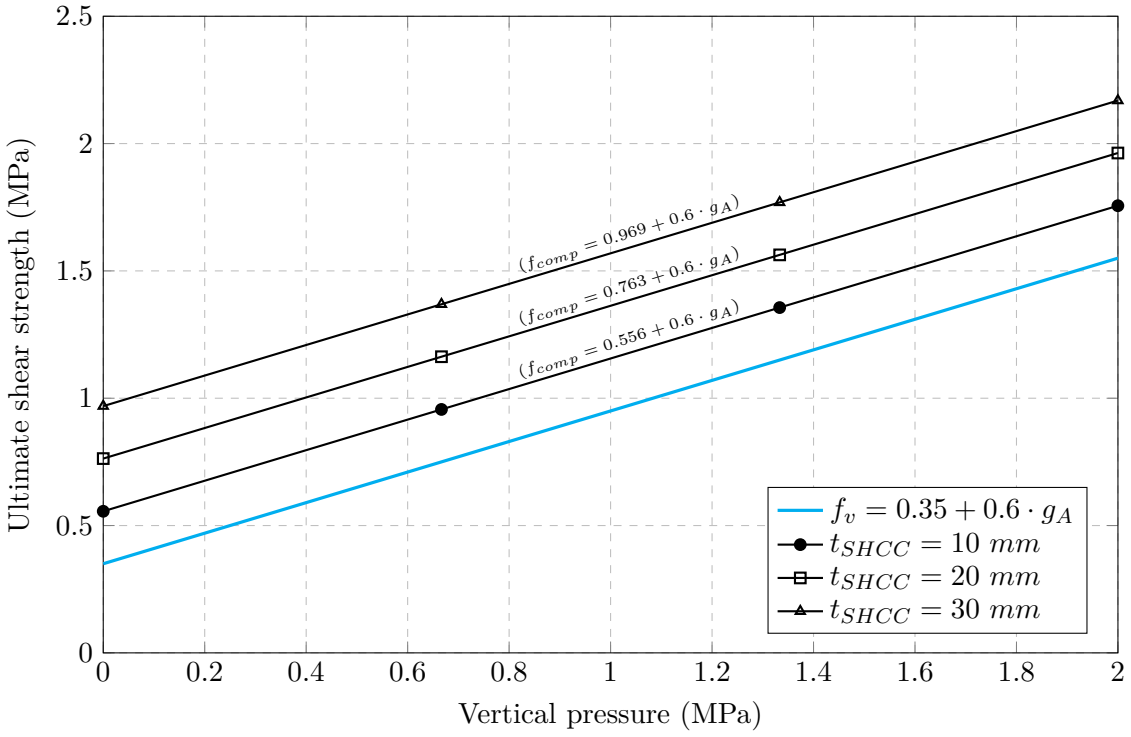

Figure 5.39: Design prediction illustrated, 220 mm thick class I masonry.

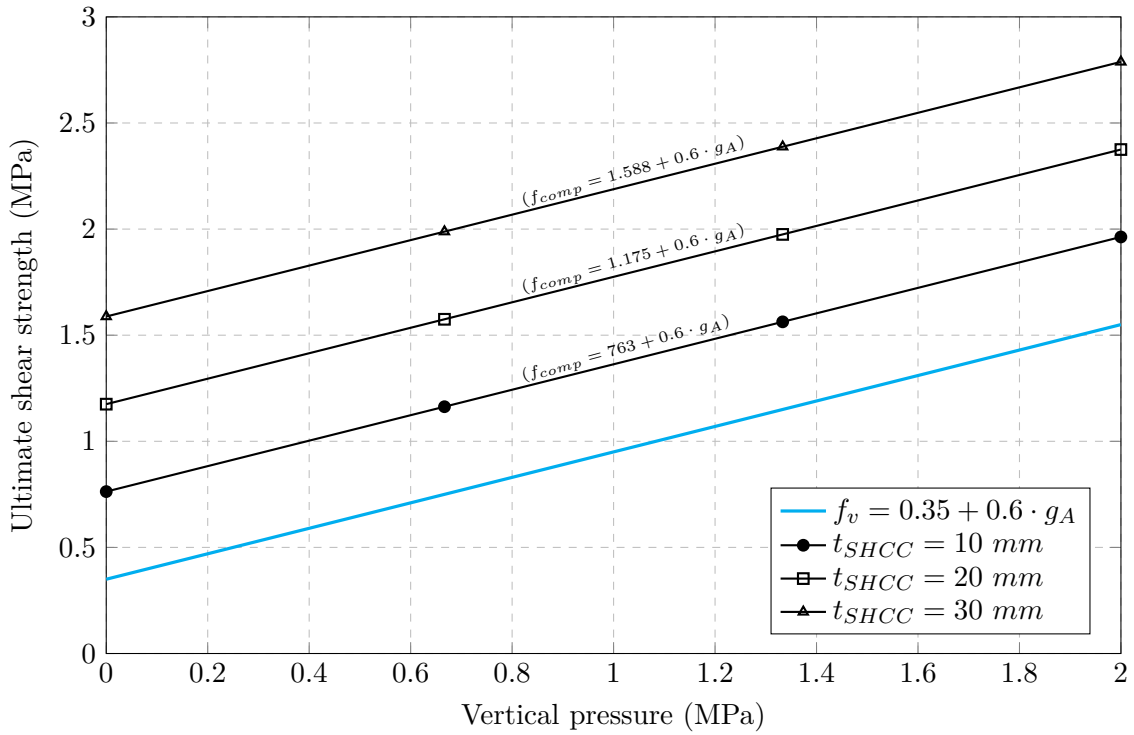

Figure 5.40: Design prediction illustrated, 110 mm thick class I masonry.

5.6 Concluding summary

From the material characterization tests and results presented in Section 5.2, conclusions were drawn and presented in Section 5.2.5. Recall that a shear bond strength of 2.30 MPa, and an effective shear strength of 5.06 MPa was found for the SHCC used in this research.

From the SW test results presented in Section 5.3, and compared in Section 5.4 the following summary and concluding remarks can be drawn:

- Testing SWS under normal (0.35 MPa) vertical pressures results in rocking and sliding failures, and further FE analysis, to investigate the formation of diagonal shear cracks in masonry shear walls under these pressures, is encouraged, with the goal to form a standardized test for large SWS.
- Static push over tests, with a increasing vertical force, were successfully performed on large SWS, with all the samples showing diagonal shear failure.
- The control specimen showed a sudden drop in resistance after the diagonal shear crack formed and continued to have a resistance from the friction along the horizontal bed joints. This may seam like a ductile failure, but the energy diserpation of this friction is small compared to that of the SHCC overlay. This is shown in Figure 5.33, where the area under the friction parts of the control specimen is small compared to the area under phase 2 (recall, phase 2 is where masonry is cracked and the force is resisted by friction along the bed joints and the SHCC overlay) of the retrofitted specimen.

- The retrofitted SWS with a thin SHCC overlay showed enhanced strength and ductility. A diagonal shear failure with multiple cracking through the overlay was observed.
- From SW-220-0 a trend line with a R^2 value of 0.930 was produced indicating the control SWS to have a initial shear strength of 0.15 MPa and a frictional angle of 0.6775. This performance differs from the results from the triplet tests, where a initial shear strength of 0.277 MPa and a frictional angle of 1.08 was determined. The SW test is however considered to be a more accurate representation of SW behaviour in a URM building, where there is shear and bending in a wall oppose to the triplet test where a more pure shear force is exerted.
- An average effective shear strength of 6.543 MPa with a CoV of 19% for the SHCC overlay was determined, showing the potential of SHCC as a retrofitting solution. This effective SHCC shear strength is also in reasonable agreement with the strength of 5.06 MPa determined during the MT tests.

The following summary and concluding remarks are drawn about the design model presented in Section 5.5:

- The design model presented uses the effective shear strength determined from the SW tests to calculate an increase in the initial shear strength.
- The model is limited to the specific material used in this research and additional tests have to be conducted for the use of other SHCC and masonry.
- The model shows the potential of SHCC overlays as a retrofitting strategy with increased initial shear strength values. Increases in shear strength (compared with masonry) of 0.2 MPa and 1.24 MPa were calculated for 220 mm thick walls with a 10 mm overlay and 110 mm thick walls with a 30 mm overlay respectively.
- Additional tests with more variables (other overlay thicknesses and different brick types) are advised to improve and generalize the model.

Chapter 6

Conclusions and Recommendations

6.1 Conclusions

This study followed from the need to retrofit URM buildings vulnerable to seismic action, as seismic design standards in South-Africa were only introduced in 1989. This means that most of the URM buildings in the South Western part of the Western Cape region were not adequately designed for seismic activity, putting a large number of lives at risk. In-plane shear strength is the main focus, as diagonal shear cracking is a main cause of collapse for URM buildings during seismic activities. In follow-up research, out-of-plane resistance, and connections between structural parts will be studied by the research group.

Sprayable SHCC overlays as an in-plane shear strengthening mechanism were investigated. A SHCC mixture was successfully adjusted for spraying onto masonry without running off, while maintaining it's mechanical properties. Material characterization tests and full scale SW tests led to the development of a prediction model for in-plane shear resistance of such a retrofitted wall.

This thesis is a contribution to the process of redressing the shortage of literature and design guidance for retrofitting masonry using bonded SHCC overlays. The following notable conclusions can be drawn from the work presented in this thesis.

6.1.1 Development of spray-able SHCC

- SHCC can be applied by spraying and trowelled flat to provide an acceptable finish.
- The viscosity development of SHCC can be adjusted with the addition of small quantities of CAC.
- A 5% replacement of cement with CAC proved to be the optimal replacement for minimal run off after 15 min rest time.
- Overlay thickness's up to 60 mm can be achieved.
- Deformability of $1.1 < \Gamma < 1.3$ is required for pumping and spraying of SHCC without running off.

- A circumferential air supply nozzle provides improved compaction and a smaller spray angle and is thus advised for spraying of SHCC.

6.1.2 Mechanical performance of sprayed SHCC

- Higher percentage inclusion of FA increased the strain capacity and a 140% ratio to cement showed the highest strain capacity.
- CAC replacement of cement has no clear effect on the strength or strain capacity of SHCC.
- The mechanical properties of sprayed SHCC were lower than those of the cast specimens, with a 26.1% and 32.1% decrease in ultimate tensile strength and strain capacity respectively.
- An average of 2.26% strain and 2.20 MPa tensile strength for the sprayed SHCC is considered sufficient for retrofitting application.
- The elastic modulus of both the sprayed and cast SHCC was 15.26 GPa.

6.1.3 Shrinkage of overlay

- The sprayed SHCC had an average free shrinkage of 655 micro strain, while the shrinkage at the top of a 30 mm restrained overlay was on average 594.4 micro strain after 56 days.
- No cracking of the SHCC overlay was observed for the restrained shrinkage specimen.
- Restrained shrinkage is not detrimental to sprayed SHCC overlays on masonry tested in this project. The relatively low free shrinkage values and high relaxation potential combined with high tensile strain capacity hold potential for highly favourable composite behaviour of a masonry wall with a bonded SHCC overlay. No debonding or localized cracking was observed.
- Crack patterns on the SW overlays were observed, with crack widths of 10 μm and smaller and are considered insignificant and possibly limited to the surface. These restrained drying shrinkage cracks were regularly spaced at an average of 44 mm in 15 mm thick overlays and 33 mm in 30 mm thick overlays.

6.1.4 Bonded overlay characterization

Two triplet shear tests, the standardized Triplet (T) and the Modified Triplet (MT) shear tests, were successfully applied on masonry specimens with and without SHCC overlays, which resulted in the following conclusions:

- From the standard triplet (T) test results, the initial shear bond strength of the mortar joint was determined to be 0.277 MPa, with a friction coefficient of 1.08. The initial shear strength is lower than that specified in SANS 10164-1 (1989) of 0.35 for a class I mortar, but a friction angle of 1.08 is far greater than 0.6 as specified in SANS 10164-1 (1989). From these results it is recommended that the values provided in SANS 10164-1 (1989) be reviewed and possibly adjusted for specific brick types.

- Using the same test, the shear bond strength of the SHCC overlay was determined to be 2.30 MPa for the materials tested. The test showed a brittle bond failure, where a sudden drop after peak force occurs. This is considered to be a significant bond resistance, while surface preparation effects are still to be researched.
- From the larger control specimen results of the MT shear test, the test method was deemed satisfactory for determining the additional shear strength and ductility that SHCC brings about, as similar results as those from the standardized test were achieved.
- In a modified triplet test with larger specimens and 10 mm thick bonded SHCC overlays on both faces, multiple shear cracking formed in the overlays, leading to ductile shearing response of these specimens. The MT specimens with an overlay, showed an ultimate resistance increase of 5.2 times, compared to the control specimen, with the SHCC having an effective shear strength of 5.06 MPa. A significant (6.4 times) increase in post-peak ductility was evident for all specimens with overlays, compared with the control specimens.
- The specimens with a 10 mm overlay on both sides showed a ductile post peak response, due to the multiple fine cracking phenomenon. After the initial cracks formed, localized debonding occurred around the crack region followed by the next crack through the SHCC. This proses continued until a localization cracked formed. The SHCC on the smooth face showed a debonding and crack kinking behaviour with a wider area and number of cracks forming. The localization crack on the smooth face formed away from the shear plane, while a more localized shear failure around the mortar shear plane, with a narrower cracking area was observed on the grooved face.

6.1.5 Shear wall tests

Large scale Shear Wall (SW) tests were successfully performed on control and SHCC retrofitted specimens in diagonal shear, which resulted in the following conclusions:

- Testing SW specimens under normal (0.35 MPa) vertical pressure results in rocking and sliding failures, and further FE analysis, to investigate the formation of diagonal shear cracks in masonry shear walls under these pressures, is encouraged, with the goal to form a standardized test for large SWS.
- The control specimen showed a sudden drop in resistance after the diagonal shear crack formed and continued to have a resistance from the friction along the horizontal bed joints. The retrofitted SW specimens with a thin SHCC overlay showed enhanced strength and ductility, with increasing resistance after the masonry cracked along head and bed joints. A diagonal shear failure with multiple cracking through the overlay was observed.
- From the 220 mm thick control specimen a trend line with a R^2 value of 0.930 was produced indicating the control SWS to have an initial shear strength of 0.15 MPa and a frictional angle of 0.6775. This performance differs from the results from the triplet tests, where a initial shear strength of 0.277 MPa and a frictional angle of 1.08 was determined. The

SW test is however considered to be a more accurate representation of SW behaviour in a URM building, where there is shear and bending in a wall as apposed to the triplet test where a more pure shear force is exerted. It should be kept in mind that a non-uniform pressure distribution arose in the SWS due to the particular constraint in the shear wall test, which may represent the case of a confinement by stiff floors and upper storey structural elements.

- An average effective shear strength of 6.543 MPa with a CoV of 19% for the SHCC overlay was determined, showing the potential of SHCC as a retrofitting solution. This effective SHCC shear strength is also in reasonable agreement with the strength of 5.06 MPa determined during the MT tests.

6.1.6 Design model

The SW test data was used to formulate a design model. The model is based on the shear strength as described in SANS 10164-1 (1989), with an additional term accounting for the SHCC overlay providing an advanced shear strength. The following conclusions about the model can be made:

- The model is limited to the specific materials used in this research and additional test have to be conducted for the use of other SHCC and masonry.
- The model shows the potential for SHCC as a retrofitting strategy with increased initial shear strength values. Increases in shear strength (i.t.o. masonry) of 0.2 MPa and 1.24 MPa was calculated for 220 mm thick walls with a 10 mm overlay and 110 mm thick walls with a 30 mm overlay respectively.
- Additional tests with more variables (other overlay thicknesses and different brick types) are advised to improve and generalize the model.

6.2 Recommendations for future studies

From the insight gained in this research project, the following are identified as issues to be researched further:

- Material development of spray-able SHCC to optimize the mix design for ultimate strain and strength, taking into account the ageing effects of SHCC.
- Determine the effect of spraying SHCC at different deform-abilities (Γ) on the strain capacity and density.
- Determine the relaxation and strength development of sprayed SHCC, to predict shrinkage cracking behaviour.

- Determine the performance of bonded SHCC on other types of bricks, for example concrete blocks and hollow core clay bricks.
- Determine the effect that surface preparation has on the bond and cracking behaviour of SHCC overlays.
- Conduct more SW tests with different overlay thickness's to validate and possibly improve prediction the model.
- Perform cyclic and dynamic tests on retrofitted SHCC SW's and compare results with static push over results presented in this study.
- Evaluate the possible increase in behaviour factor (q) due to the ductility of the overlay.
- Model the individual tests using FE and compare results to the characterising tests. Calibrate the FE model then to the SW behaviour and use this model to then predict URM performance during earthquakes in a dynamic or transient response analysis.
- Assess the out-of-plane performance enhancement that SHCC will bring about, when retrofitted on a single and on both faces.
- Determine the durability advantages of using SHCC on masonry i.t.o moisture ingress.

References

ACI Committee 224 (2007). *Causes, Evaluation, and Repair of Cracks in Concrete Structures.* ACI224.1 R-07. American Concrete Institute.

Alexander, Mark and Beushausen, H.D. (2009). *Fulton's Concrete Technology.* Vol. 9. Cement and Concrete Institute, Midrand, South Africa. Chap. 8, pp. 111–146. ISBN: 978-0-9584779-1-8.

ASTM C109 (2010). 'Standard Test Method for Compressive Strength of Hydraulic Cement Mortars (Using 2-in . or [50-mm] Cube Specimens) 1'. In: *Annual Book of ASTM Standards* i.C, pp. 1–9. DOI: 10.1520/C0109.

ASTM C1437 (2007). 'Standard test method for flow of hydraulic cement mortar'. In: *Annual Book of ASTM Standards* C, pp. 1–2.

ASTM E519 (2002). 'Standard test method for diagonal tension (shear) in masonry assemblages, masonry test methods and specifications for the building industry'. In: *Annual Book of ASTM Standards* C, pp. 2–14.

Basoenondo, Assy Arijoeni (2008). 'Lateral load response of Cikarang Brick wall structures- an experimental study'. Phd Thesis. Centre of Build Environment and Engineering Reseach, Queensland University of Technology.

Beushausen, H.D. (2005). 'Performance of bonded concrete overlays subjected to differential shrinkage.' Phd Thesis. University of Cape Town, South Africa.

Beushausen, H.D. and Alexander, M. G. (2006). 'Failure mechanisms and tensile relaxation of bonded concrete overlays subjected to differential shrinkage'. In: *Cement and Concrete Research* 36.10, pp. 1908–1914. ISSN: 00088846.

Beushausen, H.D. and Alexander, M (2007). 'Localised strain and stress in bonded concrete overlays subjected to differential shrinkage'. In: *Materials and structures.* Pp. 189–199.

Beushausen, H.D. and Chilwesa, Masuzyo (2013). 'Assessment and prediction of drying shrinkage cracking in bonded mortar overlays'. In: *Cement and Concrete Research*, pp. 256–266. ISSN: 00088846. DOI: 10.1016/j.cemconres.2013.07.008.

Boshoff, William Peter (2007). 'Time-Dependant Behaviour of Engineered Cement-Based Composites'. PhD thesis. University of Stellenbosch.

Bruedern, A, Abecasis, D and Mechtcherine, V (2009). 'Development of Strain-Hardening Cement-based Composites for the strengthening of masonry'. In: *Concrete Repair, Rehabilitation and Retrofitting II - Proceedings of the 2nd International Conference on Concrete Repair, Rehabilitation and Retrofitting, ICCRRR*, pp. 887–894.

BS EN 1052-3 (2002). 'Methods of test for masonry-Part3: Determination of initial shear strength.' In: *British Standards Institution. London,United Kingdom.*

BS EN 772-1 (2011). 'Methods of test for masonry units-Part1: Determination of compressive strength.' In: *British Standards Institution. London,United Kingdom.*

Carlsward, Jonas (2006). 'Shrinkage cracking of steel fibre reinforced self compacting concrete overlays'. Doctoral Thesis. Lulea University of Technology.

Chilwesa, Masuzyo (2012). 'Assessing the age at cracking of concrete repair mortars/overlays subjected to restrained drying shrinkage.' Masters Thesis. University of Cape Town.

Combrinck, Riaan (2016). 'Cracking of plastic concrete in slab-like elements.' PhD thesis. University of Stellenbosch.

Dehghani, Ayoub, Fischer, Gregor and Nateghi Alahi, Fariborz (2015). 'Strengthening masonry infill panels using engineered cementitious composites'. In: *Materials and Structures* 48.1-2, pp. 185–204. ISSN: 1359-5997. DOI: 10.1617/s11527-013-0176-4.

ElGawady, M, Lestuzzi, P and Badoux, M (2004). 'A review of retrofitting of unreinforced masonry walls using composites'. In: *Proc., 4th International Conf. ...* Pp. 1–8.

ElGawady, Ma, Lestuzzi, P and Badoux, M (2006). 'Retrofitting of masonry walls using shotcrete'. In: *2006 NZSEE Conference, Yeni ...* 45, pp. 45–54.

Esmaeeli, Esmaeel, Manning, Elizabeth and Barros, Joaquim A O (2013). 'Strain hardening fibre reinforced cement composites for the flexural strengthening of masonry elements of ancient structures'. In: *Construction and Building Materials* 38, pp. 1010–1021. ISSN: 09500618. DOI: 10.1016/j.conbuildmat.2012.09.065.

Hancilar, U, Durukal, E and Erdik, M (2008). 'Seismic assessment and rehabilitation of historical unreinforced masonry (URM) buildings in Istanbul'. In: *The 14th World Conference on Earthquake Engineering, Oct 12-17, Beijing, China*, pp. 1305–1316.

Iosipescu, N. (1967). 'New accurate method for single shear testing of metals'. In: *Journal of Materials*, pp. 537–566.

Kesner, K.E, Billington, S.L. and Douglas, K.S. (2003). 'Cyclic response of highly ductile fibre-reinforced cement-based composites'. In: *ACI Materials Journal* 100.5, pp. 381–390.

Kim, Yun Yong, Kong, Hyun Joon and Li, Victor C. (2003). 'Design of Engineered Cementitious Composite Suitable for Wet-Mixture Shotcreting'. In: *ACI Materials Journal* 100.6, pp. 511–518. ISSN: 0889325X. DOI: 10.14359/12958.

Li, M. (2006). 'Behaviour of ECC/Concrete Layered repair system under drying shrinkage conditions'. In: *Restoration of Buildings and Monuments* 12.2, pp. 143–160.

Lin, Yi Wei, Wotherspoon, Liam, Scott, Allan and Ingham, Jason M. (2014). 'In-plane strengthening of clay brick unreinforced masonry wallettes using ECC shotcrete'. In: *Engineering Structures* 66, pp. 57–65. ISSN: 01410296. DOI: 10.1016/j.engstruct.2014.01.043.

Loser R, Leemann A (2009). 'Shrinkage and restrained shrinkage cracking of self-compacting concrete compared to conventionally vibrated concrete'. In: *Mater Struct* 42, pp. 71–82.

Matsumura, A, ed. (1990). *Planar shear loading test on reinforced fully grouted hollow clay masonry walls.* Vol. I, pp. 347–358.

Neville, A.M (1970). 'Creep of Concrete: Plain, reinforced and prestressed'. In: *North Holland publishing company,Amsterdam.*

Page, A.W., ed. (1989). *A parametric study of the behaviour of masonry shear walls.* 1 vols. Vancouver, Canada, pp. 817–826.

Paul, Suvash Chandra (2015). 'The Role of Cracks and Chlorides in Corrosion of Reinforced Strain Hardening Cement-Based Composite (R/SHCC)'. Phd thesis. University of Stellenbosch.

Sahmaran, Mustafa, Al-Emam, Muhannad, Yildirim, Gürkan, Simsek, Yunus Emre, Erdem, Tahir Kemal and Lachemi, Mohamed (2015). 'High-early-strength ductile cementitious composites with characteristics of low early-age shrinkage for repair of infrastructures'. In: *Materials and Structures* 5, pp. 1389–1403. ISSN: 1359-5997.

SANS 10160-4:2011 (2011). 'Basis of structural design and actions for buildings and industrial structures, Part 4: Seismic actions and general requirements for buildings'. In: *SANS.*

SANS 10164-1 (1989). 'The structural use of masonry, part 1: Unreinforced masonry walling '. In: *SANS.*

SANS 10249 (2012). 'Masonry walling'. In: *SANS.*

Schaaf, RA (2009). *Investigation into the Seismic Resistance of a Typical Unreinforced Masonry Structure used as Low Cost Housing Units in the Western Cape.* Final year project. University of Stellenbosch.

Shang, Q (2006). 'Shear behaviour of Engineered Cement-based Composites'. MScEng Thesis. University of Stellenbosch.

Song, Gao (2005). 'Matrix manipulation to stady ECC behaviour'. MScEng Thesis. University of Stellenbosch.

Stander, H (2007). 'Interfacial bond properties for ECC overlay systems'. MScEng Thesis. University of Stellenbosch.

Tomazevic, M (1999). 'Earthquake-resistant design of masonry buildings'. In: *Imperial College Press, London, England*.

Van der Mersch, W.A. (2015). 'Modelling the Seismic Response of an Unreinforced Masonry Structure'. PhD thesis. TUDelft.

Van Zijl, Gideon P. A. G., Slowik, Volker, Toledo Filho, Romildo D., Wittmann, Folker H. and Mihashi, Hirozo (2016). 'Comparative testing of crack formation in strain-hardening cement-based composites (SHCC)'. In: *Materials and Structures* 49.4, pp. 1175–1189. ISSN: 1359-5997. DOI: 10.1617/s11527-015-0567-9.

Van Zijl, Gideon P.A.G (2004). 'Modeling masonry shear-compression: Role of dilatancy highlighted'. In: *Journal of Engineering Mechanics-Asce* 130.11, pp. 1289–1296. ISSN: 0733-9399. DOI: 10.1061/(ASCE)0733-9399(2004)130:11(1289).

Van Zijl, Gideon P.A.G. (2005). 'The role of aggregate in HPFRCC'. In: *Concrete , Beton* 110, pp. 7–13.

Van Zijl, Gideon PAG (2007). 'Improved mechanical performance: Shear behaviour of strain-hardening cement-based composites (SHCC)'. In: *Cement and Concrete Research* 37.8, pp. 1241–1247. DOI: 10.1016/j.cemconres.2007.04.009.

Van Zijl, GPAG and Wittmann, FH (eds.) (2011). 'Durability of Strain-Hardening Fibre Reinforced Cement Based composites (SHCC), State-of the art report'. In: *Rilem TC 208 HFC*.

Van Zijl, GPAG, de Vries, PA and Vermeltfoort, AT (2004). 'Masonry wall damage by restraint to shrinkage'. In: *ASCE Journal of Struc Engineering Mechanics* 130(7), pp. 1075–1086.

Visser, Christo Riaan (2007). 'Mechanical and structural characterisation of extrusion moulded SHCC'. MScEng Thesis. University of Stellenbosch.

Wang, Shuxin and Li, Victor C (2006). 'High-early-strength engineered cementitious composites'. In: 103.2, p. 9. ISSN: 0889325X.

Zang, Jin (2015). 'Developing non-heat treated UHPC in South-Africa'. Phd thesis. University of Stellenbosch.

Zhou, Deyuan, Lei, Zhen and Wang, Jibing (2013). 'In-plane behavior of seismically damaged masonry walls repaired with external BFRP'. In: *Composite Structures* 102, pp. 9–19. ISSN: 02638223. DOI: 10.1016/j.compstruct.2013.01.031.

Appendices

Appendix A

Addtional Figures

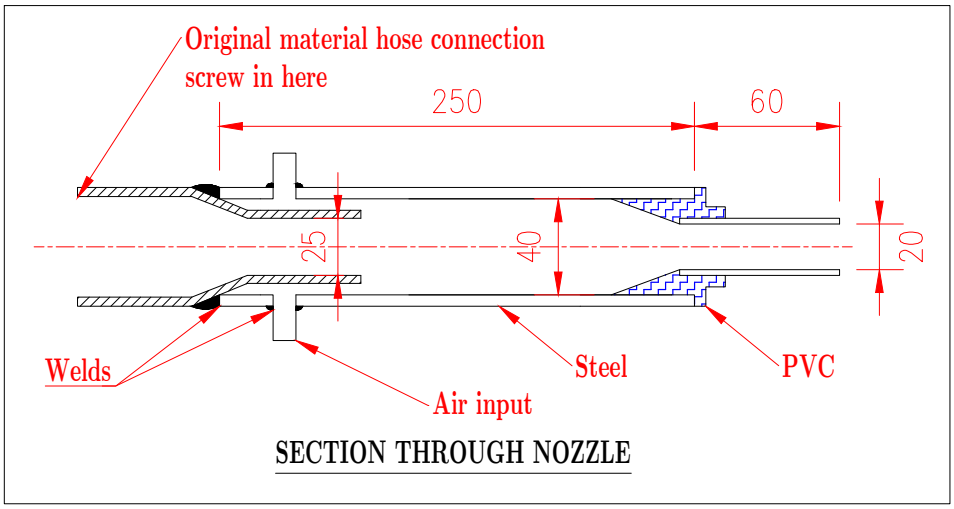

Figure A.1: Nozzle design drawing for nozzle with air supplied along the full circumference of the material

(a) (b)

Figure A.2: Dumbell specimen before and after grinding.

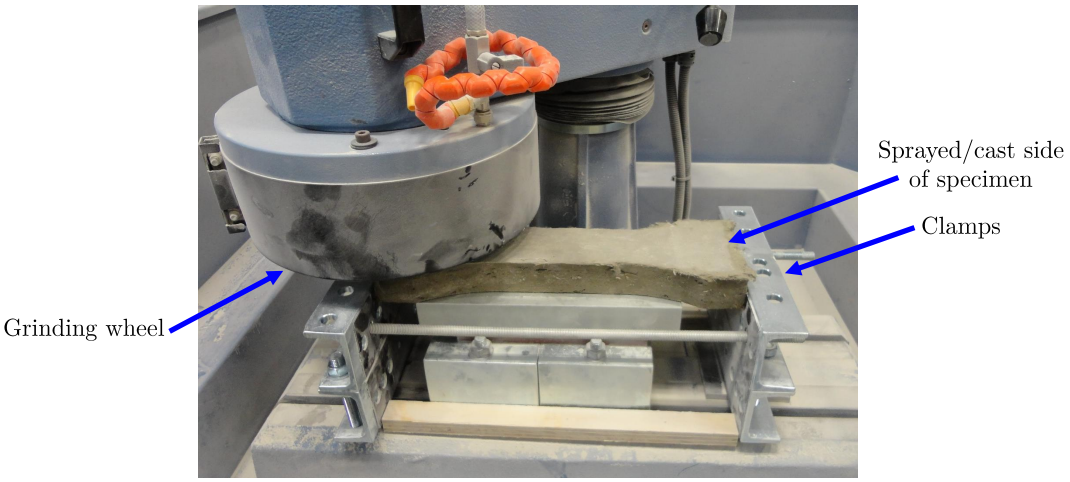

Figure A.3: Kingtest specimen grinding machine.

(a) (b)

Figure A.4: Stored specimens (a) triplet and (b) modified triplet.

Figure A.5: Stored SWS

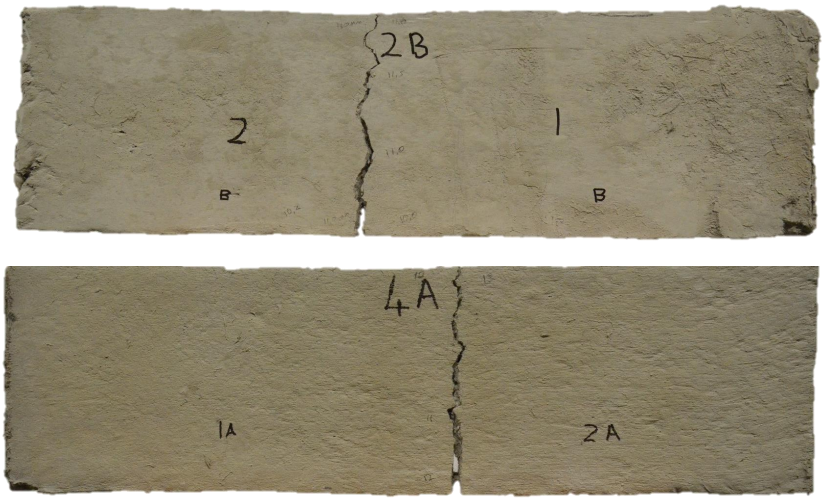

Figure A.6: Flexural failure of specimens MT-110-20-2&4.

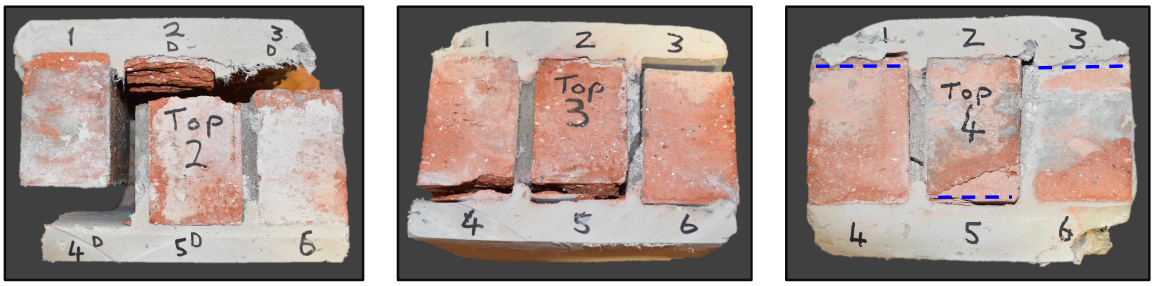

(a) (b) (c)

(d) (e) (f)

Figure A.7: SHCC shear bond test failure mechanisms: (a,d) T0-110-60-2; (b,e) T0-110-60-3; (c,f) T0-110-60-4.

(a) (b) (c)

Figure A.8: Crack growth during test SW-220-0-1 with cracks documented at: (a) at ultimate shear force, (b) 5 seconds after ultimate shear force (failure occurred in less than half a second and remained at that position until photograth was taken) and (c) at the end of the test.

Figure A.9: SW-110-30-2 Flexural crack opening.

Figure A.10: SW-110-30-2 Top beam sliding failure.

(a) (b) (c)

Figure A.11: SW-220-15-2 (a) before SHCC cracking (b) Localized SHCC crack formed (c) Corner debonded and localized cracked open wider.

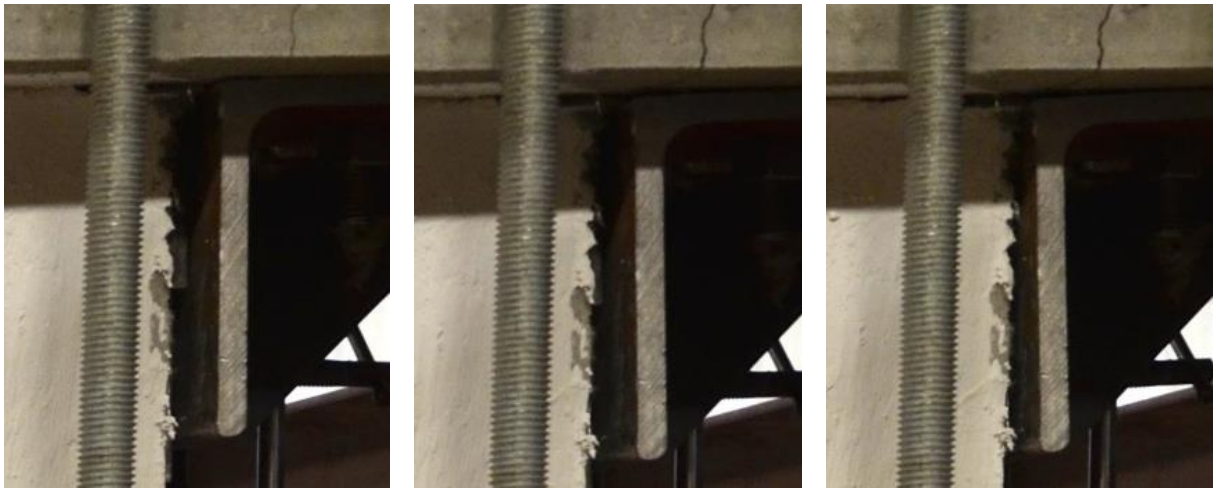

(a) (b) (c)

Figure A.12: SW-220-15-2 focused on top right corner (a) before SHCC cracking (b) Localized SHCC crack formed (c) Corner debonded and localized cracked open wider

(a) (b)

Figure A.13: SW-220-15-3 (a) Bottom corner debond ; (b) Top corner debond.

Appendix B

Triplet results

B.1 0 MPa confinement pressure

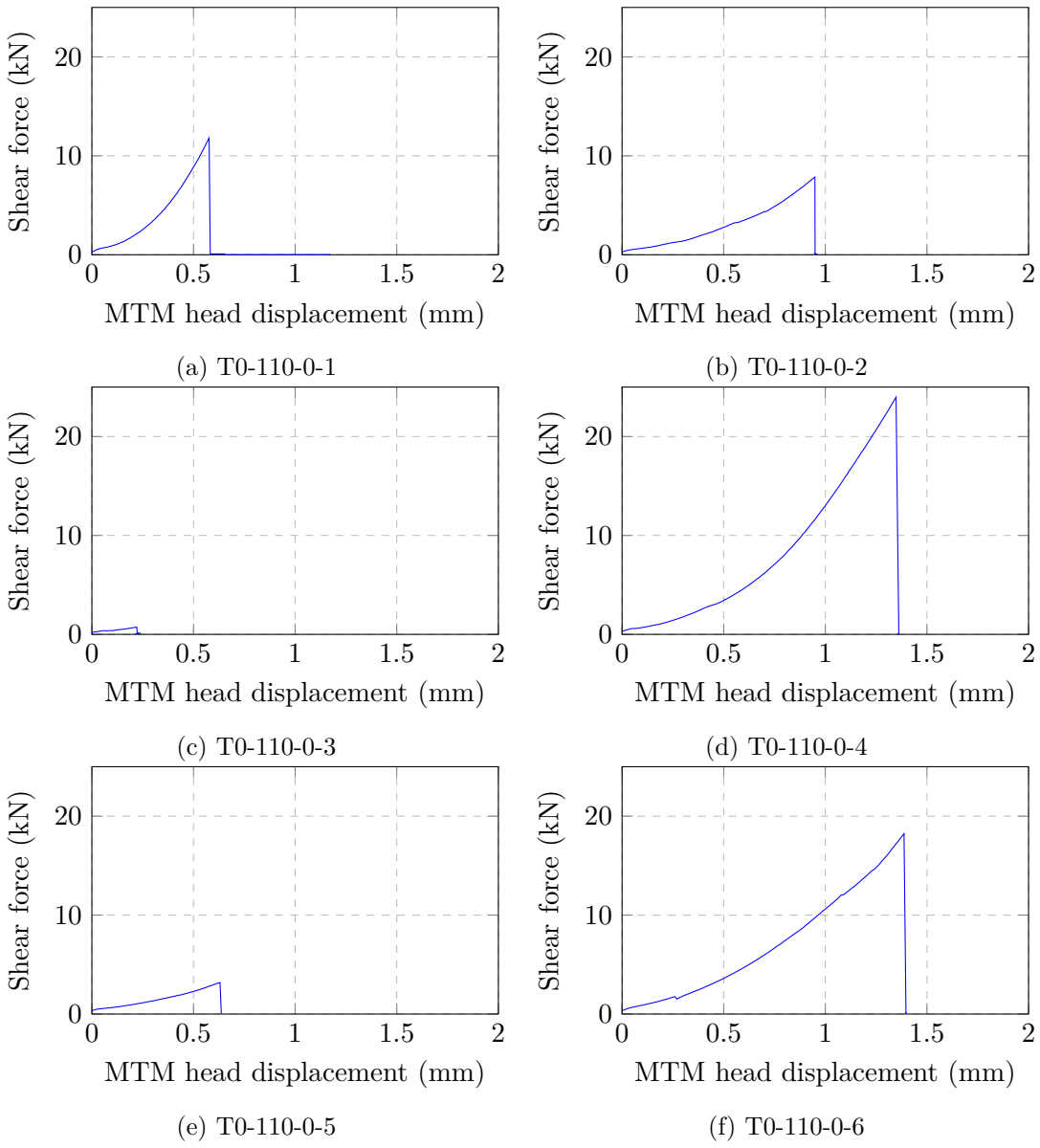

(a) T0-110-0-1

(b) T0-110-0-2

(c) T0-110-0-3

(d) T0-110-0-4

(e) T0-110-0-5

(f) T0-110-0-6

Figure B.1: 0 MPa confinement pressure

B.2 0.3 MPa confinement pressure

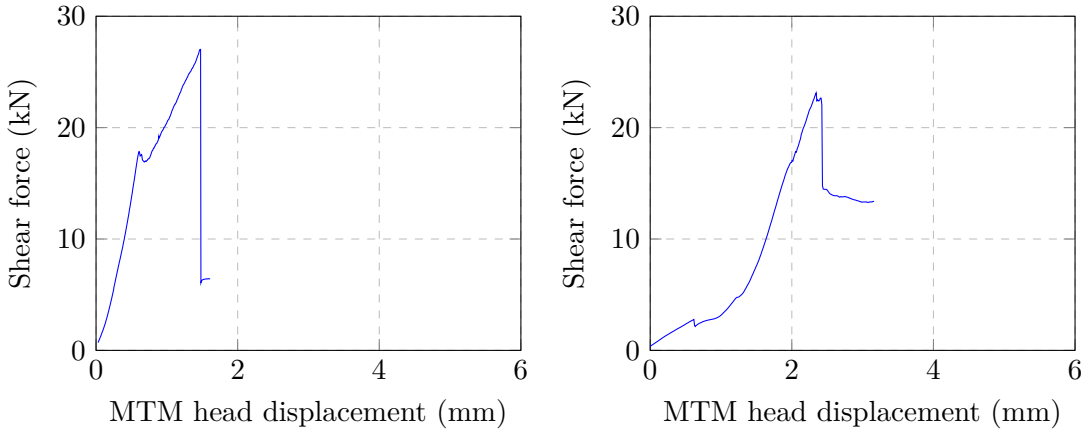

(a) T03-110-0-1

(b) T03-110-0-2

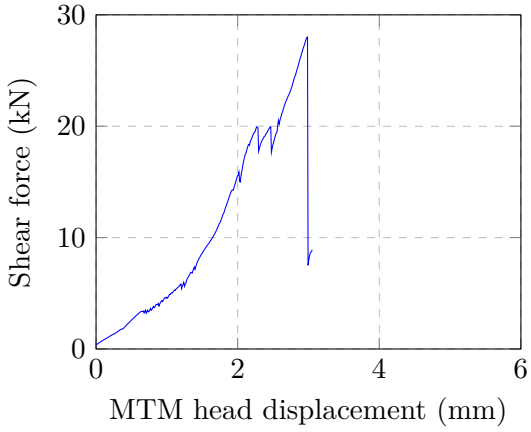

(c) T03-110-0-3

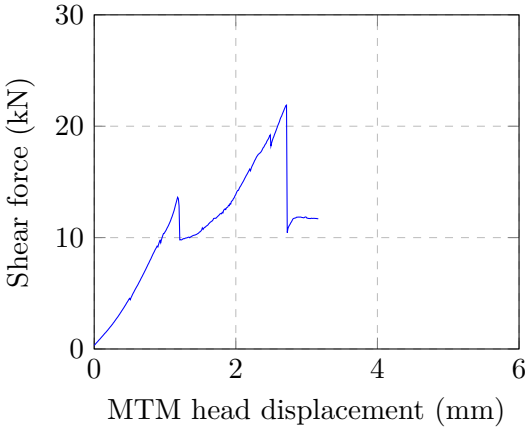

(d) T03-110-0-4

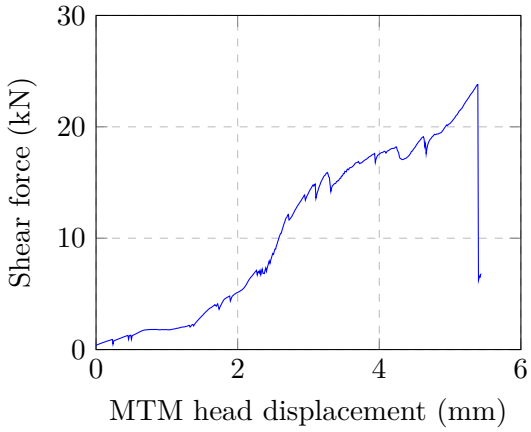

(e) T03-110-0-5

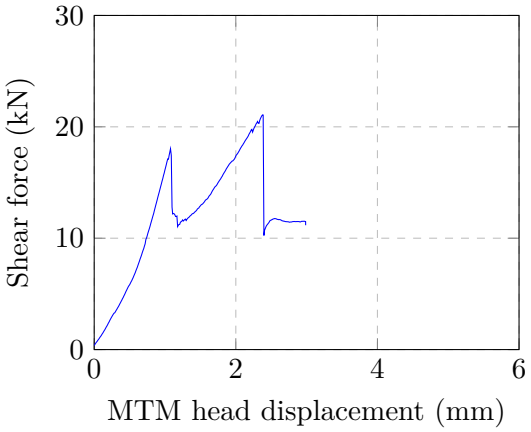

(f) T03-110-0-6

Figure B.2: 0.3 MPa confinement pressure

B.3 0.6 MPa confinement pressure

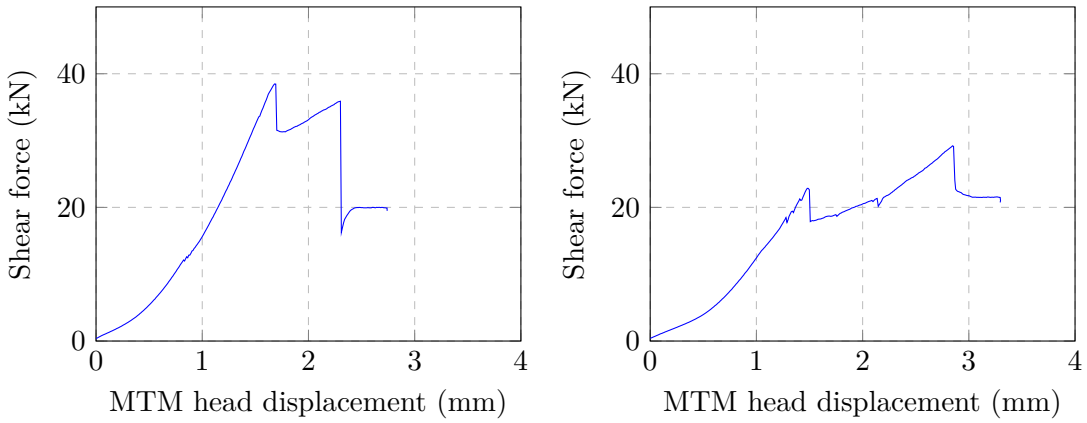

(a) T06-110-0-1

(b) T06-110-0-2

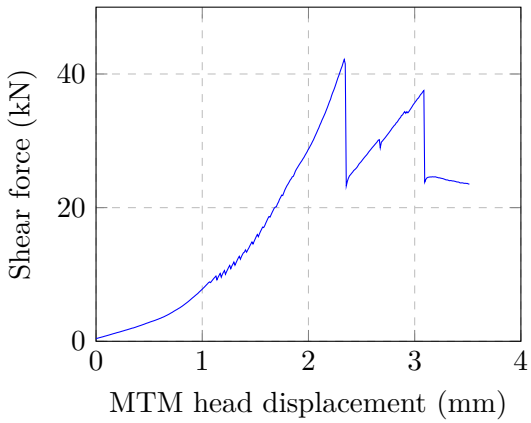

(c) T06-110-0-3

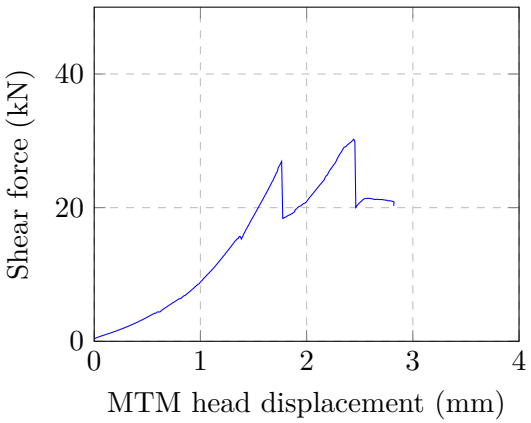

(d) T06-110-0-4

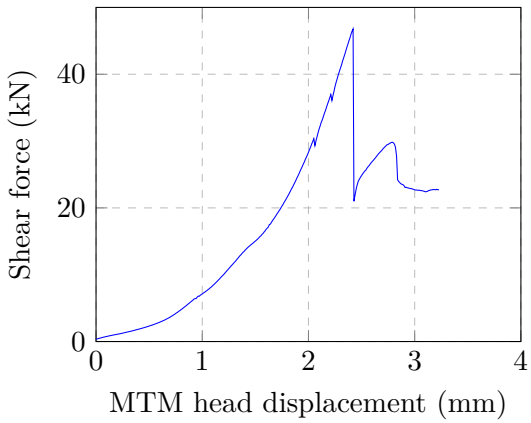

(e) T06-110-0-5

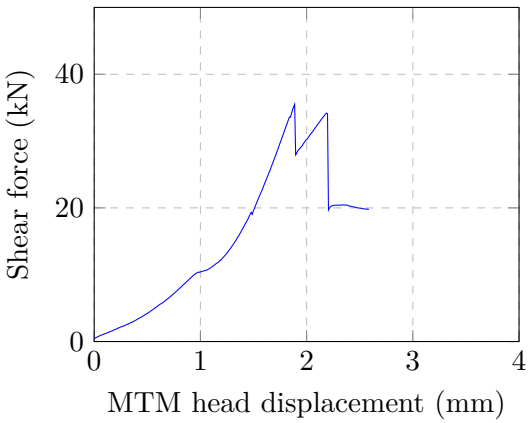

(f) T06-110-0-6

Figure B.3: 0.6 MPa confinement pressure

Appendix C

MT Addtional Results

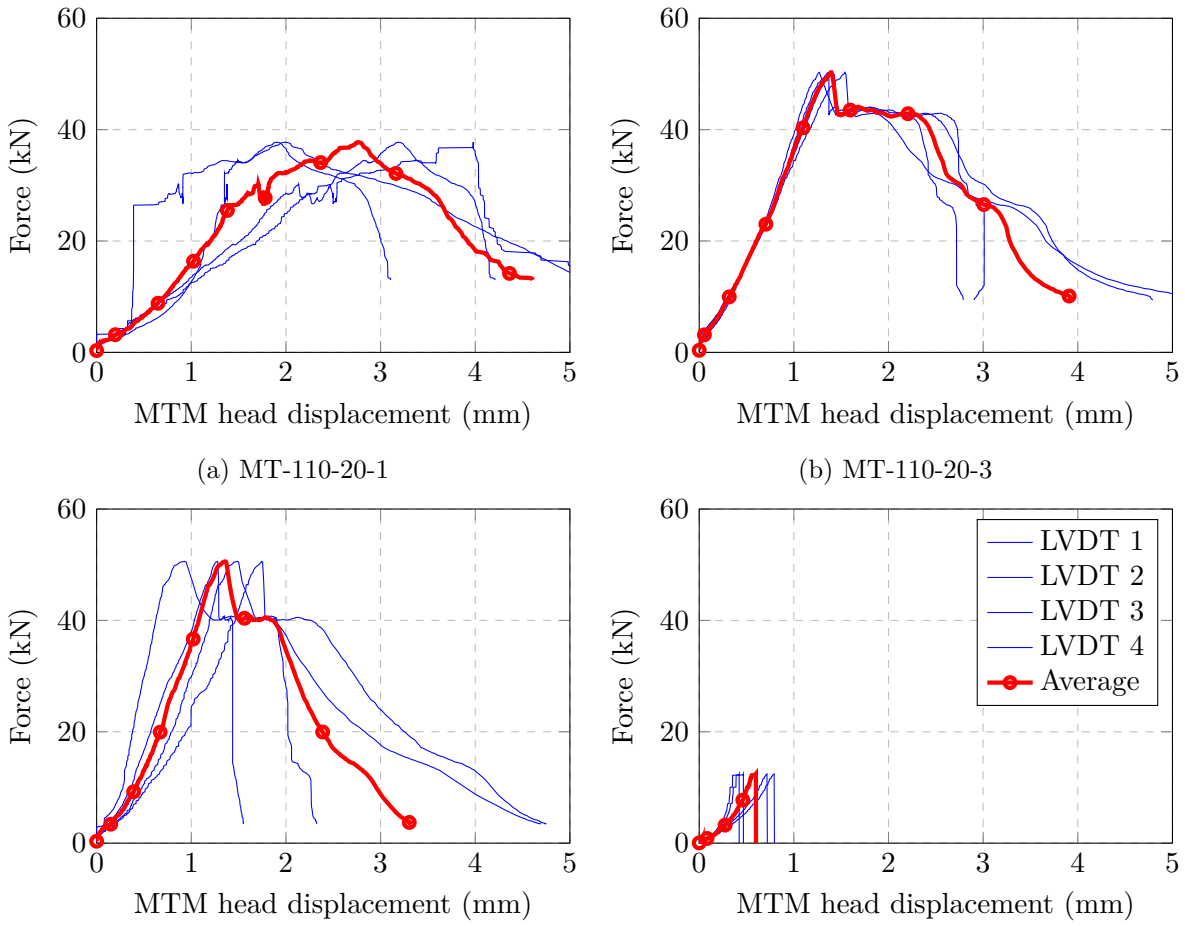

(a) MT-110-20-1

(b) MT-110-20-3

(c) MT-110-20-5

(d) MT-110-0-5

Figure C.1: Force against the four bottom displacements and the average shown for MT-110-20.

Appendix D

Results of SWS-110-0 & 30-1

D.1 SWS-110-0-1

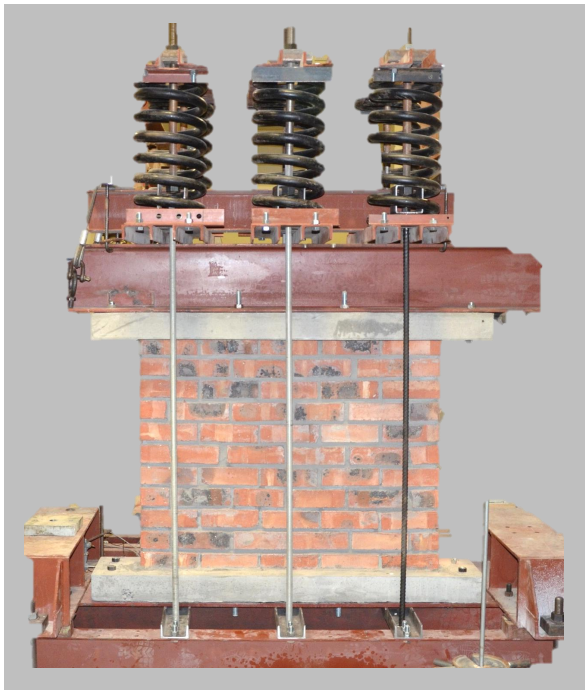

Figure D.1: Constant vertical force test setup.

Figure D.2: Flexural crack opening.

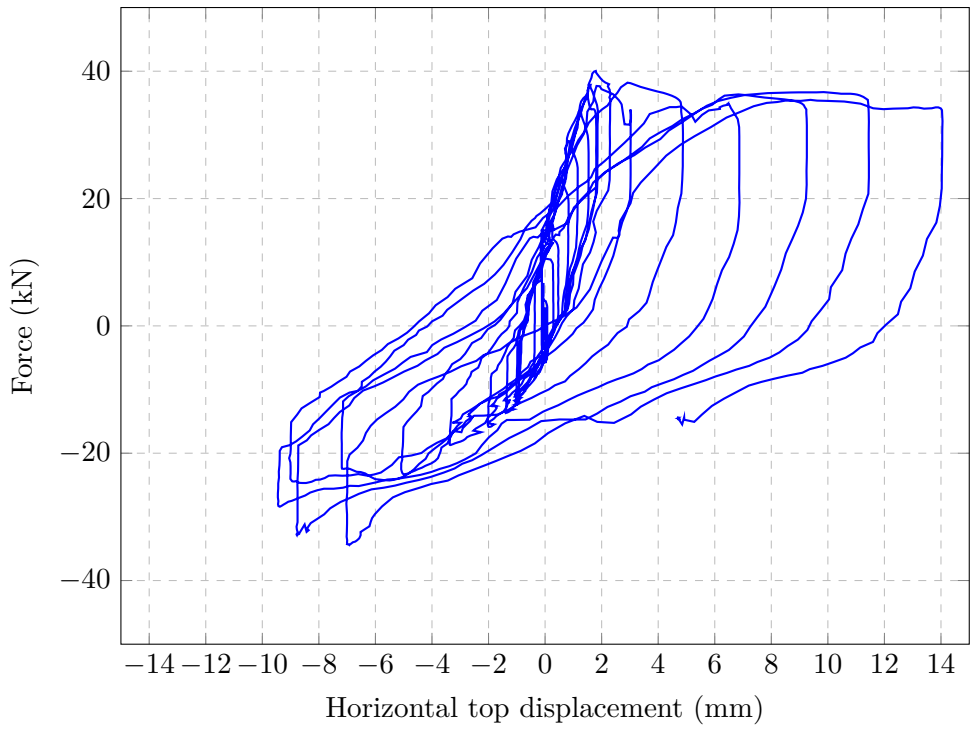

Figure D.3: SW-110-0-1 load vs displacement under cyclic loading.

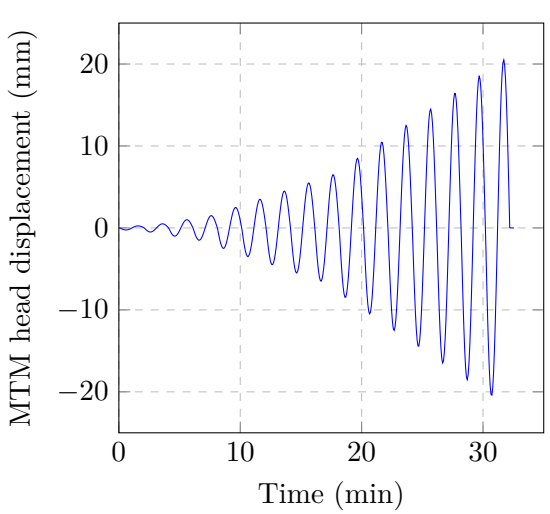

(a) Displacement control cyclic loading applied.

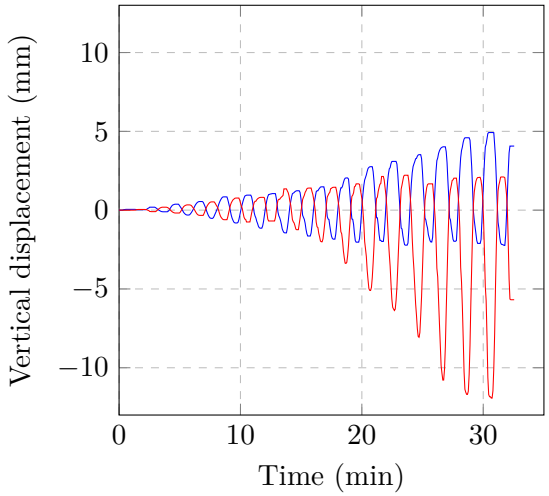

(b) Vertical displacement of both sides over time.

Figure D.4: SW-110-0-1 Horizontal (MTM head displacement) and Vertical displacement over time.

D.2 SWS-110-30-1

Figure D.5: Cyclic test setup with foot stops at both ends.

(a) (b)

Figure D.6: Toe crushing failure.

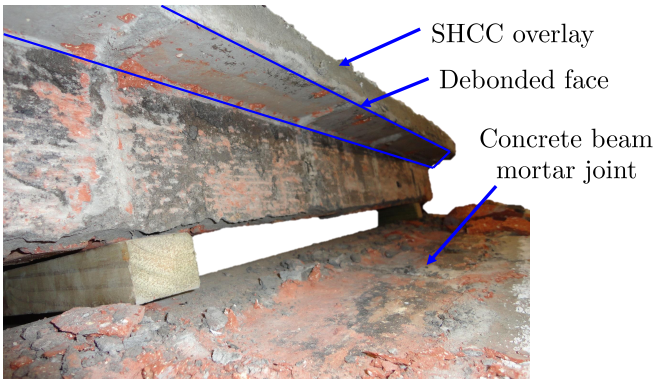

Figure D.7: SHCC overlay debonding from the bottom row of bricks. (Photograph taken from the bottom, after the wall was places horizontally, and bottom row of bricks removed by hand, to show the debonding face of the SHCC overlay.)

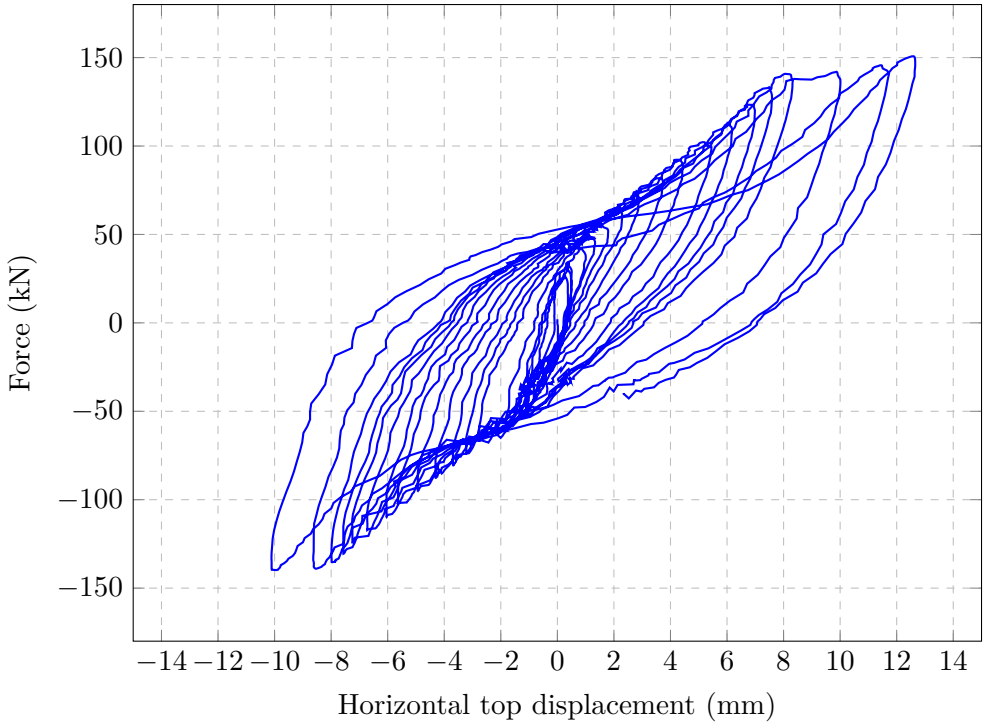

Figure D.8: SW-110-30-1, shear force vs displacement under cyclic loading.

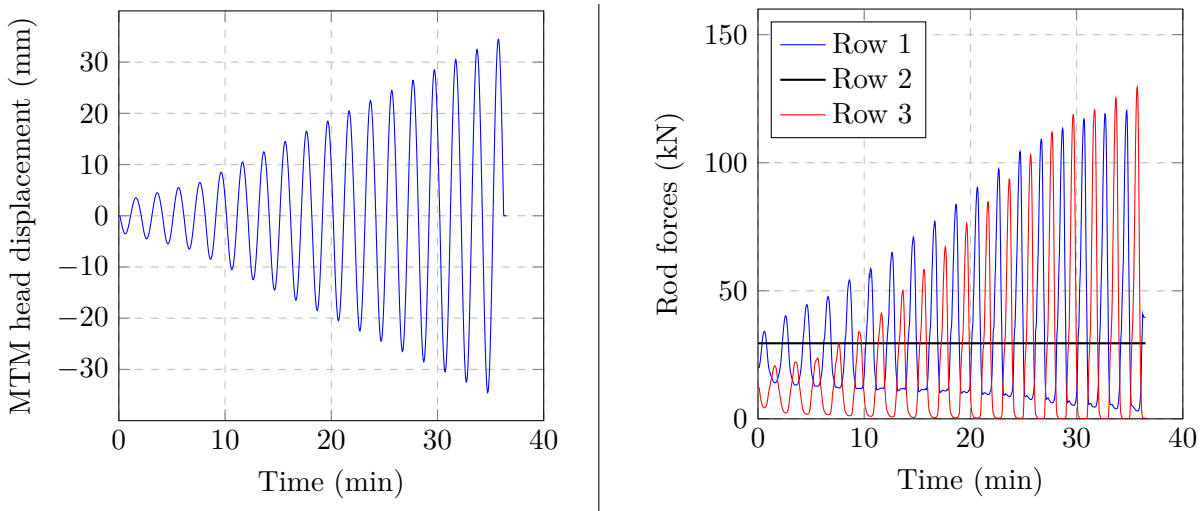

(a) Displacement control cyclic loading applied.

(b) Rod forces over time.

Figure D.9: SW-110-0-1 Horizontal displacement and rod forces over time.